NONLINEAR DYNAMICS OF CARDIOVASCULAR AGING

by

Yuri Shiogai

(Master, Kyoto University)

SUBMITTED IN PARTIAL FULFILMENT OF THE REQUIREMENTS FOR THE DEGREE OF
DOCTOR OF PHILOSOPHY

DEPARTMENT OF PHYSICS
LANCASTER UNIVERSITY
LANCASTER, UK, JULY 2007

CONTENTS

DECLARATION

This thesis is my original work and has not been submitted, in whole or in part, for a degree at this or any other university. Nor does it contain, to the best of my knowledge and belief, any material published or written by another person, except as acknowledged in the text.

ABSTRACT

The application of methods drawn from nonlinear and stochastic dynamics to the analysis of cardiovascular time series are applied with particular interests in the identification of changes associated with aging. Scale invariant and scale dependent approaches are studied. Using signals measured from healthy adults of all age (16-82 years, 71 men and 47 women), four different approaches to investigate cardiovascular aging are considered: (a) complexity and fractal analysis of heart rate variability (HRV); (b) spectral analysis of HRV using the wavelet transform; (c) spectral analysis of blood flow signals recorded with iontophoresis, using the wavelet transform; and (d) cardiorespiratory synchronization analysis. In (a) detrended fluctuation analysis (DFA) comprises a modified root-mean-square (rms) analysis of a random walk and has been developed to detect the fractal (self-similar) correlation property of non-stationary time series. Approaches (b), (c) and (d) focus on nonlinear oscillatory dynamics. In this approach non-stationarity is perceived as time- variability of oscillatory components. The cardiovascular system is perceived as being composed of many nonlinear oscillators of different physiological origin, interacting with each other and subject to noise. The understanding of coupled nonlinear oscillators has progressed rapidly in recent years, especially after the phase description was established. We show how these ideas can be applied to the cardiovascular system. As a first step in studies (b) and (c), we use wavelet analysis to separate the frequency components of nonlinear oscillations of different physiological origin into six intervals. We discuss the age-related changes in each of these frequency components and show how there changes are related to the results of the DFA. As the second step, we study the interaction between cardiac (I) and respiratory (II) systems, by the application of synchronization analysis. Finally, we present an overview of cardiovascular aging in terms of nonlinear dynamics and identify the further problems that remain to be tackled.

ACKNOWLEDGEMENTS

I gratefully acknowledge my supervisors, Dr. Aneta Stefanovska for giving me a whole guidance to this study and Prof. Peter McClintock for general supports which have been necessary to accomplish the work. Dr. Dmitry Luchinskyy also gave me good influence on my physical thinking and life.

Dr. Peter Clarkson in royal Lancaster infirmary also helped me in getting substances which I needed for measurements. Without him, I could not have accomplished the huge amount of measurements.

I also acknowledge my colleges in Lancaster, Andriy Bandrivskyy, Srefano Beri, Alexandra Pershakova, Rodrigue Tindjong, Jose Suarez-Vargas, Jane Sheeba, David Kenwright, Andrea Duggento and Laurence Sheppard for a lot of support in research and life. It was a great pleasure to work with good students from all over the world in the same group. It was also useful to discuss with Dr. Igor Khovanov, Dr. David Garcia-Alvarez and Dr. Alireza Bahraminasab.

The Colleges in Ljubljana, Alan Bernjak and Bojan Musizza, also helped me a lot in computing and life when I stayed there as a visitor. With their help, I could enjoy the study and life very much in Slovenia, a really beautiful country.

An ex-supervisor, Prof. Yoshiki Kuramoto, sent me documents to study the theory of coupled oscillators again. A theoretical basis of my work is largely dependent on his work.

I acknowledge all the volunteers who spared some time to be measured. Due to them, I could get a good statistics.

I appreciate my parents very much for have been supporting me to finish my studies for many years.

There are a lot of other friends which have helped me in every occasion. I really would like to thank all of them although I cannot mention all the names here.

Lancaster, UK Yuri Shiogai

December, 2006

LIST OF PUBLICATIONS

Parts of this thesis have been presented at conferences and published or are in the process of submission in the following.

Publication

- Y. Shiogai and Y. Kurmoto, Wave propagation in nonlocally coupled oscillators with noise, Prog. Theor. Phys. Suppl. 150 (2003) 435-438.
- Y. Kuramoto, S. Shima, D. Battogtokh and Y. Shiogai, Mean-field theory revives in self-oscillatory fields with non-local coupling, Prog. Theor. Suppl 161 (2006) 127-143.
- Y. Shiogai, A. Stefanovska and P.V.E. McClintock, Nonlinear dynamics of Aging, Physics Report (the proposal is accepted).
- Y. Shiogai, A. Stefanovska, P.J. Owen-Lynch, A. Bernjak, P. B. M. Clarkson and P. V. E. McClintock, Wavelet analysis of oscillatory components reveals age-related changes in the endothelial components of vasomotion, submitted.
- Y. Shiogai, A. Stefanovska, P.J. Owen-Lynch, Gender differences in the effects of aging on cardio-respiratory synchronization, in preparation.

Conference talks and posters

- INTAS workshop. December 2003, Ljubljana, Slovenia (Oral presentation)
- Workshop: complex dynamics of networks of oscillators: from basic research to novel therapy. November 2005, Sapporo, Japan (Oral presentation)

1. INTRODUCTION

In this thesis, methods from nonlinear science are used to identify changes in cardiovascular signals associated with the process of aging. This chapter sets the scene by considering the relevance of coupled oscillators to the cardiovascular system and by giving an overview of the complexity and spectral analysis of heart rate, age-related physiological changes in the cardiovascular system and aging studies with iontophoretic blood flow measurements. Chapter 2 gives a brief physiological explanation of the cardiovascular system. Chapter 3 describes how the measurements were made. The statistical tests are explained in Chapter 4. Phase dynamics is considered in chapter 5, together with a description of its relevance to heart rate variability. Chapter 6 describes the application of complexity analysis to heart rate and blood flow signals. Chapter 7 describes the problem to detect time varying oscillatory components. Chapter 8 gives the results of cardiorespiratory synchronization. Chapter 9 describes the correlation between different oscillatory components in blood flow signals calculated by wavelet analysis in Chapter 7. Finally in chapter 10 we summarize the results and draw conclusions.

1.1 Coupled nonlinear oscillators and the cardiovascular system

Two major milestones marked the development of coupled nonlinear oscillators: the introduction of the concept of entrainment within an ensemble of oscillators by Winfree [157]; and its analysis by Kuramoto [73] using a phase model. After Winfree had gone further into the theory of the geometry of biological time [158], Kuramoto generalized the phase dynamics approach [74] by reducing the degrees of freedom of the original dynamical system. For this to work, the original dynamics should be perturbed weakly by noise, with an external force or coupling to dynamics with a limit-cycle orbit. The latter describes dissipative systems and the form of the phase dynamics is not dependent on the form of the original model.

Numerous researchers contributed to the development of the theory, and the approach was further generalized by Strogatz [142]. Because of its universality and simplicity, phase dynamics can be applied quite generally to oscillatory phenomena in dissipative systems. It was this body of work that subsequently motivated the introduction of the theory of phase synchronization, facilitating studies of the interactions between coupled nonlinear and chaotic oscillators [116].

Coupled oscillators have been investigated by many physicists because the emergence of synchronization has similarities to phase transition phenomena, which had traditionally been studied. This synchronization transition was analyzed by the method of mean field theory in global coupled oscillators, in which one oscillator couples to all the other oscillators equally under a sine coupling function (the Kuramoto model). The stability of the macroscopic oscillation (synchronized solution) was then addressed by Croford and Strogatz [28], [29] and [141], and the coupled function was extended by Sakaguchi [124]. Not only global coupling, but also local coupling in which a given oscillator couples only to its nearest neighbors and which is equivalent to the diffusion coupling in the continuous system, has been studied extensively, eg. in the form of the Ginzburg-Landau equation [74]. An intermediate form of coupling between local and global, which is called nonlocal coupling, was suggested by Kuramoto [75, 77]. The nonlocal coupling has a finite coupling distance so that an oscillator can interact not only with its nearest neighbors, but also with some other oscillators. It differs from global coupling because an oscillator cannot in reality interact with all the others because of the finite coupling distance. Compared to local and global coupling which have been studied widely, nonlocal coupling has not been studied very much to date. But this model is expected to be useful because we can change the coupling length in the model. It is expected to encompass a lot of interesting phenomena which are as yet undiscovered. Studies of nonlocal coupling include [76, 131, 144, 130, 78].

In the human cardiovascular system, there are many phenomena to which the idea of the entrainment or synchronization of coupled oscillators can be applied. One of them is the emergence of macroscopic oscillations from the individual microscopic oscillation of each cell with slightly different frequency by entrainment. For example, it is well known [156] that the heart has pace-maker cells to which

other cells are entrained. It is also reported that the initiation of vasomotion requires the synchronization of Ca^{2+} release from the sarcoplasmic reticulum [113]. Another approach is to study the interaction of macroscopic oscillators of different physiological origin. In the latter approach, coupled oscillators were proposed as a possible description of the dynamics of the cardiovascular system [138] and synchronization between cardiac and respiratory oscillations, and their mutual modulation, were examined with particular care [89, 126, 127, 136, 137, 67, 149, 151]. The emerging picture motivated additional studies, and several methods for analysis of the direction of coupling among interacting oscillatory processes have recently been proposed [129, 121, 122, 108]. The notion of phase dynamics can be useful not only in terms of phase synchronization but also of phase-resetting [157]. The annihilation of pacemaker activity in cardiac tissues was observed via phase-resetting in [66], where current pulse was used to stimulate SA nodal pacemaker cells and observed phase-resetting phenomena. If the timing and amplitude were appropriate, the autonomous oscillatory activity stopped. There is also another study to terminate spiral waves during cardiac fibrillation via shock-induced phase-resetting [48]. The spiral waves rotating around the singularities in the heart, which is called ventricular fibrillation, can lead to death because the heart cannot pump the blood properly. In this way, phase dynamics can be applied successfully even to clinical medicine.

1.2 Time-invariant complexity analysis of heart rate variability (HRV)

The investigation of deterministic chaotic dynamics and, in particular, the introduction of measures to quantify the complexity of fractal dynamics triggered an avalanche of new studies of cardiovascular dynamics. H.E. Hurst introduced the Hurst exponent to quantify a scaling property when he investigated problems related to water storage in the Nile [59, 60]. Mandelbrot and Wallis examined and elaborated the method futher in [93, 94, 95, 96, 97, 98, 99]. Feder gives an excellent overview of the history, theory and applications, and adds some more statistical experiments in [38]. Although the estimation of the Hurst exponent was originally developed in hydrology, modern techniques for estimating the Hurst exponent come from fractal mathematics. The mathematics and images derived

from fractal geometry exploded into the world in the 1970s and 1980s. A fractal object is composed of sub-units and sub-sub-units on multiple levels that resemble the structure of the whole object (self-similarity) and it has a fractional dimension. As for chaotic dynamics, it often has a strange attractor which is characterized by fractal dimensionality D [100]. This dimension of a chaotic system is one of the ways to measure complexity. The pioneering algorithm by Grassberger and Proccacia was introduced to calculate the 'strangeness' of attractors in a easier way [45] and motivated a large number of applications. Another way to measure the complexity is based on the entropy and was also proposed by Grassberger and Proccacia [47]. The approximate dimension and approximate entropy were proposed by Kalpan *et al* [69]. Then chaotic behavior was proposed as a possible scenario [10, 117] to explain the dynamics of cardiac signals. Several methods, based on statistical physics were proposed. Scaling properties [63, 3, 54, 8, 16], multifractal properties [64, 4], and the $1/f$ spectra [72, 110, 65] of heart rate variability (HRV), were all discussed.

On the other hand, the heart rate has been known to have characteristics that differ between healthy people and people with heart disease [43]. The heart rate of healthy people is far from being a homeostatic constant state and has visually apparent non-stationarity, whereas the heart rate with heart disease is associated with the emergence of excessive regularity or uncorrelated randomness. A constant heart rate was observed in coma as well [134]. These features are thought to be related to fractal and nonlinear properties. To quantify the complexity of healthy heart rate and detect the alterations with disease and aging is a major challenge in physiology.

New methods have been developed to replace traditional methods which are suitable only for stationary signals, such as power-spectrum and autocorrelation analysis, and to quantify accurately 'long-range' correlation (see definitions in section 6.3) in non-stationary signals: the detrended fluctuation analysis (DFA) [111, 112] and the detrended moving average method (DMA) [24, 25, 26]. They are also based on the idea of a fractal in nonlinear theory. The fractal concept is extended to time series so that we can see the self-similar properties on different time scales. The DFA is a method to quantify the fractal correlation in time series by filtering out polynomial trends as explained in more detail in chapter 6. Then

to avoid the assumption that the trend is polynomial, the DMA method was introduced to estimate the correlation properties of non-stationary signals without any assumption of trends, the probability distribution or other characteristics of stochastic processes. These methods have been applied to financial [25], physiological [34, 52, 53] and biological signals [105].

It has been suggested that the HRV of healthy subjects shows self-similar (scale-invariant) fluctuations over a wide range of time scales, and that disease or aging make HRV less complex (with higher regularity and predictability). Actually it was reported that the complexity decreases with increasing age by using DFA in some studies such as [114, 143]. The physiological background to the loss of complexity with age has been studied extensively, yet it has not been fully elucidated. However, a balance between two branches of the autonomic nervous system is thought to attribute to the change of the complexity of heart rate [150].

In our study, we will confirm the previous results and extend them.

1.3 Spectral analysis of heart rate variability (HRV) and aging

With the advent of computers, starting in the 1960s, it became possible to sample physiological variables in real time and to store data for analysis. The resultant time series (signals) immediately introduced a need for tools for studying the dynamical properties of the underlying physiological processes. Because of the complexity of the time series the tools developed for spectral analysis were applied mainly with the aim of filtering out the noise, thereby reducing the complexity. Various methods of linear filtering were introduced, as was also a fast algorithm for calculation of the Fourier transform (now well known as the fast Fourier transform, or FFT). Application of the FFT to the most studied cardiovascular signal, the ECG, immediately showed that it possesses oscillatory components by Penaz *et al.* [109]. In their pioneering work Hyndman *et al.* [61] pointed to the generally oscillatory nature of physiological control systems. Sayers [125] and Luczak and Lauring [90] also did initiative work for rhythms in beat-to-beat heart rate signals. The spectral analysis of heart rate variability (HRV) was introduced by Akselrod *et al.* in 1981 [2] as a noninvasive means to evaluate quantitatively the beat-to-beat cardiovascular control. Besides the respiratory oscillations around

0.3 Hz (HF), several peaks were observed in the spectrum analysis around 0.1 Hz (LF) and below 0.05 Hz (VLF) in the frequency domain [2] [61]. It has been revealed in many papers that sympathetic and parasympathetic activities affect these components. HF is considered to represent vagal control of heart rate and LF is jointly contributed by both vagal and sympathetic nerves. The ratio LF/HF is considered as sympathovagal balance by many researchers [79].

However, the majority of the studies were done by FFT and autoregressive (AR) spectrum estimation [145]. By these methods, the frequency below 0.05 Hz was not studied. To overcome this, the wavelet transform was used for spectrum analysis by Lotrič [89], where age-related changes in the spectrum from 0.0095-0.6 Hz were studied. In this thesis, we add a new frequency interval from 0.005-0.0095 Hz to the previous study by Lotrič. Moreover the gender difference, which was not mentioned there, will be discussed, as well as aging.

1.4 Structural and functional changes in the cardiovascular system with age

Cardiovascular structure and function change with age, affecting the function of the heart and other organs, and perhaps causing diseases.

One of the major changes with aging is the remodelling of large arteries, when there is an increase in wall thickness and lumen enlargement. Arterial stiffening is another hallmark of arterial aging [85]. The geometry and diastolic function of the left ventriculum alters substantially with age [106].

Aging is also associated with alterations in the function of endothelium, the layer of cells between the blood and vascular smooth muscle cells in blood vessels. The endothelial control of vasomotor tone is altered with age and the alteration impairs the vascular adaptation to changes in flow, especially those induced by exercise and ischemia. Endothelium normally releases vasoactive substances such as nitric oxide (NO). Its ability to release them is also altered by aging. The impairment of endothelial dependent relaxation, which is especially mediated by NO, is observed in aged subjects. Most studies indicate that aging is associated with a decrease in NO production and release [23].

1.5 Blood flow with iontophoresis and aging

Endothelium was once thought to serve just as lining for the blood vessels. However after Furchgott and Zawadzki 1980 [40] found out that the relaxation evoked by acetylcholine in the rabbit aorta is mediated only in the presence of endothelium, numerous studies have demonstrated that endothelium plays an important role in regulating local vascular tone by releasing vasodilating and vasoconstricting substances.

Iontophoresis, which allows the transdermal delivery of polar drugs containing vasoactive endothelial-dependent and endothelial-independent substances such as acetylcholine (ACh) and sodium nitroprusside (SNP), has been widely used to assess how endothelial vasodilation changes with essential hypertension, heart failure, arteriosclerosis and exercise, as well as aging. Blood flow was measured by using laser Doppler flowmetry (LDF) at the sites into which ACh and SNP were delivered by iontophoresis and then the blood flow signals were analyzed by wavelet transform according to [139] This is a non-invasive measurement and one can acquire data to make an assessment of the human cardiovascular system in vivo. In earlier studies [80, 81, 82, 83, 84, 139], it was revealed that there are several peaks in the frequency domain arising from different physiological origins such as endothelial, neurogenic, myogenic, respiratory and cardiac components. In addition, a large number of studies were done to reveal the physiological origin of the oscillatory components [132]. By this method of analysis, the endothelial function can be compared among different ages by looking into the frequency interval corresponding to the endothelial activity.

In physiology, a lot of aging studies of blood flow by iontophoresis have been done and some of them reported that endothelial-dependent vasodilation decreased with increasing age [36, 42]. There are also some studies which observed gender difference in endothelial dependent vasodilation [27, 1]. However wavelet analysis and any oscillatory components analysis have not yet been combined with iontophoresis studies of aging. Here we present novel results about aging by LDF measurement of blood flow with both iontophoresis and wavelet analysis.

2. PHYSIOLOGICAL BACKGROUND

In this chapter, I briefly review the physiological background of the cardiovascular system according to [156]

2.1 Electric activity in the cell

First, I describe the electrical activity in a single cell, which provides the basis for the subsequent sections.

The predominant solutes in the extracellular fluid are sodium and chloride ions. The intracellular fluid contains high concentrations of potassium ions and ionized non-diffusible molecules, particularly proteins, with negatively charged side chains and phosphate compounds. Electrical phenomena result from the distribution of these charged particles and occur at the cell plasma membrane.

All cells under resting conditions have a potential difference across their plasma membranes. The inside is negatively charged with respect to the outside. This potential is the membrane resting potential.

By convention, the extracellular fluid is assigned a voltage zero and the polarity of the membrane potential is stated in terms of the sign of the excess charge inside the cell. The magnitude of the resting potential is from -5 to -100 mV depending on the type of the cell. The resting potential is steady unless a movement of charged particles occurs between the inside and the outside. The distribution of charged particles inside and outside the cell is shown schematically in Fig. 2.1.

Transient changes in the membrane potential from the resting level produce electrical signals. These signals occur in two forms, graded potential and action potential. Graded potentials are important in producing signals over short distances whereas action potentials produce signals over long distances. Graded potentials arise in all the cells but action potentials do not. The latter needs some specific function in the membrane. Here I refer only to the action potential since it bears on the following sections.

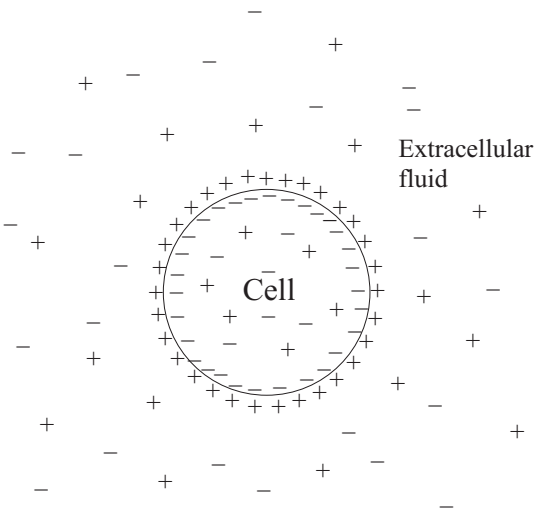

Fig. 2.1: The distribution of charged particles inside and outside a cell.

The term 'depolarize', 'repolarize', 'hyperpolarize' are used to describe the direction of changes in the membrane potential relative to the resting potential (Fig. 2.2). The membrane is said to be depolarized when its potential is less negative than its resting state. Overshoot is a reversal of the membrane potential polarity. When a membrane potential that has been depolarized returns toward the resting value, it is said to be repolarizing. The membrane is hyperpolarizing when the potential is more negative than the resting level.

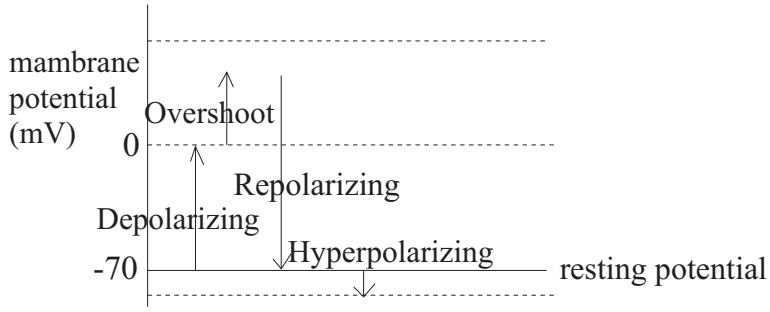

Fig. 2.2: The change of membrane potential.

Action potentials are rapid and large alterations in the membrane potential (Fig. 2.3). They may occur at a rate of 1000 per second. Membranes which are able to produce an action potential are called excitable membranes and the ability to generate action potentials is called excitability. If a stimulus is not strong

enough, an action potential does not occur. Only when the stimulus is strong enough to make membrane the potential reach the threshold potential, it triggers an action potential.

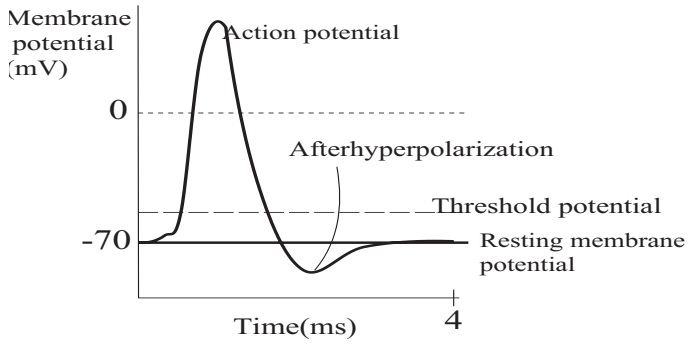

Fig. 2.3: Action potential.

2.2 The circulatory system

The heart, the vascular system (blood vessels) and the blood are the three principle components that make up the circulatory system. As reported by the British physiologist William Harvey in 1628, the cardiovascular system forms a closed loop, so that blood pumped out of the heart through one set of vessels returns to the heart via a different set. The whole system can be divided into two circuits, the pulmonary circulation and the systemic circulation (Fig. 2.4b). Both start and end in the heart. Both the right and left sides of the heart have two chambers: the upper chamber is the atrium and a lower chamber is the ventricle. There is flow from the atrium to the ventricle on each side of the heart but there is no direct flow between the two atria or two ventricles.

The pulmonary circulation includes blood pumped from the right ventricle through the lungs and then to the left atrium. It is then pumped through the systemic circulation from the left ventricle through all the organs and tissues of the body except the lungs, and to the right atrium. In both circuits, the vessels which carry blood away from the heart are called the arteries and those which carry blood towards the heart are called veins.

In the systemic circuits, blood leaves the left ventricle via a single large artery, the aorta (Fig. 2.4a). The arteries of the systemic circulation branch off the aorta,

dividing into smaller vessels. The smallest arteries branch into arterioles, which branch into a huge number of very small vessels, the capillaries. The capillaries unite to form vessels with larger diameter, the venules and then veins. The flow in arterioles, capillaries and venules is termed microcirculation.

In the pulmonary system, blood leaves the right ventricle via a single large artery, the pulmonary trunk, which divides into two pulmonary arteries, one supplying the right lung and the other the left. In the lungs, the arteries continue to branch and form the capillaries that unite into venules and then veins. The blood leaves the lungs via four pulmonary veins, which empty into the left atrium.

As blood flows through the lung capillaries, it picks up oxygen supplied to the lungs by breathing. So the blood in the pulmonary veins, the left side of the heart, and the systemic arteries has a higher oxygen content. And the blood of the other side of the circulatory system has a lower oxygen content.

2.3 The heart

2.3.1 Anatomy

The heart is a muscular organ enclosed in a fibrous sac, the pericardium, and located in the chest. The walls of the heart are composed primarily of cardiac muscle cells and termed the myocardium. The inner surface of the cardiac chambers, as well as the inner wall of the blood vessels, is lined by a thin layer of cells known as endothelium.

The human heart is divided into right and left halves, each consisting of an atrium and ventricle. Located between the atrium and ventricle in each half of the heart are the atrioventricular (AV) valves, which permit blood to flow from atrium to ventricle but not from ventricle to atrium (Fig. 2.4a).

The opening and closing of the AV valves is a passive process resulting from pressure difference across the valves. When the blood pressure in an atrium is greater than in the ventricle, the valve is pushed open and flow proceeds from atrium to ventricle. In contrast, when a contracting ventricle achieves an internal pressure greater than that in its connected atrium, the AV valve between them is forced to close.

The openings of the right ventricle into the pulmonary trunk, and of the left ventricle into the aorta, also contain valves, the pulmonary and aortic valves,

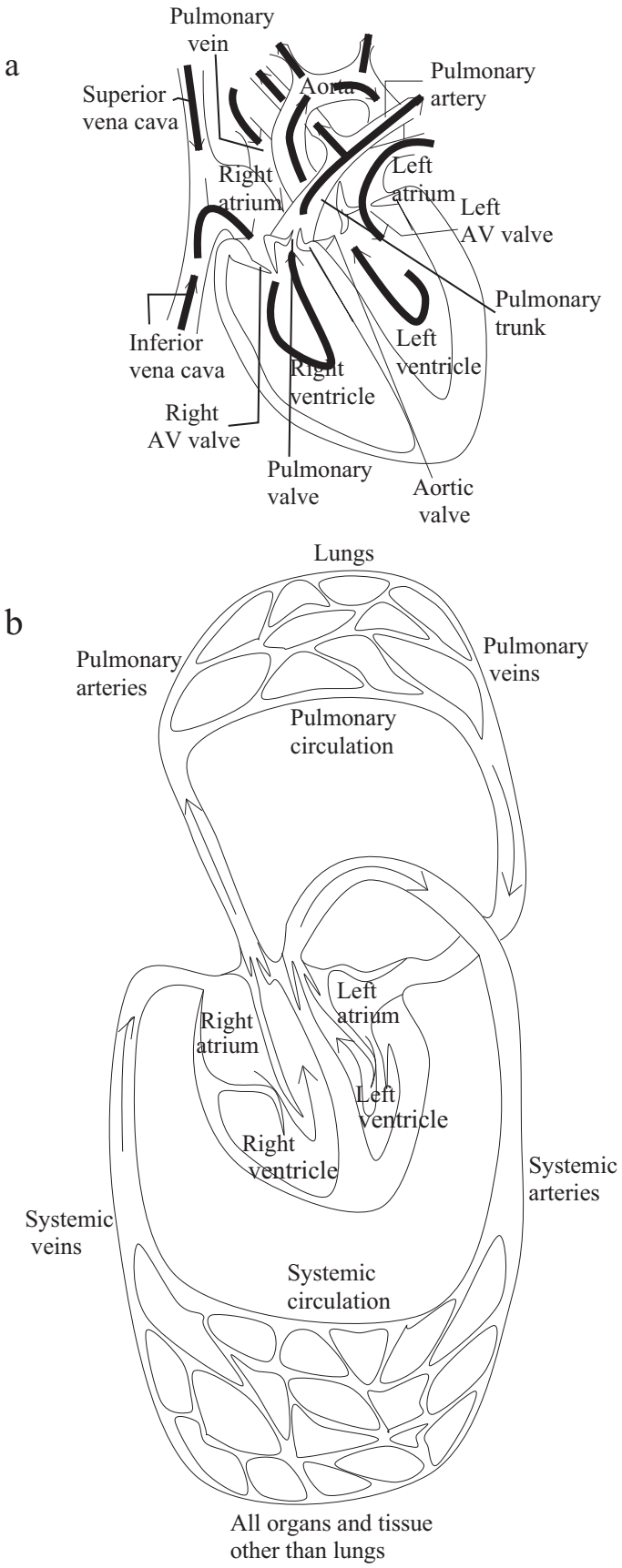

Fig. 2.4: The systemic and pulmonary circulation.

respectively (Fig. 2.4a). These valves permit blood to flow into the arteries during ventricular contraction but prevent blood from moving in the opposite direction during ventricular relaxation. They also act in a passive way like the AV valves and they are either open or closed depending on the pressure differences across them.

2.3.2 Heartbeat coordination

The heart is a dual pump in that the left and right sides of the heart pump blood separately but simultaneously. The atria contracts first, followed almost immediately by the ventricles. Contraction of cardiac muscle is triggered by depolarization of the plasma membrane. The gap junctions that connect myocardial cells allow the action potential to spread from one cell to another. Thus, the excitation of one cardiac cell results in the excitation of all the cardiac cells. This initial depolarization normally arises in a small group of cells, the sinoatrial (SA) node, located in the right atrium near the entrance of the superior vena cava (Fig. 2.5). The action potential spreads from the SA node throughout the atria and then throughout the ventricles. So the SA node works as the pacemaker for the entire heart and its discharge rate determines the heart rate, the number of times the heart contracts per minute.

The action potential initiated in the SA node spreads throughout the right atrium, and from the right atrium to the left atrium, so rapidly that the two atria contract at the same time.

The spread of the action potential to the ventricles involves the rest of the conducting system, a portion of which is called the atrioventricular (AV) node. The AV node is located at the base of the right atrium (Fig. 2.5). The action potential spreading through the right atrium causes depolarization of the AV node. Because the propagation of the action potential through the AV node is relatively slow, atrial contraction is completed before ventricular excitation occurs.

After leaving the AV node, the impulse enters the interventricular septum between ventricles. This pathway has conducting-system fibers termed the bundle of His (Fig. 2.5). The AV node and the bundle of His constitute the only electrical link between the atria and ventricles.

Within the interventricular septum the bundle of His divides into right and

left bundle branches, which leave the septum to enter the walls of both ventricles (Fig. 2.5). These fibers contact with Purkinje fibers, large conducting cells that rapidly distribute the impulse thorough much of the ventricles. Finally the Purkinje fibers make contact with ventricular myocardial cells, by which the impulse spreads through the rest of the ventricles.

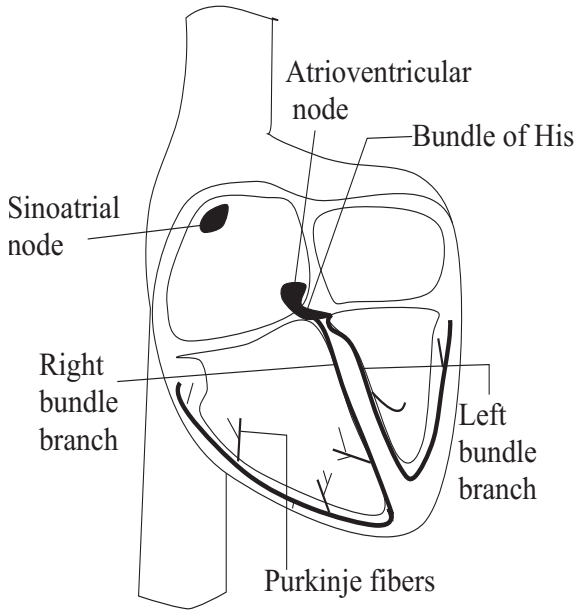

Fig. 2.5: Conducting system of the heart.

2.3.3 Mechanical event of the cardiac cycle

The cardiac cycle is divided into two major phases, both named for events in the ventricles. The period of ventricular contraction and blood ejection is called systole, and its alternates with a period of ventricular relaxation and blood filling, diastole. At an average, one cardiac cycle lasts approximately 1.0 second, with 0.4 seconds in ventricular systole and 0.6 seconds in ventricular diastole.

Both systole and diastole can be subdivided into two periods. During the first part of the systole, the ventricles are contracting but all the valves in the heart closed and no blood can be ejected. This period is termed isovolumetric ventricular contraction because the ventricular volume is constant. The ventricular walls are developing tension and squeezing the blood they enclose.

Once the rising blood pressure in the ventricles exceeds that in the aorta and

pulmonary trunk, the aortic and pulmonary valves open, and the ventricular ejection period of the systole occurs.

During the first part of diastole, the ventricles begin to relax and the aortic and pulmonary valves close as well as the AV valves. No blood is entering and leaving the ventricles and its ventricular volume is not changing. Therefore this period is called isovolumetric ventricular relaxation. The AV valves then open and ventricular filling occurs as blood flows in from the atria. Atrial contraction occurs at the end of diastole after most of the ventricular filling has taken place.

2.3.4 Control of the heart rate

The isolated heart, disconnected from the nervous system beats, approximately at a rate of 100 beats/min. The heart rate in the body may be much lower or higher than this; the SA node is usually under the influence of nerves and hormones. A large number of parasympathetic and sympathetic fibers end on the SA node. Activity of the parasympathetic nerves causes the heart rate to decrease whereas that of sympathetic nerves causes the heart rate to increase. In the resting state, there is considerably more parasympathetic activity to the heart than sympathetic, so the normal resting heart rate of about 61 beats/min is well below the inherent rate of 100 beats/min.

2.4 The vascular system

The functional and structural characteristics of the blood vessels change with successive branching. But there is one structural component in common in the entire cardiovascular system. It is a smooth single-celled layer of endothelial cells or endothelium, which lines the inner surface of the vessels. Capillaries consist only of endothelium, whereas all other vessels have additional layers of connective tissue and smooth muscle.

2.4.1 Endothelium

The endothelium is located at the interface between the blood and the vessel wall. The cells are in close contact and form a layer that prevents blood cell interaction with the vessel wall as blood moves through the vessel lumen. The endothelium is a layer of cells that lines the lumen of all blood vessels. It plays a critical role in

the mechanics of blood flow, the regulation of coagulation, leukocyte adhesion, and vascular smooth muscle cell growth, and also serves as a barrier to the transvascular diffusion of liquids and solutes.

It was first reported by Furchgott and Zawadzki in 1980 that the intact endothelium produces a factor which causes relaxation of vascular smooth muscle. This was originally named endothelium-derived relaxing factor (EDRF) and now it has been found out to be nitric oxide (NO). Nitric oxide is released continuously by endothelium in the arterioles and contributes to arteriolar vasodilation in the basal state. The production of NO can be stimulated by a variety of endothelial antagonists, including acetycholine, as well as by shear stress resulting from an increase of blood flow or pressure. In addition to NO, endothelium releases other vasodilators such as prostacyclin (PGI_2) and vasoconstrictors such as endothelin-1 (ET-1) [101].

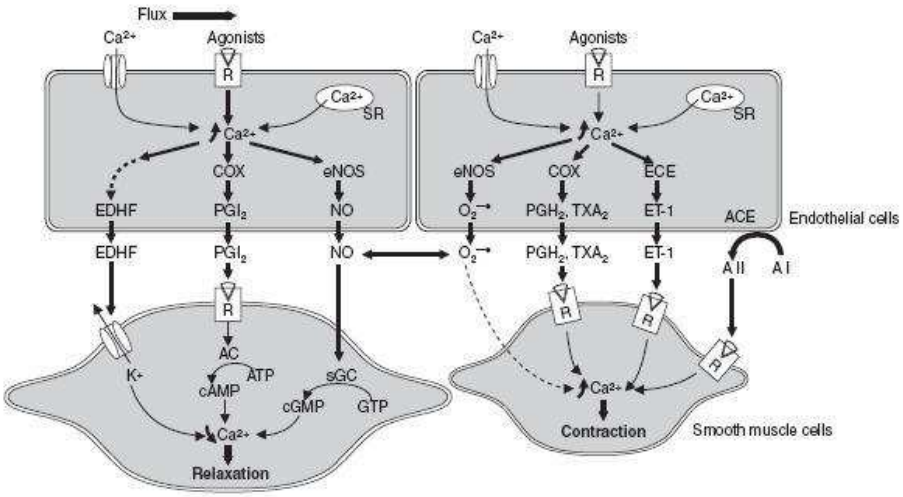

Fig. 2.6: Release of relaxing and contracting factors from endothelial cells and their effects on vascular smooth muscles. **AC** = adenylyl cyclase; **ACE** = angiotensin converting enzyme; **ATP** = adenosine triphosphate; **A I** = angiotensin I; **A II** = angiotensin II; **cAMP** = cyclic adenosine monophosphate; **cGMP** = cyclic guanosine monophosphate; **COX** = cyclo-oxygenase; **ECE** = endothelin converting enzyme; **EDHE** = endothelium-derived hyperpolarising factor; **eNOS** = endothelial nitric oxide synthase; **ET-1** = endothelin-1; **GTP** = guanosine triphosphate; **NO** = nitric oxide; $\mathbf{O_2^{-\bullet}}$ = superoxide anions; $\mathbf{PGH_2}$ = prostaglandin H_2; $\mathbf{PGI_2}$ = prostacyclin; **R** = recepter; **sGC** = soluble guanylyl cyclase; **SR** = sarcoplasmic reticulum; $\mathbf{TAX_2}$ = thromboxane A_2.
The picture is taken from [101].

2.4.2 Vascular smooth muscle

The vascular smooth muscle cells are arranged in helical or circular layers around larger blood vessels and in a single layer around arterioles. Vascular muscle cells provide active tension in the vessel wall and regulate the diameter of the vessels.

In many vessels there are smooth muscles that undergo spontaneous depolarization. Their cells act as pacemakers and excite neighboring cells, thus providing background tension, the myogenic basal tone. Their activities are independent of innervation. The property is similar to that of the heart, but the contractile characteristics and the mechanisms that cause contraction of vascular smooth muscle are very different from those for cardiac muscle. Vascular smooth muscle undergoes slow, sustained, tonic contractions, whereas cardiac muscle contractions are rapid and of relatively short duration (a few hundred milliseconds).

Contraction in vascular smooth muscle can be initiated by mechanical, electrical, or chemical stimuli. Passive stretching of vascular smooth muscle can cause contraction that originates from the smooth muscle itself and is therefore termed a myogenic response. Electrical depolarization of the vascular muscle cell membrane also elicits contraction, most likely by opening voltage dependent calcium channels and causing an increase in the intracellular concentration of calcium. Finally, a number of chemical stimuli such as norepinephrine, angiotensin II, vasopressin and endothelin-1 can cause contraction. Each of these substances bind to specific receptors on the vascular smooth muscle cell (or to receptors on the endothelium), which then leads to vascular smooth muscle contraction.

The arterioles consist of both smooth muscle and endothelium, whose structure is shown in Fig. 2.7.

2.5 The nervous system

2.5.1 Innervation of the heart

There are two divisions of the autonomic nervous system which affect the heart's activities, the parasympathetic nervous system and the sympathetic nervous system.

Parasympathetic innervation is achieved by two vagus systems. The right vagus affects the SA node predominantly. This nerve has an ability to slow SA nodal

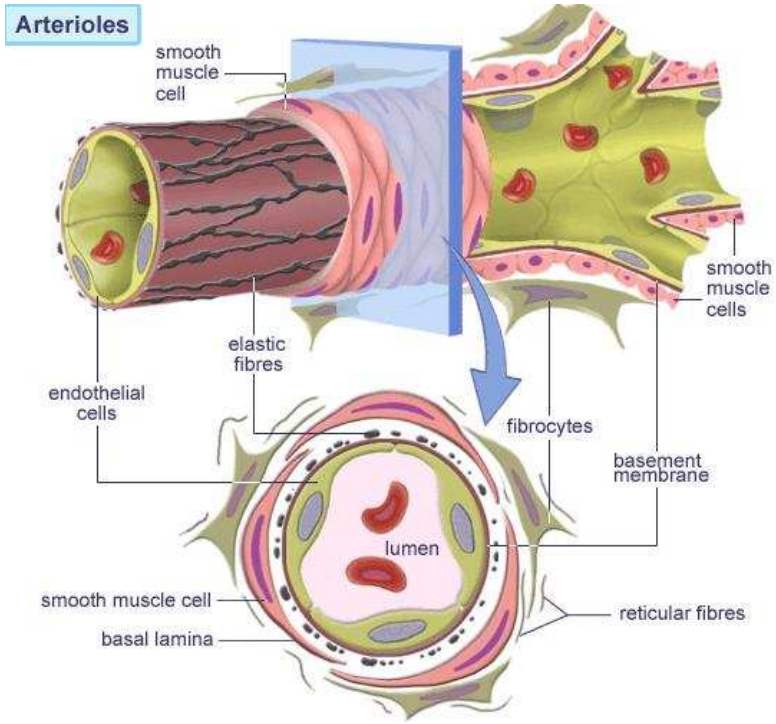

Fig. 2.7: The structure of arterioles.

firing and even stop it for several seconds. The left vagus nerve mainly inhibits AV conducting tissues. The sympathetic nerve supply is nearly uniformly distributed in the heart. Increased sympathetic activity produces an increase in the heart rate and velocity and force of contraction.

Both divisions of the autonomic nervous system have a tonic influence on the cardiac pacemaker, the SA node. The sympathetic nerve system enhances the autorhythmicity, whereas the parasympathetic nervous system inhibits it. Parasympathetic nerves predominate in healthy, resting individuals. After a parasympathetic blockage, the heart rate increases substantially and after sympathetic blockade, it decreases slightly. After a blockade of both divisions, the heart rate is about 100 beats per minute for young adults.

2.5.2 Innervation of the vessels

Most of the arteries and veins are innervated by the sympathetic nervous system. The fibers have a tonic contractile effect on the blood vessels.

2.6 Substances

In this section, details of the substances, ACh and SNP, are described.

2.6.1 Acetylcholine

Acetylcholine (ACh) is a neurotransmitter that is released from the terminal of parasympathetic nerve or motor nerve. It serves as a transmitter of nervous stimulation through synapses. Its chemical formula is $CH_3COOCH_2CH_2N^+(CH_3)_3$. Its structure is presented in Fig. 2.8a.

When it binds to the acetylcholine receptors of striated muscle fibers, it stimulates those fibers to contract. ACh is also used in the brain, where it tends to cause excitatory actions. The glands that receive impulses from the parasympathetic part of the autonomic nervous system are also stimulated in the same way. This is why an increase in ACh causes a decreased heart rate and increased production of saliva.

Acetylcholine was first identified in 1914 by Henry Hallett Dale, then confirmed as a neurotransmitter by Otto Loewi in 1921. For their work, they received the 1936 Nobel Prize in Physiology or Medicine.

Later it was found out in rabbits experiments that the removal of endothelium prevented the ACh-induced vasodilation [40].

2.6.2 Sodium Nitroprusside

Sodium nitroprusside (SNP) breaks down in the blood and releases a chemical called nitric oxide (NO). Nitric oxide enters the muscle cells in the walls of the blood vessels and causes them to relax. When the muscles relax, the blood vessels become wider and the blood pressure decreases.

Its chemical formula is $Na_2[Fe(CN)_5NO]$ and its structure is presented in Fig. 2.8b.

Sodium nitroprusside is used for the emergency treatment of high blood pressure (hypertensive crisis). It is also used to produce controlled hypotension (low blood pressure) in anesthetized patients during surgery. It had been used in the emergency treatment of severe heart failure to reduce heart workload. However, it has side effects and is no longer used for clinical treatment of hypertension.

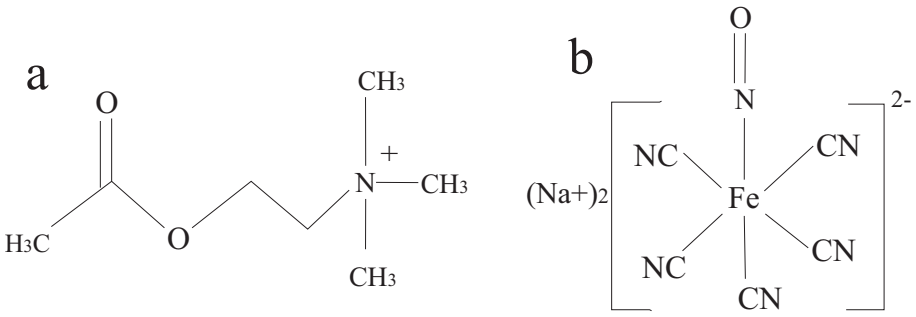

Fig. 2.8: The structure of ACh (a) and SNP (b).

3. MEASUREMENT

3.1 Measurement time

In living systems, there are several rhythmic processes with different time scales. For example, seasonal growth and involution has the time scale around years, reproduction around months, sleep-wakefulness cycle around days, sleep cycle and smooth muscle tone around hours, blood distribution around minutes, respiration and heart beat around seconds and nervous action around tenths of seconds [57]. The measurement time should be longer than the time scale of the phenomena in which we are interested. In our study, we are interested in phenomena whose scale is of the order of the blood distribution time. Under steady conditions in resting subjects, the volume of blood pumped by the heart in one minute is on average equivalent to the whole amount of blood in the humans [156]. Thus, the dynamics of the blood distribution can be analyzed on the time scale of minutes. We are especially interested in oscillations from 0.005 to 2.0 Hz whose period is from 0.5 to 200 seconds. Their physiological origins will be described below in section 7.2.1.

If a signal is periodic, two periods are enough to specify them. However, signals from the human cardiovascular system are not periodic, but quasiperiodic and their period fluctuate constantly. In that case, the measurement should be long enough to contain at least several periods. On the other hand, the longer a signal, the more pronounced the effects of non-stationarity becomes. For example, changes of physiological conditions or physical movement can occur during measurements. Therefore we chose 30 minutes as a compromise.

3.2 Measurement techniques

3.2.1 ECG

The electrocardiogram (ECG) is a tool for evaluating the electrical events in the heart. ECG measurements have been used for diagnostic purposes for more than

a century. The action potential of cardiac muscle cells can be viewed as batteries that cause charge to move throughout the body fluids. These moving charges are caused by all the action potentials occurring simultaneously in many individual myocardial cells and can be detected by recording electrodes at the surface of the skin. ECG is not a direct record of the changes in membrane potential across individual muscle cells. Instead, it is a measure of the currents generated in the extracellular fluid by the changes occurring simultaneously in many cardiac cells on the surface of the body.

A conventional 3-lead measurement of the ECG is done by using three leads which are put on the right and left shoulder bones for the first and second leads and on the left leg or limb bone for the third lead.

The P wave is the first deflection and represents the electrical impulse through the atrial musculature (depolarization). The second deflection is the QRS complex and represents the spread of the electrical impulse through the ventricular musculature, which triggers the ventricular contraction. The P-R interval is measured from the beginning of the P wave to the beginning of the QRS complex. It reflects the time taken by impulse to travel the entire distance from the SA node to the ventricular muscle. The final deflection is the T wave and represents the period of recovery for the ventricles (repolarization).

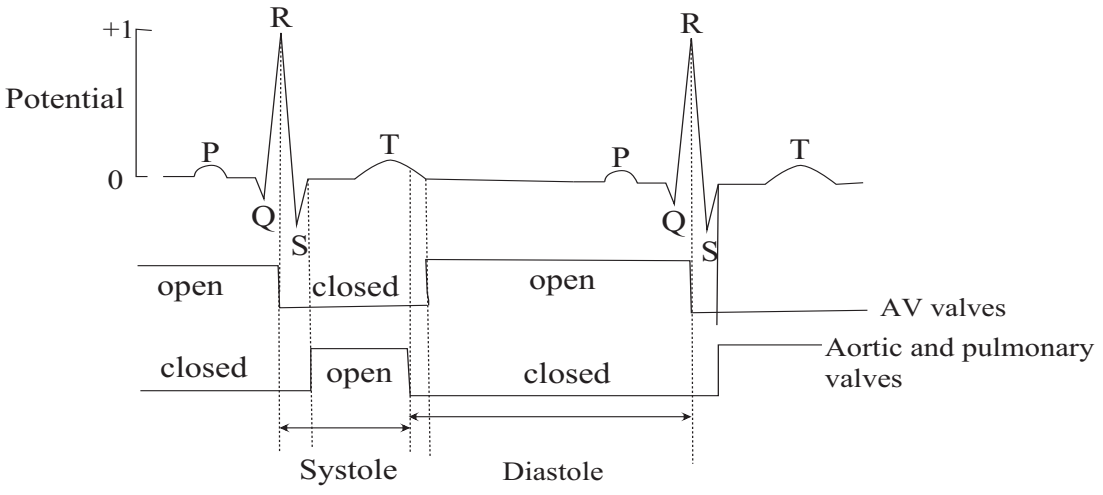

Fig. 3.1: Cycles of ECG signal.

3.2.2 Respiration

Respiration is what we do constantly to exchange oxygen and carbon dioxide between our organism and the external environment. In humans, the respiratory system includes the oral and nasal cavities, the lungs, the series of tubes leading to the lungs and the chest structures which move the air into and out of the lungs. In respiration, there are two movements: inspiration and expiration. Inspiration is the movement of air from the external environment into lungs which increases the volume of the lungs. Expiration is the movement in the opposite direction. One cycle of respiration consists of an inspiration and expiration. In our study, respiration was measured by a belt around the thorax which can detect the change of the volume of the lungs by inspiration and expiration during breathing (Respiratory effort trans, TP-TSD201, BIOPAC Systems, Inc. Goleta, CA, USA).

3.2.3 Blood flow

3.2.3.1 Laser Doppler flowmetery

After the first laser was demonstrated by Maiman [91], Cummins *et al.* proposed a way to measure the velocity of particles in solution by using the Doppler frequency-shifted light [30]. After some years, Riva *et al.* applied this technique to the measurement of the velocity of red blood cells in the glass tube flow model [119] and Stern used the laser Doppler technique for blood perfusion measurement in the undisturbed microcirculation [140].

The laser Doppler technique measures blood flow in the very small blood vessels of the microvasculature, such as the low-speed flows associated with nutritional blood flow in capillaries close to the skin surface and flow in the underlying arterioles and venules involved in regulation of skin temperature. The tissue thickness sampled is typically 1 mm, the capillary diameters 10 microns and the velocity spectrum measurement typically 0.01 to 10 mm/s. The technique depends on the Doppler principle by which low power light from a monochromatic (single wavelength) stable laser is scattered by moving red blood cells and as a consequence frequency is broadened. The frequency broadened light, together with laser light scattered from static tissue, is photodetected and the resulting photocurrent processed to provide a blood flow measurement. Because of this mechanism, there are two optic fibers in laser Doppler probes. One is to deliver light to the tissues

and the other is to collect the scattered light. Bonner and Nossal showed that after filtering the scattered light, they could get an output which is proportional to the velocity and the number of red blood cells in the measured volume but is not related to the direction of the blood flow [20].

The corresponding instruments for blood flow measurement were developed by Watkins and Holloway [154], Nilsson *et al.* [104] and Fischer *et al.* [39]. They demonstrated a good correlation between the output of the devices and the blood flow.

In our study, a near-infra-red laser of wavelength 785 nm is used to measure the velocity and concentration of red blood cells within the volume covered by the laser light. The covered volume depends on several factors: optical density of the tissue, separation of the probe fibres and the power and wavelength of the laser. From imaging at this wavelength by a commercially available instrument (DRT4, Moor Instruments, Axminster, Devon, UK), it is known that the full dermal thickness (about 1 mm) is probed, so from simple geometry a hemisphere of radius 1mm gives a volume of order 2 mm^3, in which 'of order' has to be emphasized.

Because of the fact that there is a residual value called the *biological zero* in the case of occlusion [138], we can not use an absolute unite (e.g $ml/s/mm^3$) but arbitrary unit (AU) for the flow. The residual value comes from the Brownian motion of remaining red blood cells. To obtain an absolute measure, the biologocal zero has to be determined for every measurement by doing probe calibration in the water with polystyrene microspheres.

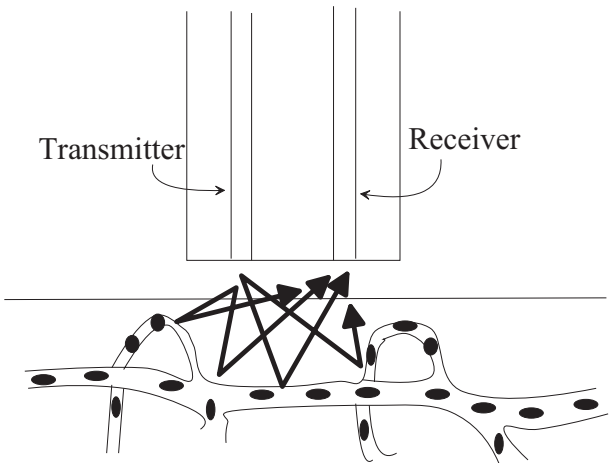

Fig. 3.2: Sketch showing how a probe detects flow.

3.2.3.2 Iontophoresis

Iontophoresis is widely used for transcutaneous delivery of ionized drugs for the assessment of skin microvascular function. A small electrical current is used to transfer locally vasoactive substances such as endothelial-dependent ACh and endothelial-independent SNP across the dermal barrier as unipolar currents of relatively large molecules. As discussed in subsection 2.6.2, SNP breaks down to yield nitric oxide (NO) directly, which acts on vascular smooth muscle cells, while ACh acts on the intact vascular endothelium and makes the endothelium release NO. SNP acts directly on smooth muscles but ACh acts through the endothelium. Therefore the oscillations related to endothelial activity can be extracted by seeing the difference between them, in this way oscillation around 0.01 Hz and 0.07 Hz were identified in previous studies to be endothelial-dependent [80, 83, 139]. ACh and SNP are relatively high conductivity solutions and have different polarity. Therefore we need to apply anodal iontophoresis to ACh and cathodal iontophoresis to SNP.

However there are some methodological problems related to iontophoresis. It is known that blood flow is increased in response to the current without vasoactive drugs but with pharmacologically neutral electrolytes such as H_2O [17, 35] or NaCl solution [7]. This phenomenon is known as the *galvanic effect*, or *current-induced vasodilation*. The mechanism is unclear but could involve, for example, local heating due to the voltage required to convey the ions through the dermal barrier. It was shown in [13] that the magnitude of the voltage between an chamber and the adjacent cells needed to sustain the chosen iontophoresis current is not an important factor in causing changes in blood flow using H_2O and NaCl with anodal and cathodal iontophoresis, ACh with anodal iontophoresis and SNP with cathodal iontophoresis. There is another study [153] in which H_2O and NaCl were used with the same protocol as used in this thesis and with anodal and cathodal iontophoresis. They concluded that the differing responses of the 0.01 Hz spectral component to ACh and SNP may be interpreted with confidence as a specific effect of substances, and not of the iontophoresis current itself.

Currents were delivered from a battery-powered constant-current iontophoresis controller (Moor Instruments MIC1-e). The iontophoresis probehholders were of perspex with internal platinum wire electrodes. Their internal diameter was 8 mm,

giving an area of 1 cm^2 in contact with the skin. The dosages of the drugs delivered are proportional to the total charge (Q) in millicoulombs (mC) which migrates through skin surface, determined by the product of constant current measured in milliamperes (mA) and the duration (t) of current flow in seconds. We used a protocol that passes a charge of 2 mC (100 μA for 20 seconds) followed by a 240 seconds interval seven times in one measurement, thus filling the 30 minutes of recording.

3.2.4 Measurement set up

The measurement of two blood flow channels with ACh and SNP was obtained by laser Doppler flowmetry (LDF) with DRT4. A battery powered constant current stimulator for iontophoresis was connected to DRT4 and the probeholders for ACh and SNP. The chambers combined with laser Doppler MP1 probes were placed on the anterior side of the left forearm on the different sites under which the vessel densities were similar. 1 % w/v ACh and 1 % w/v SNP were put into the holes of the iontophoretic chambers. The cahmbers also served as the support for the probes of the LDF measurements.

The measurement of basal blood flow was obtained with other instruments (moorLAB server and moorLAB satellite, Moor Instruments, Axminster, Devon, UK). Two Laser Doppler probes were fixed on the right wrist and on the inner right ankle respectively.

The cut-off frequency of the low-pass filter of 22.5 kHz and a time constant of 0.1 second were selected thus allowing the dynamics of the slow oscillatory processes to be optimally captured.

The flow measured by the LDF instrument depends largely on the site of the probe because some areas contain a high density of arteriovenous anastomoses [19] which can cause high shunt flow, whereas most of the skin is perfused by capillaries with low flow. So we chose measurement sites on bony prominence so as to avoid high density of arteriovenous anastomoses and large arteries.

The ECG was set up as described in subsection 3.2.1. Respiration was measured with Biopac respiratory effort transducer placed around the thorax which can convert the stretch of the belt to an electric signal. The ECG and respiration signals were amplified by a signal conditioning unit (Cardiosignals, Jozef Stefan

Institute, Ljubljana, Slovenia). All signals were sampled at 400 Hz by a 16-bit A/D converter (National Instruments) and stored in a personal computer.

3.3 Subjects

118 healthy individuals were measured including 71 males (42.6 ± 15.1 years, range 16-74 years) and 47 females (45.8 ± 16.6 years, range 18-82 years). They had not had any medication nor any history of cardiovascular disease prior to recordings. They were asked not to eat or drink coffee for one hour before the measurement.

Subject lay on a bed in a supine position and were asked to relax while peripheral blood flow, ECG and respiration were recorded throughout 30 minutes. The measurements were done at room temperature 22 ± 1 °C.

3.4 Results: obtained signals

3.4.1 ECG and respiration

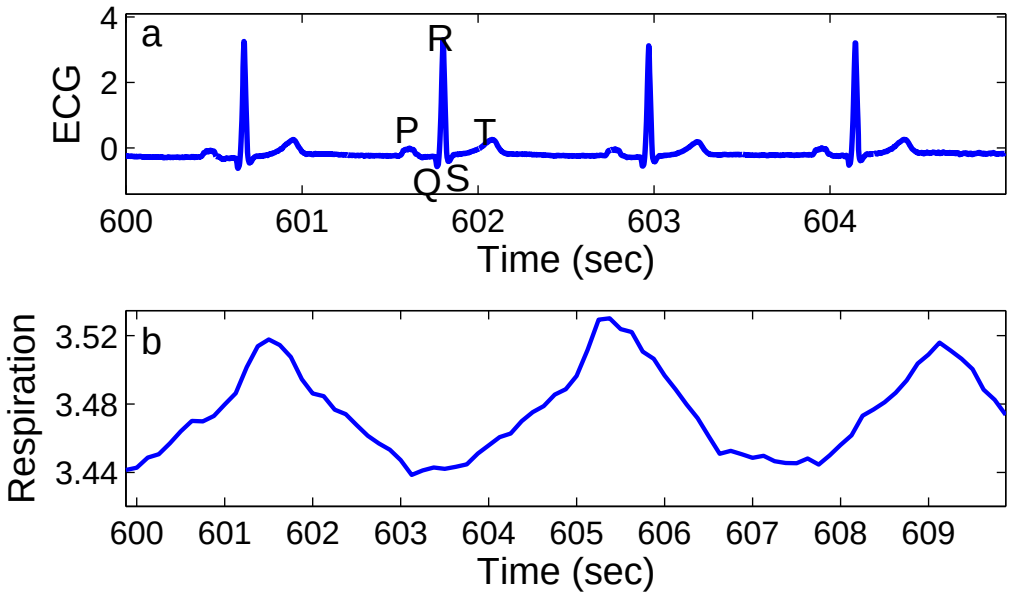

Fig. 3.3: An ECG typical signal (a) and a respiratory signal (b) obtained from measurement. The PQRST events are shown in (a).

For the first several decades of ECG measurements, attention was focussed mainly on the detailed *shape* of the approximately periodic pulses seen in the

signal. As discussed in subsection 3.2.1, a typical ECG signal consists of the P wave, the QRS complex, and the T wave as shown with the marks of PQRST events in Fig. 3.3a. A respiratory signal is shown in Fig. 3.3b. The maximum in each period represents inspiration and the minimum expiration.

3.4.2 Blood flow with iontophoresis

Blood flow signals with iontophoresis are shown in Fig. 3.4. In (a) and (b), slow oscillation is shown from the record of 30 minutes of the whole measurement. In (d) and (e), 10 seconds of record is shown to see faster oscillation. It has to be noted that the flow and its oscillations increase more than 10 times after applying the substances.

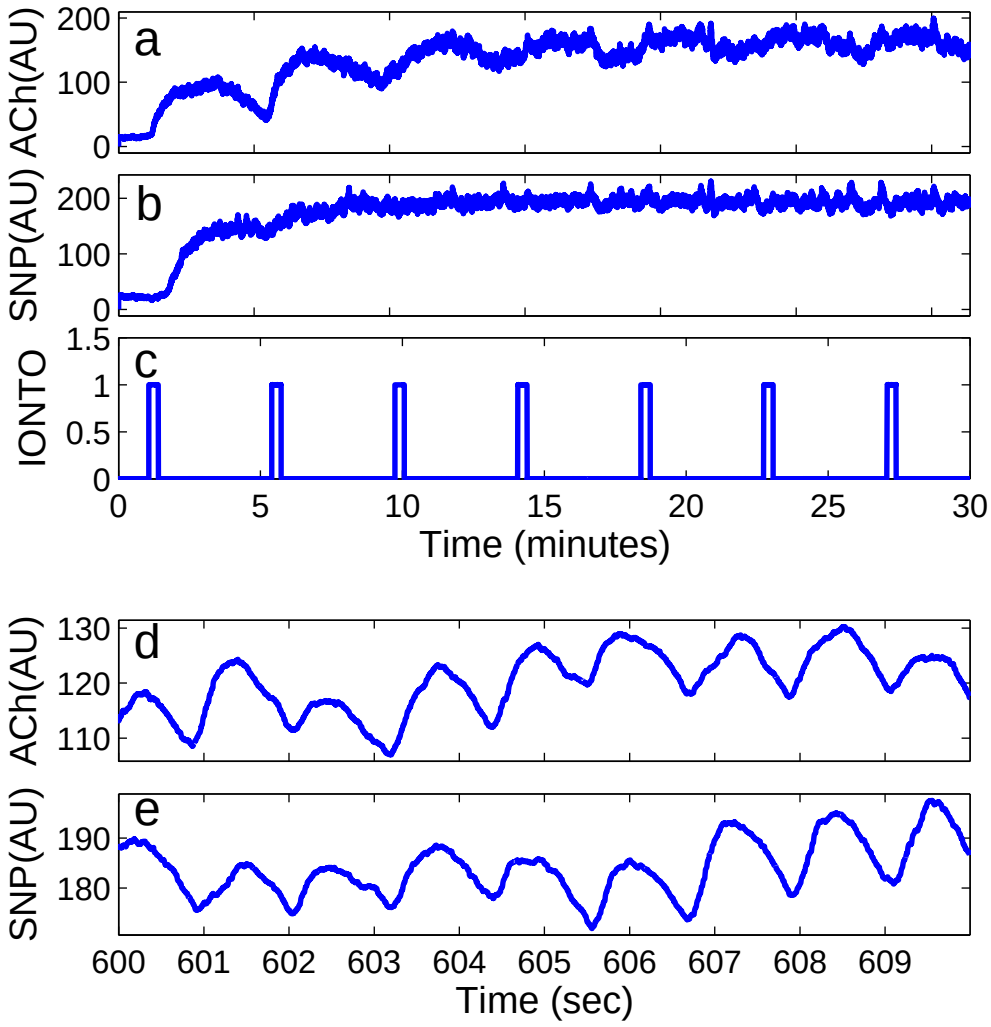

Fig. 3.4: The blood flow measured with ACh (a) and SNP (b), and the iontophoretic current pulses (c) shown for q whole measurement of for 30 minutes. To see faster variations, 10 seconds of the record are shown for ACh (d) and SNP (e).

4. METHODS OF STATISTICAL TESTS

A statistical significance test is used to determine the statistical significance of an observation. In this chapter, the statistical tests used in this thesis are explained.

With an assumption of the underlying distribution of the data, a parametric test are conducted. For example, the t-test is a typical parametric test [44]. It is used to test whether two Gaussian populations have different statistical distributions. On the other hand, when the underlying distribution of data is unknown, a non-parametric test should be conducted. In our studies, we use the Wilcoxon rank sum test, a non-parametric test, to test the difference of the distributions of two groups because we have no prior knowledge of the distribution of samples. In section 4.1, the details of the significance tests are explained. Correlation analysis is used to draw inferences about the strength of the relationship between two or more variables. In section 4.2, the details of correlation analysis will be explained.

4.1 Significance tests

A conjecture concerning the unknown distribution of a random variable is called a statistical hypothesis. The aim of a significant test is to test whether the hypothesis is true or not. If the probability that the hypothesis holds is below the threshold chosen for statistical significance, the hypothesis is rejected. The statistical significance is usually set to 0.05 and the same value was used in this thesis. These statistical significance tests were conducted using MatLab (MatWorks).

4.1.1 The T-test

In this subsection, a typical parametric test, the t-test, is explained briefly. The t-statistic was introduced by William Sealy Gosset for cheaply monitoring the quality of beer brews. Gosset published the t-test in Biometrika in 1908, but was forced to use a pen name, Student, by his employer who regarded the fact that they were using statistics as a trade secret.

Given two data sets X_1 and X_2, each characterized by its mean $\bar{X}_1$ and $\bar{X}_2$, standard deviation s_1 and s_2 and number of data points n_1 and n_2, we can use a t-test to determine whether the means are distinct under the assumption that the underlying distributions can be assumed to be normal. All such tests are usually called Student's t-tests. Strictly speaking that name should only be used if the variances of the two populations are also assumed to be equal. The test used when this assumption is dropped is sometimes called Welch's t-test. There are different versions of the t-test depending on whether the two samples are independent of each other (e.g., individuals randomly assigned into two groups), or paired so that each member of one sample has a unique relationship with a particular member of the other sample (e.g., the same people measured before and after an intervention, or IQ test scores of a husband and wife).

In the case that two samples are independent, the t-value is calculated as

$$t = \frac{\bar{X}_1 - \bar{X}_2}{s_{X_1 - X_2}}, \text{ where } s_{X_1-X_2} = \sqrt{\frac{(n_1-1){s_1}^2 + (n_2-1){s_2}^2}{n_1+n_2-2}(\frac{1}{n_1}+\frac{1}{n_2})}. \quad (4.1)$$

Once a t-value is determined, a p-value can be found using a table of values from the t-distribution with (n_1+n_2-2) degrees of freedom. The t-distribution f_T is a symmetric bell-shaped distribution with heavier tails than the normal distribution as shown in Fig. 4.1. The t-distribution is defined as

$$f_T(t) = \frac{\Gamma((k+1)/2)}{\sqrt{k\pi}\Gamma(k/2)}(1+t^2/k)^{-(k+1)/2} \quad (4.2)$$

where k is the degree of freedom. The p-value is calculated as

$$p = 2\int_t^\infty f_T(t)dt, \quad (4.3)$$

If the p-value is below the threshold chosen for statistical significance (usually 0.05), then the null hypothesis H_0 that the distributions of the two groups are identical is rejected in favor of an alternative hypothesis, which typically states that the groups do differ.

The t-test is also used to examine whether the slope of a regression line differs significantly from 0.

4.1.2 Rank sum test

The rank sum test is a big category of non-parametric tests [32]. The general idea is that instead of using an original observed data, we list the data in ascending

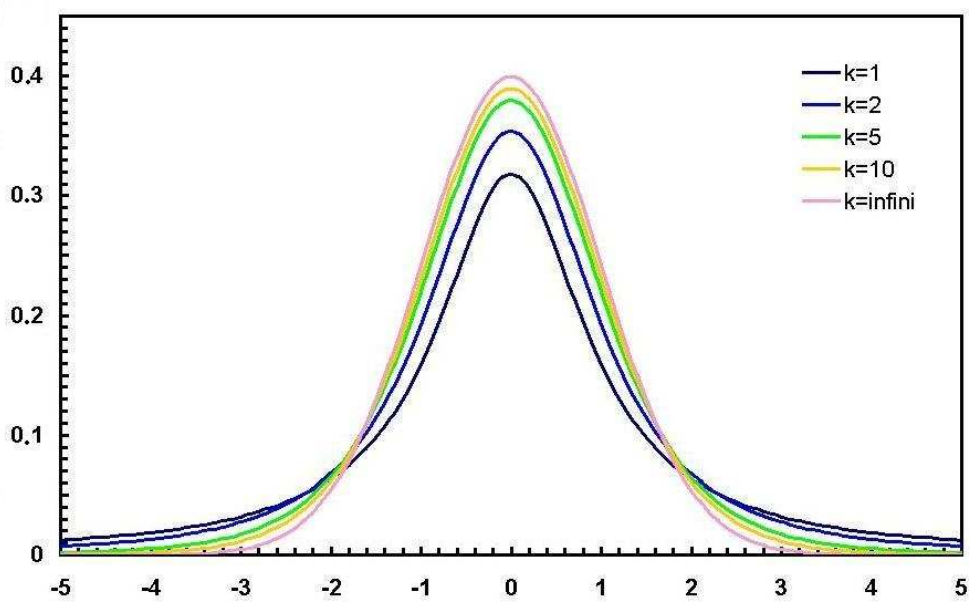

Fig. 4.1: The t-distribution with various degrees of freedom k. The graph is taken from Wikipedia, http://en.wikipedia.org/.

order and assign a rank to each item, the position where the item appears in the sorted list. Using the ranks instead of the original observed data makes the test much less sensitive to outliers and noise than parametric tests.

Depending on the number of classes in the data sets, there are different kinds of rank sum tests. The Wilcoxon rank sum test [155] is a non-parametric alternative to the t-test. Here we focus on the Wilcoxon rank sum test. We demonstrate how to conduct the Wilcoxon rank sum test by taking an example. Let us take two groups X and Y. X contains 11 samples and Y contains 7 samples as shown in Tab. 4.1. We want to test whether the null hypothesis H_0 that the distribution of samples X is identical to that of samples Y is true or false.

Types	Number	Values										
X	11	33	14	12	11	22	28	10	8	18	19	20
Y	7	17	28	15	35	27	32	29				

Tab. 4.1: Values of two groups.

We combine all the samples of X and Y and sort them in the ascending order. The ranks are assigned to the samples based on the order. If k samples have the same rank of i, than all k samples have an average rank $i + (k-1)/2$. The results

of the example are shown in Tab. 4.2

Values	8	10	11	12	14	15	17	18	19
Types	X	X	X	X	X	Y	Y	X	X
Ranks	1	2	3	4	5	6	7	8	9
Values	20	22	27	28	28	29	32	33	35
Types	X	X	Y	X	Y	Y	Y	X	Y
Ranks	10	11	12	13.5	13.5	15	16	17	18

Tab. 4.2: Assigned ranks to each sample.

Suppose that n_1 and n_2 are the numbers of the smaller sample size and the larger sample size, respectively. In this example, $n_1 = 7$ and n_2=11. Then we calculate the sum of group Y and have the statistic $W = 6 + 7 + 12 + 13.5 + 15 + 16 + 18 = 87.5$. If the null hypothesis H_0 holds, the statistic W should be around the expectation value $(n_1 + n_2 + 1) \cdot n_1/2 = 66.5$. If W is too small or too large, the null hypothesis H_0 is likely to be false. Using MatLab, the p-value is calculated as $p = 0.0589$ for this example. If we set the statistical significance to 0.05, the null hypothesis H_0 can not be rejected since $0.05 < 0.0589$, whereas if we set the statistical significance 0.1, the null hypothesis H_0 is rejected.

4.2 Correlation analysis

Suppose that we have n observations of two variables, $X = x_1, \cdots, x_n$ and $Y = y_1, \cdots, y_n$. The variation of variable Y can be separated into two parts: the variation associated with variable X and the variation not associated with variable X. The fraction that is explained by the linear relationship between X and Y is called the coefficient of determination and its square root is the correlation coefficient. The correlation coefficient r can be expressed [9] as

$$r = \frac{\sum_{i=1}^{n} x_i y_i - \frac{1}{n}(\sum_{i=1}^{n} x_i)(\sum_{i=1}^{n} y_i)}{\sqrt{\sum_{i=1}^{n} x_i^2 - \frac{1}{n}(\sum_{i=1}^{n} x_i)^2}\sqrt{\sum_{i=1}^{n} y_i^2 - \frac{1}{n}(\sum_{i=1}^{n} y_i)^2}}. \tag{4.4}$$

The estimated correlation coefficient r is a random variable and each random variable has a distribution function. The distribution of r is a function of the sample size n and the real correlation coefficient ρ. A correlation coefficient of zero means that there is no linear relationship between the two variables. To test

whether two variables are linearly related, we set the null hypothesis,

$$H_0 : \rho = 0. \tag{4.5}$$

It can be shown that for $n > 2$, this hypothesis can be tested using a t-test that is given by

$$t_r = r\sqrt{\frac{n-2}{1-r^2}}. \tag{4.6}$$

The value t_r is a random value with a t-distribution with $n-2$ degrees of freedom. The p-value is defined as

$$p = 2\int_{t_r}^{\infty} f_T(t)dt. \tag{4.7}$$

If the p-value is lower than statistical significance, then the null hypothesis is rejected and the correlation coefficient is considered statistically significant. In our study, the statistical significance was chosen 0.05.

It is important to check the relationship between variables graphically before performing the correlation analysis in order to to check whether there is no outlier in the data. In the t-test, an outlier can affect the statistics significantly. In some cases, variables have a nonlinear relationship and this can be identified graphically as well. The nonlinearity may result in low correlation and may sometimes be improved by using a log-plot.

In this thesis, we calculated linear regression, correlation coefficients and their significance were determined using MatLab (MatWorks). The values of r_m and p_m represent correlation with age and the probability for males, and the values of r_f and p_f represent those for females. The blue line and dots represent males and the red females in all the graphs throughout the thesis.

5. BACKGROUND OF PHASE DYNAMICS

5.1 Description of phase dynamics

In this section, we review phase dynamics following Kuramoto [74]. Phase dynamics provides a way of describing a system with only one variable, the phase. In this subsection, we explain how the phase is defined and its dynamics is obtained by one of the reduction methods, which will be explained later in more detail.

5.1.1 Small perturbations in general

Suppose that $\mathbf{X}(t)$ develops its dynamics according to $d\mathbf{X}/dt = \mathbf{F}(\mathbf{X})$ and that there is a linearly stable T-periodic solution $\mathbf{X_0}$ which statisfies

$$\frac{d\mathbf{X_0}}{dt} = \mathbf{F}(\mathbf{X_0}), \quad \mathbf{X_0}(t+T) = \mathbf{X_0}(t). \tag{5.1}$$

Let C denote the closed orbit corresponding to $\mathbf{X_0}$. Clearly a phase ϕ can be defined on C as a variable linearly increasing with time, as follows,

$$\frac{d\phi(\mathbf{X})}{dt} = \omega, \quad \omega = \frac{2\pi}{T}, \quad \mathbf{X} \in C. \tag{5.2}$$

Now let us add a small perturbation $\mathbf{p}(t)$ to the dynamics. At this stage, $p(t)$ is restricted to a small perturbation. It may depend on the variable X or on the variables of other oscillators. Then the dynamics of X is expressed by the following equation,

$$\frac{d\mathbf{X}}{dt} = \mathbf{F}(\mathbf{X}) + \mathbf{p}(t). \tag{5.3}$$

Once the perturbation is added, the orbit does not correspond exactly to C but is expected to be away a bit from C. In that case, the phase needs to be defined in the region close to C. The definition can be extended to the region G containing all neighborhood of C by using the dynamical system $d\mathbf{X}/dt = \mathbf{F}(\mathbf{X})$. Here I introduce the so-called ischrone $I(\phi)$. If the points starting from a plane approach the point starting from $X_0(\phi)$ on C, the crossing point of C and $I(\phi)$ (shown in

Fig. 5.1), as $t \to \infty$, we call the plane the isochrone $I(\phi)$. It means that the phase of the same isochrone remains the same. The following equation then leads

$$(\mathrm{grad}_{\mathbf{X}}\phi, \mathbf{F}(\mathbf{X})) = \omega. \tag{5.4}$$

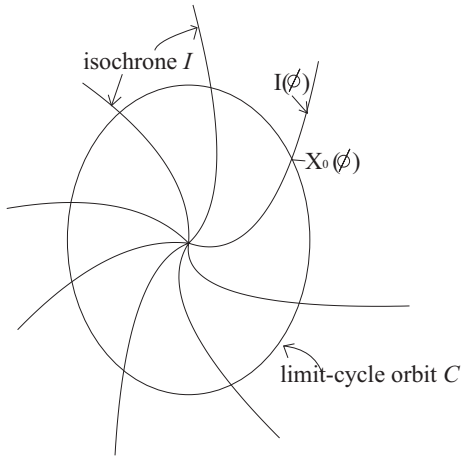

Fig. 5.1: Explanation of the isochrone. The circle is the limit cycle orbit C. A curve on which all the points have the same phase is called an isochrone and is denoted by $I(\phi)$. The crossing point between C and $I(\phi)$ is denoted by $X_0(\phi)$. The center of the limit cycle C, where all the isochrones cross, is the singular point where the phase cannot be defined.

Note that the definition of phase is made for the system without perturbation by the Eq. (5.2), but it can be extended to the system with the perturbation by using the notion of the isochrone. By introducing this phase variable, the dynamics in the region G is finally described as

$$\frac{d\phi(\mathbf{X})}{dt} = (\mathrm{grad}_{\mathbf{X}}\phi, \mathbf{F}(\mathbf{X}) + \mathbf{p}(t)) = \omega + (\mathrm{grad}_{\mathbf{X}}\phi, \mathbf{p}(t)). \tag{5.5}$$

It should be noted that $\mathrm{grad}_{\mathbf{X}}\phi$ on the right hand side is a function of the position X and Eq. (5.5) is not a closed equation of the phase ϕ. However, if the perturbation is small, the value can be approximated by the value on C as

$$\mathbf{U}^*(\phi) \equiv \mathrm{grad}_{\mathbf{X}}\phi|_{\mathbf{X_0}(\phi)}. \tag{5.6}$$

By using $\mathbf{U}^*$, the function of ϕ , the phase equation under perturbation $\mathbf{p}(t)$ can be obtained as

$$\frac{d\phi}{dt} = \omega + (\mathbf{U}^*(\phi), \mathbf{p}(t)). \tag{5.7}$$

If the perturbation is given as a function of ϕ, the Eq.(5.7) can be closed in terms of ϕ. We will look at a few examples in the subsequent subsections.

5.1.2 Small deviation from the original dynamical system

In this subsection, we discuss the case where the dynamical equation is deviated from $\mathbf{F}(\mathbf{X})$ to $\mathbf{F}(\mathbf{X}) + \delta\mathbf{F}(\mathbf{X})$. In this case, $\mathbf{p}(t) = \delta\mathbf{F}(\mathbf{X})$ and Eq. (5.7) becomes

$$\frac{d\phi}{dt} = \omega + (\mathbf{U}^*(\phi), \delta\mathbf{F}(\mathbf{X})). \tag{5.8}$$

In the first approximation, $\delta\mathbf{F}(\mathbf{X})$ can be replaced by $\delta\mathbf{F}(\mathbf{X_0}(\phi))$. Then Eq. (5.8) becomes

$$\frac{d\phi}{dt} = \omega + (\mathbf{U}^*(\phi), \delta\mathbf{F}(\mathbf{X_0}(\phi))). \tag{5.9}$$

This is a closed equation for ϕ. Another important operation called averaging is used in the next step. To do this, we introduce a new variable ψ as

$$\phi = \omega t + \psi. \tag{5.10}$$

Without the perturbation, ψ is a variable which represents the initial phase, but under small perturbation it is a variable which changes slowly with time. The dynamics of ψ becomes

$$\frac{d\psi}{dt} = (\mathbf{U}^*(\omega t + \psi), \delta\mathbf{F}(\mathbf{X_0}(\omega t + \psi))). \tag{5.11}$$

Since the dynamics of ψ is very slow, ψ can be considered as approximately constant during the period $2\pi/T$. In fact, ψ is so slow compared to ωt that it is expected that averaging of the right hand side occurs on the time scale of ψ. Then the dynamics of ψ can be expressed as

$$\frac{d\psi}{dt} = \delta\omega, \tag{5.12}$$

$$\delta\omega \equiv \frac{1}{2\pi}\int_0^{2\pi} d\theta(\mathbf{U}^*(\theta + \psi), \delta\mathbf{F}(\mathbf{X_0}(\theta + \psi))). \tag{5.13}$$

It should be noted that $\delta\omega$ is not dependent on ψ, but constant, since the integrated function on the right hand side is a 2π-periodic function. The equation

$$\frac{d\phi}{dt} = \omega + \delta\omega \tag{5.14}$$

indicates that the deviation of the original dynamical system leads to a deviation of the frequency in the phase dynamics.

5.2 Analytical methods to detect the instantaneous phase

The first thing which we have to do is to define the phase of signals numerically. There are three methods to define the instantaneous phase. They are based on peak-detection, the Hilbert transform and wavelet transform. The method based on peak-detection was used to study entrainment between cardiac and respiratory signals by calculating their frequency ratio[128] or to obtain the instantaneous phase [115]. The method based on Hilbert transform was originally introduced by Gabor [41] and brought into the context of synchronization of chaotic oscillators by Rosenbulm *et al.* [120]. The third method was introduced by Bandrivskyy *et al.* [14]. They makes use of phase of wavelet analysis, which is explained in section 7.1.4, to detect the instantaneous phase of signals of skin temperature and blood flow.

5.2.1 Marked events

If each cycle of a signal contains events which can be marked to characterize the oscillator and is possible to detect them, the phase is defined by using the times of these events,

$$\phi(t) = 2\pi \frac{t - t_k}{t_{k+1} - t_k} + 2\pi k, \quad t_k < t < t_{k+1}, \tag{5.15}$$

where t_k and t_{k+1} are the time of the k-th and $k+1$-th marked events. By this definition, the phase increases linearly with time. It should be noted that this method corresponds to the phase definition by a Poincaré section [115]. In some cases, we can find a projection of an orbit on a plane (x, y) that rotates around a point (x_0, y_0). We can choose a Poincare section and t_k is the time of the k-th crossing of the Poincare surface. In our case, the Poincaré section is defined by the plane of $y =$ maximum.

5.2.2 Hilbert transform

When a signal $g(t)$ is obtained, there is a way to analyze its amplitude and phase by constructing the so-called analytic signal $\zeta(t)$ from the original signal $g(t)$, according to the following equation

$$\zeta(t) = g(t) + \imath g_H(t) = A(t)e^{\imath\phi(t)}, \tag{5.16}$$

where $g_H(t)$ is the Hilbert transform of $g(t)$ written as

$$g_H(t) = \pi^{-1}\mathrm{PV}\int_{-\infty}^{\infty}\frac{g(\tau)}{t-\tau}d\tau. \tag{5.17}$$

Here PV means the integral in the sense of Cauchy principal value. The instantaneous amplitude $A(t)$ and phase $\phi(t)$ are determined by Eq. (5.16). Then the phase can be calculated as

$$\phi(t) = \arctan\frac{g_H(t)}{g(t)}. \tag{5.18}$$

Note that the phase obtained by this method ranges from $-\pi$ to π.

From Eq. (5.17), it can be seen that the Hilbert transform is the convolution of the functions $g(t)$ and $1/\pi t$. According to a property of convolution, the Fourier transform $\hat{g}_H$ of $g_H(t)$ is the product of the Fourier transform of $g(t)$ and $1/\pi t$. For physically relevant Fourier frequencies $f > 0$,

$$\hat{g}_H(f) = \int_{-\infty}^{\infty} dt\exp(-2\pi f\imath t)g(t) * \int_{-\infty}^{\infty} dt\frac{\exp(-2\pi f\imath t)}{\pi t}, \tag{5.19}$$

which is equivalent to $\hat{g}_H(f) = -\imath\hat{g}(f)$. This means that the Hilbert transform can be seen as a filter whose amplitude response is unity and whose phase response is a $\pi/2$ lag at all frequencies [120].

A harmonic oscillation $g(t) = A\cos(\omega t)$ is often represented by in the complex form as $A\cos(\omega t)+\imath A\sin(\omega t)$. This means that the real oscillation is complemented by the imaginary part whose phase delay by $\pi/2$, which is related to $g(t)$ by the Hilbert transform [116].

It should be remarked that this method is reasonable only when the original signal $g(t)$ is a narrow band-signal. Real signals usually contain wide range of frequencies because of noise or other factors, and some filtering may be necessary in order to use this method.

5.2.3 Application to real data

To define the phase of the heartbeat and respiration from acquired signals, the method based on marked events was used. This was because of the weak points of the Hilbert transform described above. The R-peak was used as a marked event in each heartbeat in ECG signals, and the maximum point corresponding to inhalation in respiratory signals was used as marked event in each respiratory cycle.

5.3 Results

5.3.1 Heart rate variability (HRV) and respiratory rate variability (RRV)

The instantaneous frequencies were introduced by using the times of marked events described above. If the k-th and $k+1$-th marked events occur at t_k and t_{k+1} respectively, the instantaneous frequency f_i is defined as

$$f_i(t_{k,k+1}) = \frac{1}{(t_{k+1} - t_k)} \quad \text{where} \quad t_{k,k+1} = \frac{(t_k + t_{k+1})}{2}. \tag{5.20}$$

The instantaneous frequency between $t_{k,k+1}$ and $t_{k+1,k+2}$ is defined by linear interpolation as

$$f_i(t) = \frac{f(t_{k+1,k+2}) - f(t_{k,k+1})}{t_{k+1,k+2} - t_{k,k+1}}(t - t_{k,k+1}) + f_i(t_{k,k+1}), \;\; t_{k,k+1} < t < t_{k+1,k+2}. \tag{5.21}$$

This method was applied to both the ECG and respiratory signals. The dependence of instantaneous frequency with time are called heart rate variability (HRV) and respiratory rate variability (RRV) respectively. HRV is one of the indicators for cardiac regulation. The existence of fluctuation of heart rate was noticed as early as 1733 by Hales [51], related to the respiratory oscillation. This modulation is known as respiratory sinus arrhythmia (RSA). These values represent the change of the period during which the phase starts from zero and resets to 2π. Actual examples of HRV and RRV signals are shown in Fig. 5.2, where the RSA can be seen. As explained in subsection 5.1.2, the variation of the frequency of HRV and RRV can be considered to come from the term of $(\mathbf{U}^*(\phi), \mathbf{p}(t))$ in Eq. (5.7), where the perturbation $p(t)$ can be the parameter change described in subsection 5.1.2 and the coupling with other oscillators such as respiratory oscillation as we will explain below in section 8.1. The respiratory oscillation seems to have an especially important role in modulating the heart rate since the heart rate is known to contain an oscillatory component which corresponds to respiration [138]. The results of spectral analysis of HRV will be discussed in subsection 7.2.1 and the origin of other oscillatory processes which modulate the heart rate will be also explained there.

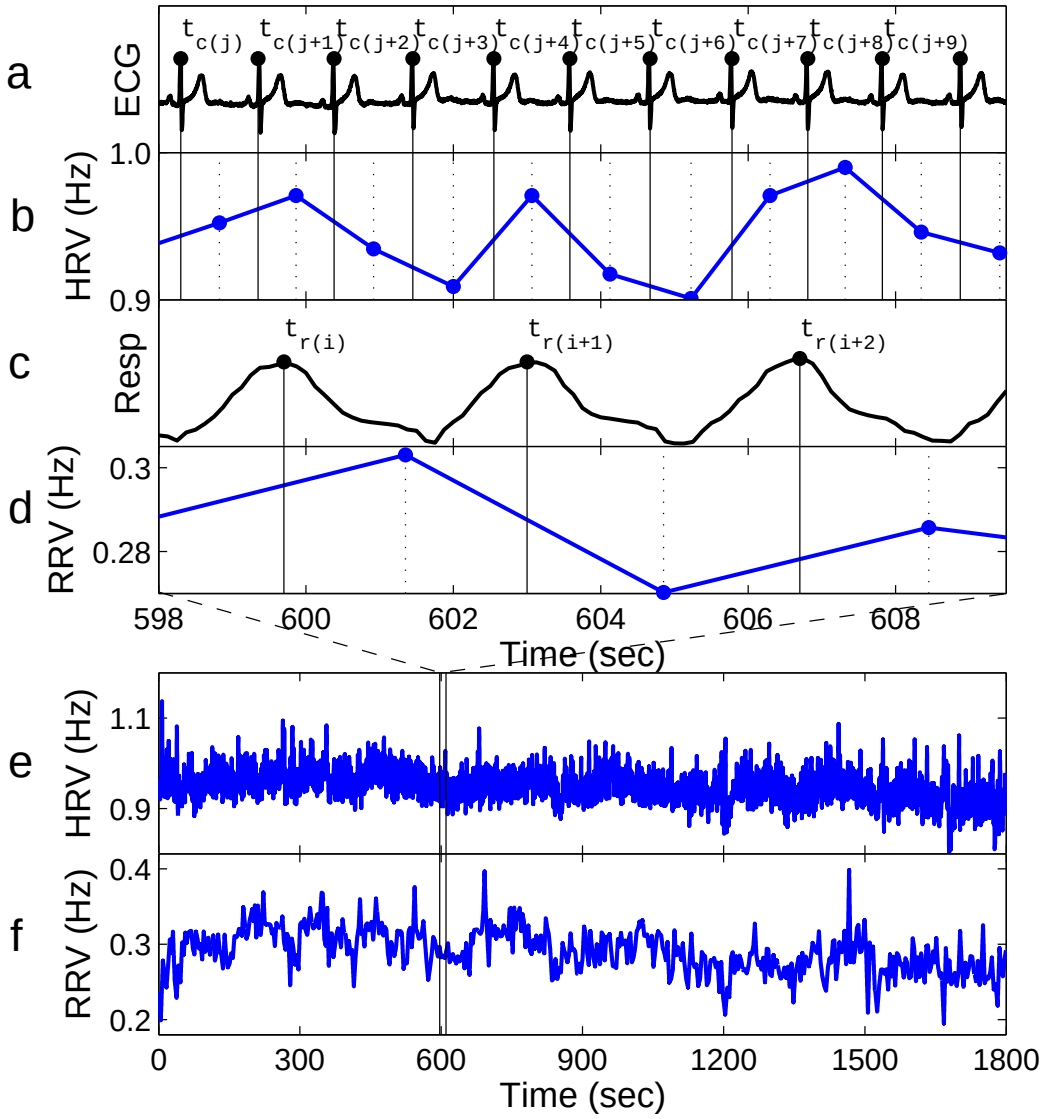

Fig. 5.2: (a) an ECG signal during a time segment where R-peaks are marked at time $t_{c(j+k)}$ for $k = 0, \ldots, 9$, (b) the instantaneous frequency $1/(t_{c(j+k+1)} - t_{c(j+k)})$ marked at a time $(t_{c(j+k)} + t_{c(j+k+1)})/2$ for $k = 0, \ldots, 9$ forms a HRV signal during the time segment, (c) a respiratory signal during the time segment where maxima are marked at time $t_{r(i+l)}$ for $l = 0, 1, 2$, (d) the instantaneous frequency $1/(t_{c(i+l+1)} - t_{c(i+l)})$ marked at a time $(t_{c(i+l)} + t_{r(i+l+1)})/2$ for $k = 0, 1, 2$ forms a RRV signal during the time segment, (e) the HRV signal during the whole measurement and (f) the RRV signal during the whole measurement (f)

5.3.2 Effects of aging on HRV and RRV

The time average and standard deviation of HRV and RRV were calculated for each person and are plotted as a function of age in Fig. 5.3. There is significant correlation with age in the standard deviation of HRV both for males ($r = -0.28, p = 0.02$) and for females ($r = -0.28,\ p = 0.02$). Correlation coefficient and statistical significance were calculated with parametric statistical testing using MatLab (MatWork) in this theses (see section 4.2). The other values, average HRV, average RRV and standard deviation of RRV do not show significant correlation with age for either males or females. The average RRV of female is significantly higher than that of males in the aged population above 55 years ($p = 0.05$) whereas the other values do not show significant a gender difference (see Tab. 5.3.2).

There are already some reports of aging effects in HRV signals, for example [69, 123, 133, 152]. The significant decrease of the standard deviation of heart rate with age is common and already well known. There are also some differences from their results. For example, Stein *et al.* [133] reported that there is a significant decrease in average heart rate for male, whereas Ryan *et al.* [123] reported that the average heart rate did not change between young and aged groups, which agree with our observation. The difference probably comes from the difference of recording time and the number of subjects. Rather than discussing the details of these differences, we will focus on the connection to the results in other sections of this thesis.

Gender difference				
	HRV		RRV	
	below 40 years	above 55 years	below 40 years	above 55 years
Average	$p = 0.83$	$p = 0.18$	$p = 0.86$	$p = 0.05$ (f)
Standard deviation	$p = 0.24$	$p = 0.44$	$p = 0.14$	$p = 0.17$

Tab. 5.1: Gender difference of average HRV, average RRV, standard deviation of HRV and standard deviation of RRV. (f) means that the values of females are significantly higher than those of males.

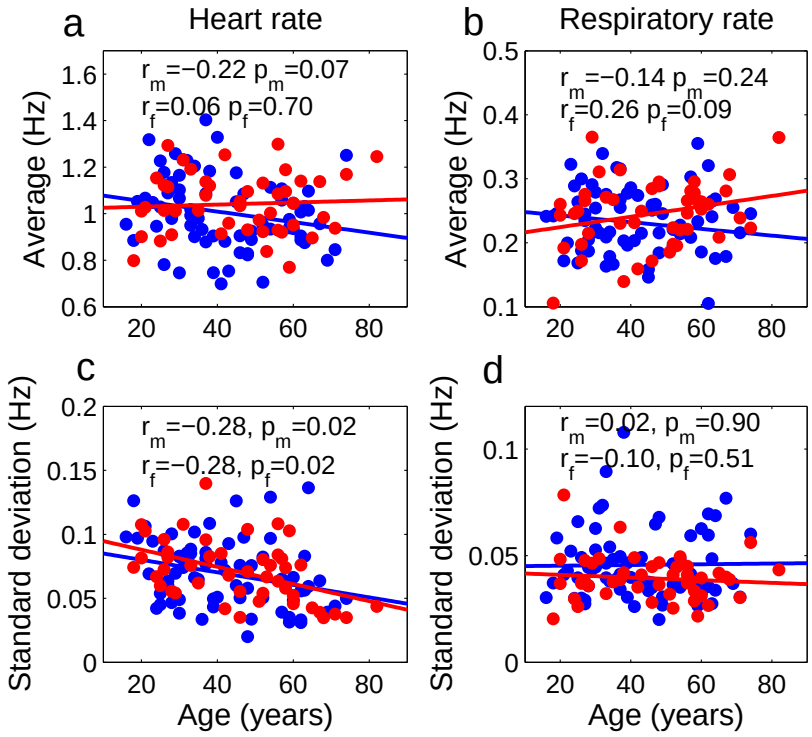

Fig. 5.3: The effect of aging on average heart rate (a), average respiratory rate (b), standard deviation of heart rate (c) and standard deviation of respiratory rate (d).

6. COMPLEXITY ANALYSIS

6.1 Overview of existing results

In this section, we will overview the results obtained but later also the introduction of detrended fluctuation analysis (DFA) and detrended moving analysis (DMA). The history of developments in this area is described in section 1.2

Complexity is independent of the mean and variance of a signal and different techniques are required for its measurement. For example, two sine waves of different amplitude can be thought to have the same complexity although they have different variances.

Chaos theory provides several meaningful ways to quantify complexity. One characteristic is the dimension, which is interpreted as the number of variables in the difference or differential equations needed to construct a dynamical system which will reproduce the measured signals. An other characteristic is entropy, which is related to the amount of information needed to predict the future state of the system. A larger dimension and a larger entropy imply greater complexity. The approximate dimension and entropy *ApEn* were calculated in the signals of the blood pressure and heart rate [69] and it was observed that younger subjects have higher complexity than older people for both blood pressure and heart rate variability. Ryan *et al.* calculated *ApEn* and reported that the complexity of heart rate dynamics are higher in women than men [123]. Higuchi suggested quantification of the complexity based on the fractal dimension [55, 56]. By using this method, fractal changes in heart rate were studied with aging and heart failure [50]. There is also a review about complexity and aging by Lipsitz *et. al.* [86].

Most of the output signals of physical, biological, physiological and economic systems are non-stationary and exhibit complex self-similar fluctuations over a broad range of space or time scales. To see the scaling property, a time series is expected to grow with the window size in a power-law way and to be unbounded. But a real signal is bounded. A method to resolve this paradox is to integrate

the signals. The integration of a signal is the critical first step common to all the methods used to calculate the complexity. Starting with an original signal $g(i)$, where $i = 1, \ldots, N$, and N is the length of the signal, the first step of the Hurst exponent, DFA, and DMA methods is to integrate $g(i)$ and obtain the integrated signal $y(i)$ as

$$y(i) = \sum_{j=1}^{i} [g(j) - \bar{g}], \tag{6.1}$$

where

$$\bar{g} \equiv \frac{1}{N} \sum_{j=1}^{N} g(j). \tag{6.2}$$

To calculate the Hurst exponent, we have to calculate the standard deviation,

$$S(N) = [\frac{1}{N} \sum_{t=1}^{N} \{g(i) - \bar{g}\}^2]^{1/2}, \tag{6.3}$$

and the range,

$$R(N) = \max_{1 \leq i \leq N} y(i) - \min_{1 \leq i \leq N} y(i). \tag{6.4}$$

The Hurst exponent H is then defined as

$$R/S = (cN)^H, \tag{6.5}$$

where the coefficient c was taken as 0.5 by Hurst. He found that the ratio R/S is very well described for a large number of natural phenomena by the above empirical relation. The relation between the Hurst exponent and the fractal dimension is simply $D = 2 - H$.

A Hurst exponent of $0.5 < H < 1$ represents persistent behavior. Persistence means that if the curve has been increasing for a period, it is expected to continue for another period. A Hurst exponent of $0 < H < 0.5$ shows anti-persistent behavior. After a period of decreases, a period of increases tends to occur.

6.2 Analytical methods: Detrended Moving Analysis (DMA) and Detrended Fluctuation Analysis (DFA)

The DFA method is a modified root-mean-square (rms) analysis of a random walk. The basic idea of these methods is based on the fractal property of a time series.

A time series is self-similar if it satisfies

$$y(i) \equiv a^{\alpha} y(\frac{i}{a}), \tag{6.6}$$

where $y(i)$ is the integrated original signal $g(i)$, and $\equiv$ means that the statistical properties of both sides of the equation are identical (both sides have the identical probability distribution as a properly rescaled process). The x-axis is rescaled as $t \to t/a$ and the y-axis as $y \to a^{\alpha}y$.

Suppose that the original signal length is n_2, and that a window of length $n_1 < n_2$ is taken to test for self-similarity compared to the original signal. Then the magnification factor of the x-axis $M_x = a$, is n_2/n_1. Suppose that the probability distribution, $P(y)$, of the variable y for the two windows before and after the magnification, where s_1 and s_2 indicate the standard deviations for these two distribution functions. Then the magnification factor of the y-axis $M_y = a^{\alpha}$ is s_2/s_1. The self-similarity parameter α is expressed as

$$\alpha = \frac{\ln M_y}{\ln M_x} = \frac{\ln s_2 - \ln s_1}{\ln n_2 - \ln n_1}. \tag{6.7}$$

To calculate s, the DFA method uses a filtering by polynomial functions. At first, the integrated signal $y(i)$ is divided into boxes of equal length n. In each box, we fit $y(i)$ using a polynomial function $y_n(i)$, which represents the local trend in that box. When a lth-order polynomial function is used for filtering, we call the method DFA-l.

Next, the integrated profile $y(i)$ is detrended by subtracting the local trend $y_n(i)$ in each box of length n and we can get Y_n as

$$Y_n(i) \equiv y(i) - y_n(i). \tag{6.8}$$

By this procedure, non-stationarity in the form of polynomial trends are eliminated.

Finally, for each box, the rms fluctuation of the integrated and detrended signal is defined as

$$F(n) \equiv \sqrt{\frac{1}{N}\sum_{i=1}^{N}[Y_n(i)]^2} \tag{6.9}$$

and $F(n)$ is then considered as s in the above discussion.

The DMA method uses a moving average method to get y_n. For example, the simple backward moving average is

$$y_n(i) \equiv \frac{1}{n}\sum_{k=0}^{n-1} y(i-k). \tag{6.10}$$

For more details, see [159]. Then we subtract the trend y_n from the original signal as in Eq. (6.8), can calculate $F(n)$ according to Eq. (6.9).

The calculation of $F(n)$ is made for varied box lengths n to obtain a power-law relationship between the rms fluctuation function $F(n)$ and the scale n in the form of

$$F(n) \sim n^{\alpha}. \tag{6.11}$$

A linear relationship between $\log(F(n))$ and $\log(n)$ indicates the presence of scaling (self-similarity). The fluctuations in the small boxes are related to the fluctuations in the larger boxes in a power-law fashion. The slope of the graph between $\log(F(n))$ and $\log(n)$ determines the self-similarity parameter α, which quantifies the presence or absence of fractal correlation properties in the signals.

Because power laws are scale-invariant, $F(n)$ is also called the scaling function and the parameter α is the scaling exponent.

These two methods are both suitable for non-stationary signals such as the physiological signals described before. Which method is better, DMA or DFA? There is a comparative study about the performance of DFA and DMA methods [159]. A study was made of how accurately these methods reproduce the exponent α and what are the limitations of the methods when applied to signals with small or large values of α. It was reported in [159] that DMA tends to underestimate the exponent if it is larger than one, whereas the DFA, especially DFA-1, shows relatively good correspondence to real values over a wide range of α. In our study, the exponents went beyond one. Therefore we adopted the DFA-1.

6.3 Relationship between the exponents obtained by DFA and from the auto-correlation function

Many simple systems have an auto-correlation function that decays exponentially with time. However it was discovered that in a system composed of many interacting subsystems, it decays not exponentially but in a power-law form [12, 110]. This implicates that there is no single characteristic time in a complex system. If correlations decay with a power-law form, the system is called ‘scale-free’ because there is no characteristic scale associated with a power law. Since at large time scales a power law is larger than an exponential function, correlations described by power laws are termed ’long range’ correlations in the sense that they are of

larger range than an exponentially decaying function. The DFA method can detect the long range correlation and here we will discuss the relationship between the exponent and the correlation function.

The exponent α (self-similarity parameter) which is calculated from an integrated time series is related to the more familiar auto-correlation function, $C(\tau)$, or the Fourier spectrum, $S(f)$, of the original (non-integrated) signal. (It is well known that $C(\tau)$ and $S(f)$ are related through the Fourier transform as $S(f) = \int_{-\infty}^{\infty} C(\tau) \exp(\imath 2\pi f \tau) d\tau$.)

White noise, whose value at each moment is completely uncorrelated with any previous value, has an auto-correlation function, $C(\tau)$, which is 0 for any non-zero τ (time-lag). The exponent α of white noise is 0.5 [38].

An exponent α greater than 0.5, and less than or equal to 1.0, indicates persistent long-range power-law correlations, i.e., $C(\tau) \sim \tau^{-\gamma}$. The relationship between α and γ is $\gamma = 2 - 2\alpha$. It should also be noted that the power spectrum, $S(f)$, of the original (non-integrated) signal is also of a power-law form, i.e., $S(f) \sim 1/f^{\beta}$. Since the power spectral density is simply the Fourier transform of the autocorrelation function, $\beta = 1 - \gamma = 2\alpha - 1$. The case of $\alpha = 1$ corresponds to $1/f$ noise ($\beta = 1$).

When $\alpha < 0.5$, power-law anti-correlations are present such that large values are more likely to be followed by small values [15].

When $\alpha > 1$, correlations exist but cease to be of power-law form; $\alpha = 1.5$ indicates brown noise, which is created by the integration of white noise. Brown noise is much more correlated than white noise, since the fluctuations at a point in time do depend on previous fluctuations and cannot stray too far from them in too short a time. Brown noise has a spectral density proportional to $1/f^2$ and has stronger modulation in slow time scales.

The exponent α can also be viewed as an indicator of the roughness of the original time series: the larger the value of α, the smoother the time series. In this context, $1/f$ noise can be interpreted as a compromise between the complete unpredictability of white noise (very rough form) and the much smoother form of brown noise [118].

6.4 Results

6.4.1 Application to HRV signals

The original HRV signals of a young female and an aged female are shown in Fig. 6.1 along with examples of white noise and brown noise. The HRV signals are determined according to R-peaks as explained in section 5.3.1. The interval between subsequent R peaks is usually around 1 second. According to Eq. (5.20), the sampling frequency of the HRV signal is also originally around 1 Hz although we made their sampling frequency 10 Hz by linear interpolation. To compare HRV signals to white noise and brown noise, we generated and recorded white noise with a sampling frequency 1 Hz and extended its sampling frequency to 10 Hz by linear interpolation, just as we did to the HRV signals. The brown noise with sampling frequency of 1 Hz was obtained by integrating the white noise with 1 Hz and its sampling frequency was also extended to 10 Hz by linear interpolation.

We take the number of points n from 20 to 2000, which means from 2 to 200 seconds. The results of DFA for white noise, brown noise and the HRV signals from a young female and an aged female are shown in Fig. 6.2. When n is smaller than 100, the slope between $\log(n)$ and $\log(F)$ deviates from 0.5 for white noise. This deviation from 0.5 in the white noise in Fig. 6.1 is thought to come from the small sampling frequency. Fig. 6.4 shows the time series of the white noise with sampling frequency of 10 Hz and the result of DFA. An exponent around 0.5 is obtained within the whole region from $n = 20$ to $n = 200$. For this reason, we only use the results for $n > 100$.

As shown in Fig. 6.2a, the exponent of white noise is 0.49, which is close to the expected value 0.5. The exponent of brown noise is 1.49, whereas it is also close to the expected value 1.50 as shown in Fig. 6.2b. The exponents of human HRV signals cannot be determined uniquely as in the case of white noise and brown noise, because the slope between $\log(F)$ and $\log(n)$ changes depending on the size of n as shown in the bottom of Fig. 6.2. We divided the range of n into two intervals so that the slope of HRV could be determined more reliably. The exponent α_i of an intermediate time scale is defined by using n from 100 to 500 (10-50 sec), while the exponent α_l of a long time scale is defined by using n from 500 to 2000 (50-200 sec). The physiological meaning of each interval will be described below in

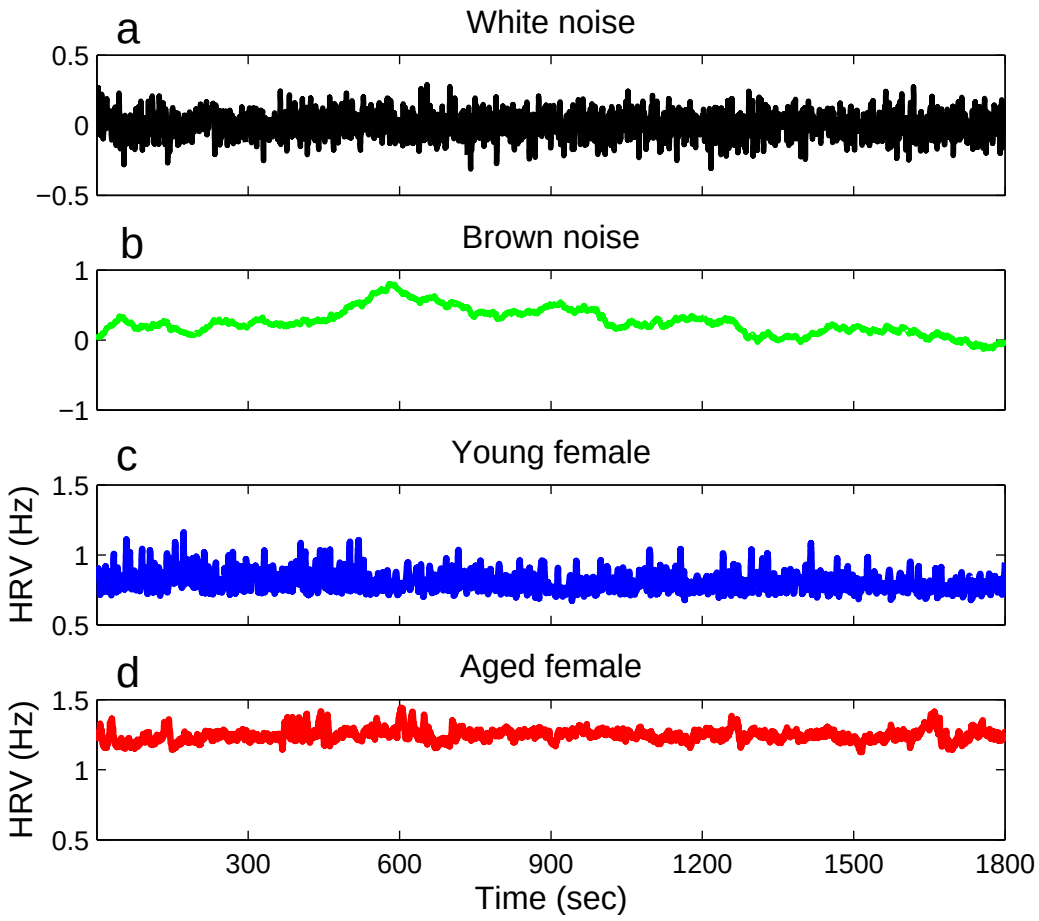

Fig. 6.1: A time series generated by white noise (a), the integrated time series (brown noise) (b), the heart rate signal of a young female (c) and the heart rate signal of an aged female (d).

section 7.2.1.

The results for all subjects are plotted separately in different colors for males and females in Fig. 6.3 (blue for males and red for females). The exponent α_i has significant correlation with age for both males ($r = 0.29,\ p = 0.01$) and females ($r = 0.37,\ p = 0.01$). There is no significant gender difference, neither in the younger age group below 40 years ($p = 0.19$), nor in the older age group above 55 years ($p = 0.06$).

In the long range (50-200 sec), there is no significant correlation related to age for either male ($r = 0.03,\ p = 0.83$) or female ($r = 0.05,\ p = 0.73$). There is no significant gender difference, neither in the younger age group below 40 years ($p = 0.35$) nor in the older age group above 55 years ($p = 0.80$).

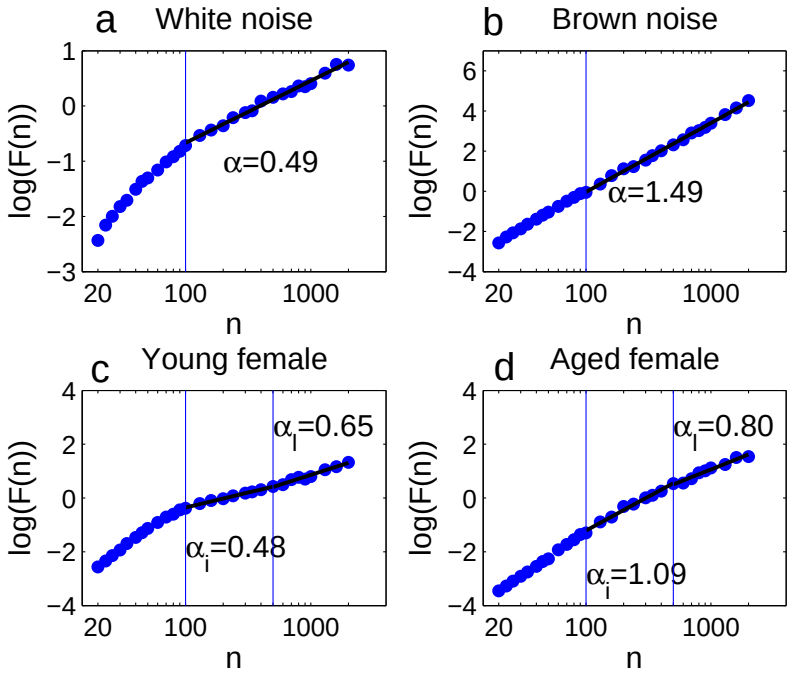

Fig. 6.2: The log-log plot between F and n of white noise (a), brown noise (b), the HRV of a young female (c), the HRV of an aged female (d). In (a) and (b), the exponent α was calculated on the right side of the line, $n = 100$. In (c) and (d), the exponent α_i was calculated between the two lines (the intermediate range), $n = 100$ and $n = 500$, whereas the exponent α_l was calculated on the right side of the line $n = 500$ (the long range).

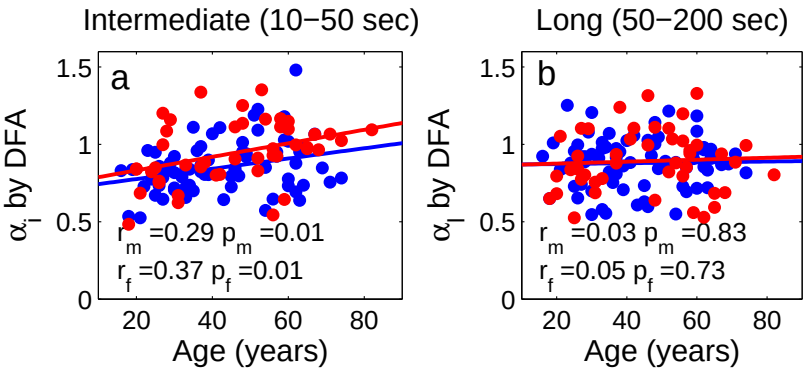

Fig. 6.3: The correlation with age of the exponent of intermediate range α_i (a) of the exponent of long range α_l (b).

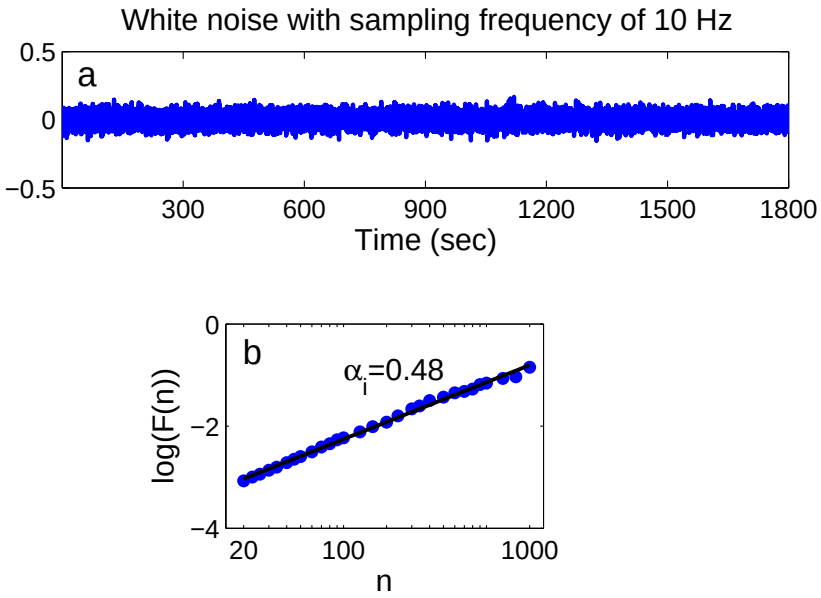

Fig. 6.4: The white noise whose sampling frequency is increased to 10 Hz (a) and its log-log plot of F and n (b). The exponent can be defined uniquely form $n = 20$ to $n = 2000$ compared with Fig 6.3a.

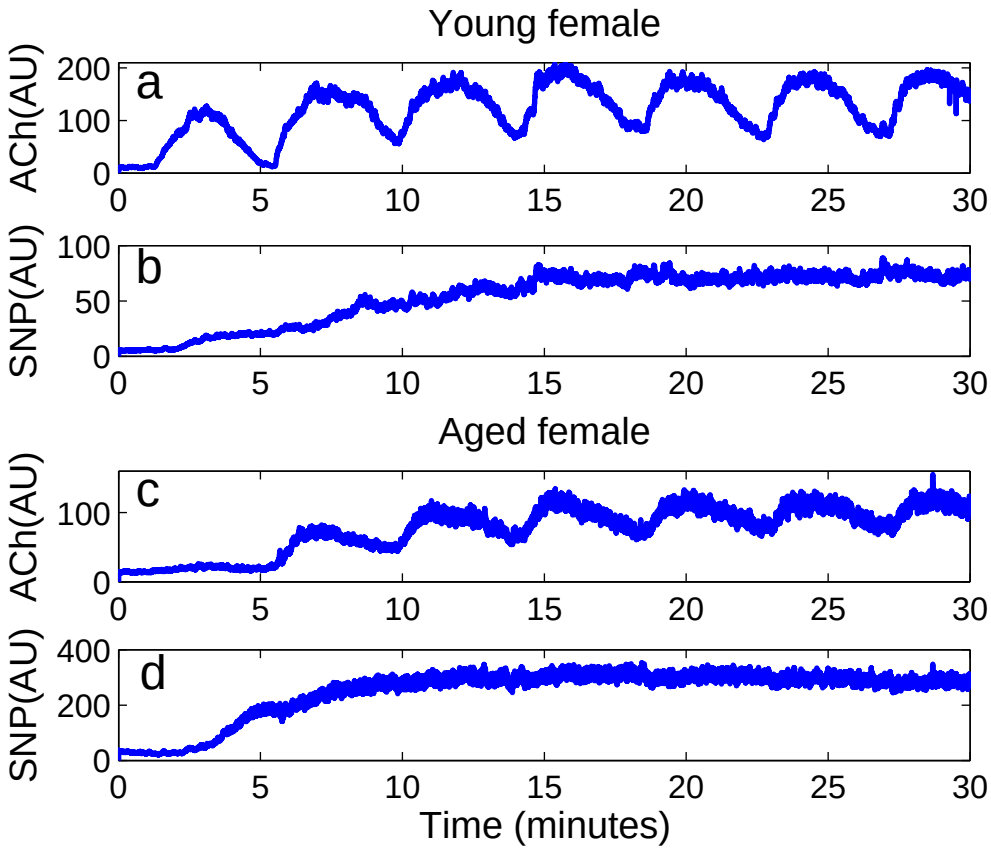

Fig. 6.5: Blood flow signals measured with ACh and SNP for a young female (a, b) and an aged female (c, d).

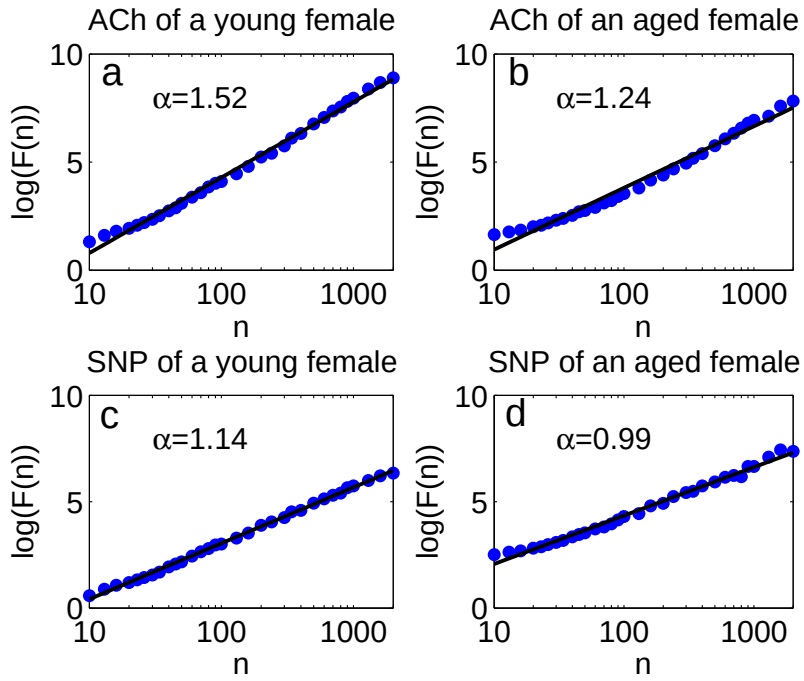

Fig. 6.6: The log-log plot between F and n for the ACh signal from a young female (a), and from an aged female (b), as well as for the SNP signal from a young female (c) and from an aged female (d).

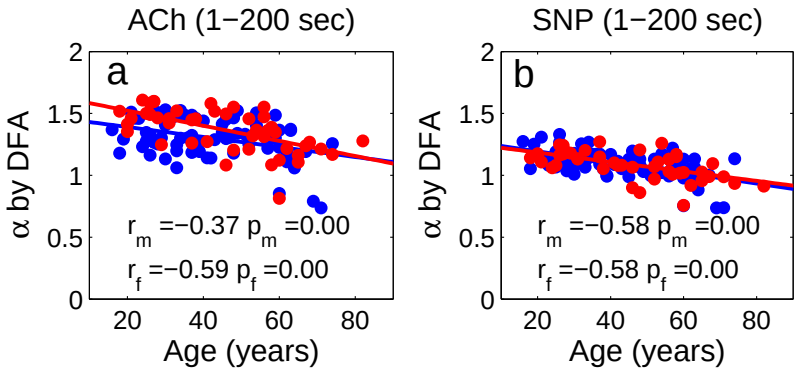

Fig. 6.7: The correlation between age and the exponent α for ACh (a) and for SNP (b). The blue line and dots represent males and the red females.

6.4.2 Application to blood flow signals

The DFA method was applied to the blood flow signals measured with ACh and SNP. The signals were resampled from 400 Hz to 10 Hz by averaging 40 points and their lower frequency oscillations below 0.005 Hz were detrended. The blood flow signals of a young female and an aged female are shown in Fig. 6.5. The results of the application of DFA to these four signals are shown in Fig. 6.6. In the case of the blood flow, the slope seems to be defined well on a time scale from 1 to 200 seconds. The plots of α with age for ACh and SNP are shown in Fig. 6.7. There is significant negative correlation with age in the ACh signals for males ($r = -0.37,\ p = 0.00$) and for females ($r = -0.59,\ p = 0.00$) and in the SNP signals for males ($r = -0.58,\ p = 0.00$) and females ($r = -0.58,\ p = 0.00$).

There is a significant gender difference for ACh in the younger population below 40 years ($p = 0.00$): the α values of young females are significantly higher than those of young males. However the difference disappears in the aged population above 55 years ($p = 0.49$). For SNP, no significant gender difference was observed both in the younger population ($p = 0.27$) and the aged population ($p = 0.95$). The exponent α for ACh is higher than that of SNP for young females, young males below 40 years and for aged males and females above 55 years ($p = 0.00$ in all cases).

6.5 Discussion

6.5.1 HRV signals

There are several studies of aging based on the use of DFA [43] [143]. They reported that the exponents of DFA increase with age, which means that the complexity decreases with age. The exponents depend on the time window in which they are calculated. They took a size of 4 to 11 seconds for the short-term exponent and a size more than 11 seconds for the intermediate-term exponent. In our case, it was found that the result below 10 seconds is not correct because of the lack of information in the original heart rate signals and we therefore discarded information below 10 seconds. For reasons which we describe below in section 7.2.1, we divided the window size into 10-50 seconds and 50-200 seconds. Our results are consistent with the earlier result that the exponent increases with age on

a time scale from 10 to 50 seconds. The HRV signals of younger subjects are relatively close to white noise, whereas those of aged subjects are relatively close to brown noise in the intermediate time scale. That means that HRV signals of aged subjects are less complex than those of young subjects. These results support the hypothesis that aging is associated with less complexity [43]. The physiological reasons which cause the effects of aging on complexity will be discussed in details below in section 7.2.1 in relation to the detailed spectral analysis of HRV signals.

Although DFA is a good way to quantify the complexity, it has to be noted that it is intended only for mono-fractal signals, to measure only one exponent characterizing a given signal. It is reported that the heart rate data of healthy subjects are not mono-fractal but multi-fractal [43]. Multi-fractal signals show self-similar (scale-invariant) fluctuation over a wide range of time scales, require a large number of indices to characterize their scaling properties and are more complex than mono-fractal signals. In this study, we found that the slope between $\log(F(n))$ and $\log(n)$ often changes dramatically around $n = 50$ as it can be seen in Fig. 6.2. This means that the DFA is not sufficient to characterize fractal correlations fully and may indicate multi-fractal properties.

6.5.2 Blood flow signals

For the blood flow signals measured with ACh and SNP, the signals of aged subjects are more complex than those of young subjects, which is opposite to the results for the HRV signals. The signals with SNP are more complex than those with ACh. The difference between ACh and SNP comes possibly from whether the respond is endothelial-related or not. Note that the sites of measurement for these two substances are quite close, and that the data wa obtained under the same physiological condition for the same subject.

It seems that a less complex responce during vasodilation means a younger vascular function. The physiological reasons for the effect of aging on complexity will be discussed later in section 7.2.2 related to the spectral analysis of the blood flow signals.

7. DETECTION OF TIME-VARYING OSCILLATORY COMPONENTS

In this section, we explain the methods used to detect oscillatory components in the measured signals.

There are two major difficulties in the frequency analysis of cardiovascular signals. The first is the time-varying nature of the characteristic frequencies. As seen in the HRV and RRV of Fig. 5.2, the signals do not have a constant period, but their inherent cycles always fluctuate. The second it the broad frequency band within which the characteristic peaks are expected. Each method suffers from limitations of the resolution in time and frequency.

The FFT is a basic method of frequency analysis, and it is still commonly used. However it has shortcomings when applied to the analysis of finite and non-stationary data. First of all, the FFT cannot chase the time varying frequency. It produces only one picture in the frequency domain from a whole signal. If the signal has a time varying frequency, the frequency peak is broadened. Moreover any abrupt change at one moment affects the whole result. To overcome these drawbacks of the FFT, a short-time Fourier transform was introduced by Gabor [41] in which a window with a certain length is shifted along the signal to obtain information about the time, and the FFT is performed within the window to get the current frequency components (see section 7.1.1). However the time and frequency resolution depend on the window length, and the detection of low frequencies demands a wide window. Wavelet analysis is more suitable for signals with time-variable frequency than Fourier analysis because a sudden change is less effective. This is a big merit because a movement of the body during measurement easily destroys the signals with FFT. Moreover, it is more accurate for low frequencies because it is a scale-independent method in terms of frequency, as we explain later in section 7.1.4.

7.1 Analytical methods

7.1.1 Fourier analysis

The Fourier transform is a method which detects the frequency components in a time-domain signal $g(u)$ by use of the following equation,

$$\hat{g}(f) = \int_{-\infty}^{\infty} g(t) e^{-2\pi\imath f u} du. \tag{7.1}$$

The original signal can be obtained by an inverse Fourier transform,

$$g(u) = \frac{1}{2\pi} \int_{-\infty}^{\infty} \hat{g}(f) e^{2\pi\imath f u} df. \tag{7.2}$$

The energy of the signal equals

$$E_{tot} = \| s \|^2 = \int_{-\infty}^{\infty} |g(u)|^2 du = \int_{-\infty}^{\infty} |\hat{g}(f)|^2 df = \| \hat{g} \|^2 . \tag{7.3}$$

This relation between $\| g \|$ and $\| \hat{g} \|$ is known as Plancherel's theorem.

7.1.2 Short time Fourier transform

The Fourier transform cannot deal with local properties in time. To overcome the short-time Fourier transform (STFT) was introduced. A window $w(u)$ with a fixed length is shifted along time to obtain the local information around t. The information of the original signal $g(u)$ in the time-frequency domain $\hat{g}(f,t)$ is then obtained from

$$G(f,t) = \int_{-\infty}^{\infty} w(u-t) g(u) e^{-2\pi\imath f u} du. \tag{7.4}$$

The original signal is reconstructed as

$$g(u) = \frac{1}{2\pi \| w^2 \|} \int_{-\infty}^{\infty} dt \int_{-\infty}^{\infty} \hat{G}(f,t) w(u-t) e^{2\pi\imath f t} df. \tag{7.5}$$

In analogy to Plancherel's theorem, the energy is expressed as

$$\| g \|^2 = \int_{-\infty}^{\infty} |g(u)|^2 du = \frac{1}{\| w^2 \|} \int_{-\infty}^{\infty} \int_{-\infty}^{\infty} |G(f,t)|^2 df dt, \tag{7.6}$$

where $\| w^2 \| = \int_{-\infty}^{\infty} |w(t)|^2 dt$.

The uncertainty principle can be used here to point out that the time and frequency resolution can not be increased at the same time.

The mean time and frequency are given by

$$t^* \equiv \frac{1}{\| w \|} \int_{-\infty}^{\infty} |w(t)|^2 t dt, \tag{7.7}$$

$$f^* \equiv \frac{1}{\| \hat{w} \|} \int_{-\infty}^{\infty} |\hat{w}(f)|^2 f df, \tag{7.8}$$

where $\| \hat{w}^2 \| = \int_{-\infty}^{\infty} |\hat{w}(t)|^2 df$. The standard deviations Δ_t and Δ_f are determined by

$${\Delta_t}^2 \equiv \frac{1}{\| w \|} \int_{-\infty}^{\infty} |w(t)|^2 (t - t*)^2 dt, \tag{7.9}$$

$${\Delta_f}^2 \equiv \frac{1}{\| \hat{w} \|} \int_{-\infty}^{\infty} |\hat{w}(f)|^2 (f - f*)^2 df, \tag{7.10}$$

The uncertainty principle states

$$\Delta_t \Delta_f \geq \frac{1}{4\pi}. \tag{7.11}$$

This means that in order to gain good time resolution, a narrow time window should be used, while a good frequency resolution and detection of low frequencies demands a wide time window.

7.1.3 Discrete Fourier transform (DFT)

In order to apply the Fourier transform to real signals, we have to think of discrete Fourier transform. Suppose that an original signal has a finite window length $T = Nt_s$ and is sampled at discrete points it_s, where $i = 0, \ldots, N-1$. The discrete Fourier transform of the signal

$$G(f_k) = \sum_{0}^{N-1} g(it_s) e^{-2\pi \imath k/N} \tag{7.12}$$

is defined only for discrete frequencies $f_k = k/T$, where $k = 0, \ldots, N-1$. The frequency resolution is determined by the length of the signal as $\triangle_f = 1/T$ and the upper frequency limit f_{max} equals $2/t_s$.

7.1.4 Wavelet Analysis

Wavelet analysis is a scale-independent method in terms of frequency. It was a mother wavelet which is based on functions of various scales. In this study, we use the Morlet mother wavelet which is written as

$$\psi(u) = \frac{1}{\sqrt{\pi}} e^{-iw_0 u} e^{-u^2/2}. \tag{7.13}$$

By use of a scaling factor s and a centered time t, a family of nonorthogonal basis functions is obtained as

$$\Psi_{s,t}(u) = |s|^{-1/2}\psi(\frac{u-t}{s}). \tag{7.14}$$

The continuous wavelet transform of a signal $g(u)$ is then defined as

$$\tilde{g}(s,t) = \int_{-\infty}^{\infty} \bar{\Psi}_{s,t}(u)g(u)du. \tag{7.15}$$

Thus any specific scale is avoided and the analysis becomes scale-independent in terms of frequency. The spectral function $\tilde{g}(s,t)$ is complex and expressed by its amplitude and phase as $\tilde{g}(s,t) = r(s,t)\exp(\imath\theta(s,t))$. The phase $\theta(s,t)$ is considered as an instantaneous phase of oscillation of a frequency scale s at a time t [14].

The energy density of the signal in the time-scale domain is expressed as [68]

$$\rho(s,t) = C^{-1}s^{-2}|\tilde{g}(s,t)|^2 \tag{7.16}$$

The total energy of the signal $g(u)$ is

$$E_{tot} = \parallel g \parallel = C^{-1}\int\int \frac{1}{s^2}|\tilde{g}(s,t)|^2 dsdt. \tag{7.17}$$

The energy in a frequency interval from f_{i2} to f_{i1}, as later used in subsection 7.2.1, is expressed as

$$E_i(f_{i1}, f_{i2}) = \frac{1}{(f_{i2}-f_{i1})(t_2-t_1)}\int_{1/f_{i1}}^{1/f_{i2}}\int_{t_1}^{t_2}\frac{1}{s^2}|\tilde{g}(s,t)|^2 dsdt. \tag{7.18}$$

If we use the relationship $s = 1/f$ and $ds = -df/f^2$, we can easily derive the following equation,

$$E_i(f_{i1}, f_{i2}) = \frac{1}{(t_2-t_1)}\int_{f_{i2}}^{f_{i1}}\int_{t_1}^{t_2}|\tilde{g}(f,t)|^2 dfdt = \parallel \tilde{g} \parallel^2 . \tag{7.19}$$

We can recover $\parallel g \parallel = \parallel \tilde{g} \parallel^2$ in analogy to the Plancherel's theorem.

The time and frequency-averaged amplitude, or wavelet amplitude, in a frequency interval from f_{i2} to f_{i1} is expressed as

$$A_i(f_{i1}, f_{i2}) = \frac{1}{(f_{i2}-f_{i1})(t_2-t_1)}\int_{fi2}^{f_{i1}}\int_{t_1}^{t_2}|\tilde{g}(f,t)|dfdt. \tag{7.20}$$

If we use the relationship $s = 1/f$ and $ds = -df/f^2$, we can quickly arrive at the following equation,

$$A_i(f_{i1}, f_{i2}) = \frac{1}{(f_{i2}-f_{i1})(t_2-t_1)}\int_{1/f_{i1}}^{1/f_{i2}}\int_{t_1}^{t_2}\frac{1}{s^2}|\tilde{g}(s,t)|dsdt. \tag{7.21}$$

Bračič and Stefanovska introduced the averaged amplitude as absolute amplitude [22].

The relative amplitude and energy are defined as the ratio of those quantities within a given frequency interval to those within the total frequency interval, in the following way,

$$a_i(f_{i1}, f_{i2}) = \frac{A_i(f_{i1}, f_{i2})}{A_{tot}}, \tag{7.22}$$

$$e_i(f_{i1}, f_{i2}) = \frac{E_i(f_{i1}, f_{i2})}{E_{tot}}. \tag{7.23}$$

The total amplitude A_{tot} and energy E_{tot} are defined in the whole interval in which we are interested.

7.1.4.1 Frequency resolution

Suppose that the mother wavelet has centers of gravity at t_0 and f_0 in time and frequency and the corresponding standard deviation is $\triangle_{t_0}$ and $\triangle_{f_0}$. The scaled mother wavelet $\Psi_{s,t}$ has a center at st_0 and deviation $s\triangle_{t_0}$ according to Eq. 7.14. The center of $\Psi_{s,t}$ in the frequency domain is expressed as

$$f(s) = \frac{1}{s} f_0, \tag{7.24}$$

and the corresponding standard deviation as

$$\triangle_{f(s)} = \frac{1}{s} \triangle_{f_0}. \tag{7.25}$$

Then the local information around f is given in the frequency interval

$$[f_0/s - \triangle_{f_0}/2s, f_0/s + \triangle_{f_0}/2s]. \tag{7.26}$$

The ratio between the center frequency $f(s)$ and bandwidth $\triangle_{f(s)}$

$$\frac{\triangle_{f(s)}}{f(s)} = \frac{\triangle_{f_0}}{f_0} \tag{7.27}$$

is independent of the scaling s. This property can be seen if time average of wavelet of simple sinus waves, $\sin(2\pi t)$, $\sin(0.2\pi t)$ and $\sin(0.02\pi t)$ are plotted on linear and semi-log scales as shown in Fig. 7.1. On the semi-log scale, the width of the peak looks the same although on the linear scale, it is quite different.

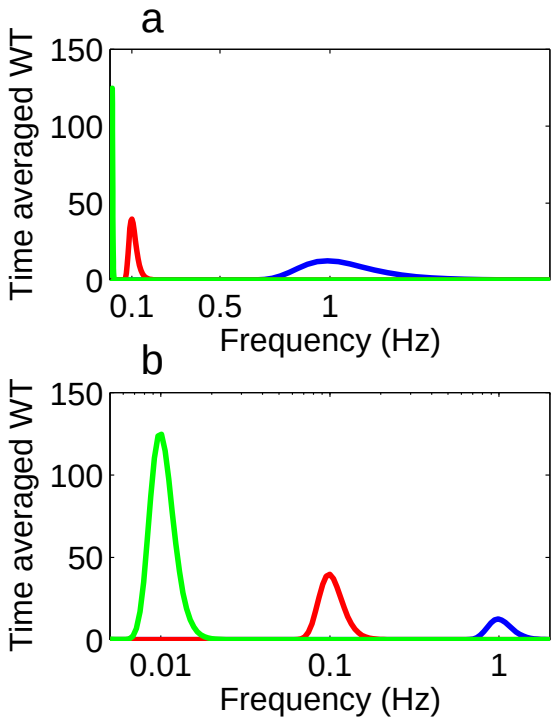

Fig. 7.1: Time averaged wavelet amplitude plotted on a linear scale (a) and a semi-log scale (b).

7.1.4.2 Energy and amplitude

Let us see the difference of the energy and amplitude of the wavelet defined by Eq. (7.18) and Eq. (7.21). As described below, our frequency interval of interest is from 0.005 to 2.0 Hz, which is divided into six subintervals (see the Tab. 7.1). According to these divisions of frequency intervals, we calculated the energy and amplitude of the sine waves, $\sin(2\pi t)$, $\sin(0.2\pi t)$ and $\sin(0.02\pi t)$ by wavelet analysis. For all the three cases, the total energy $\int |g(u)|^2 du$ is same. The absolute energy within a certain interval depends on the square of the amplitude of oscillation and does not depend on the frequency. In the case of $B\sin(\omega t)$, the total energy of wavelet depends only on B^2 but not on ω. Then the relative energy in the ith interval is proportional to $|B_i|^2 / \sum_{j=1}^{6} |B_j|^2$, where the sum of B_j is calculated for the six intervals which are listed in the Tab. 7.1.

On the other hand, the amplitude of the wavelet is affected not only by the amplitude B but also by the frequency ω. To illustrate this, we use three sine functions whose total amplitudes are different. The higher the frequency, the

higher is the total amplitude. However, if we calculate the absolute amplitude in each interval, the higher frequency produces a lower amplitude. In the case of $\sin(2\pi t)$, the total amplitude is 2.7 and A_1, which is averaged from 0.6 to 2.0 Hz, is 3.9, whereas in the case of $\sin(0.2\pi t)$, the total amplitude is 0.9 and A_3, which is averaged from 0.052 to 0.145 Hz, is 18. It is because the wavelet has the property that $\triangle_f/f$ is constant, as seen in Fig. 7.1b. If two frequencies, ω_1 and ω_2, lie in different intervals i_1 and i_2, and if the two oscillations have the same amplitude, the wavelet amplitude of the lower frequency A_{i_1} is higher than that of the higher frequency A_{i_2}. If the two frequencies lie in the same interval such as $\sin(2\pi t)$ and $\sin(2.4\pi t)$, the relative amplitude return the same value for both cases, which is obvious from its definition. But if there are several peaks in different intervals, the interpretation of relative amplitude is much more complicated since the information about amplitude and frequency in several intervals are combined.

7.2 Results

7.2.1 Components that modulate HRV

Tab. 7.1 show the frequency intervals in which we are interested for physiological reasons. A similar study but on smaller number of subjects using spectral analysis of HRV by wavelet has conducted by Lotrič *et al.* [89]. They studied the effects of aging on activity within the frequency intervals from II to V in Tab. 7.1. In this thesis, the interval VI of endothelial activity is newly added, and gender difference, which was not mentioned in [89], is discussed.

Interval	Frequency (Hz)	Physiological origin
I	0.6-2.0	cardiac activity
II	0.145-0.6	respiration
III	0.052-0.145	myogenic activity
IV	0.021-0.052	neurogenic activity
V	0.0095-0.021	endothelial metabolic activity
VI	0.005-0.0095	endothelial activity

Tab. 7.1: The frequency intervals considered in this study and their physiological origins

Lotrič *et al.* compared Fourier transform and evolutive autoregressive (AR) modelling, which are frequently used with HRV signals, with the wavelet transform. For the Fourier transform, the frequency resolution Δf is determined by

the window length and is constant for all the frequencies. For that reason, it was reported that it does not accurately locate the peaks in the low frequency interval. In contrast to the Fourier transform, $\Delta f/f$ is constant for the wavelet transform. Therefore the relative frequency resolution remains the same over all the frequency intervals. The absolute frequency resolution Δf is actually much better in the low frequency interval than in the high frequency interval for wavelet transform. Because of the wide frequency range of the intervals in Tab. 7.1, the wavelet transform is more suitable than the Fourier transform.

Autoregressive spectrum estimators avoid the problem of frequency discretization. By this method, a model of the time series is first built and the spectrum of this model is considered as an estimate of the spectrum of the original model. Linear models of different order are used to represent measured signals. An advantage of the wavelet transform compared to AR estimation is that it is calculated directly from the data and does not need modelling. The limitations of linear modelling, and the choice of model order, are avoided.

It was therefore concluded that the wavelet transform is the most suitable method of the three. We used the results of the wavelet transform.

The oscillations from intervals II to V in blood flows were studied by Bračič *et al.* [22]. In our study, the lowest frequency interval VI is added to include another endothelial-related activity.

The amplitude of the wavelet in time-frequency domain, and the time-average wavelet spectrum of HRV are presented in Figs. 7.2 and 7.3, respectively. The origins of these spectral peaks have been discussed in several papers [22, 134, 89, 139, 80, 81, 82, 83, 132, 138]. Here we review them briefly again.

(1) Interval I around 1 Hz: the cardiac activity

The basic frequency around 1 Hz in the ECG signal corresponds to the frequency of the heart activity. At rest, it varies from 0.6 in sportsmen to 1.6 Hz in subjects with impaired cardiovascular systems. The effect of the heart pumping is manifested in the vessels.

(2) Interval II around 0.2 Hz: the respiratory activity

Since Hales found out the RSA, it has been studied extensively since then [6, 5, 32, 58]. The modulation in this frequency interval corresponds well to the respiratory signal as shown in the Fig. 5.2, and the instantaneous respiratory

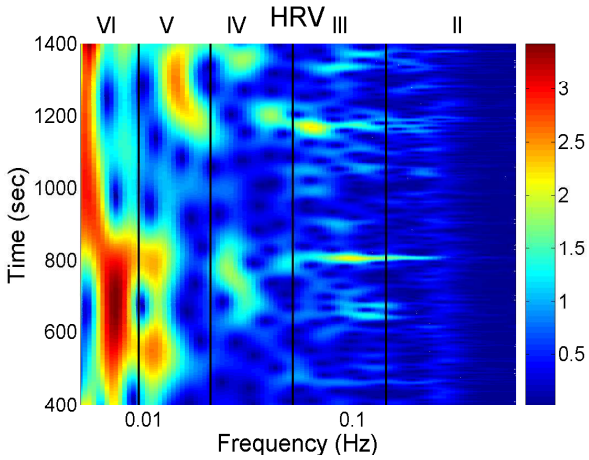

Fig. 7.2: The time frequency domain of wavelet transform of HRV.

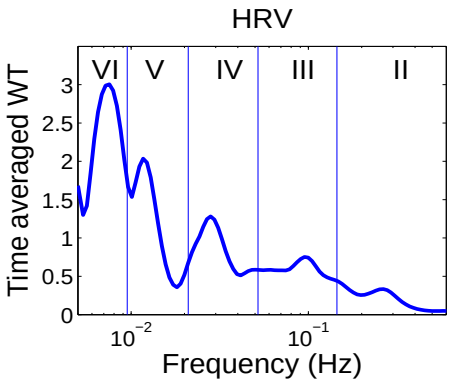

Fig. 7.3: The time-averaged amplitude of HRV.

frequency correspond well to the peak in the frequency domain of HRV wavelet analysis.

(3) Interval III around 0.1 Hz: myogenic activity

The heart and respiratory activity serve as pumps that drive blood through vessels. The vessels themselves also help to control blood flow via the mechanism called myogenic autoregulation. The vascular smooth muscles contract in response to an increase of intravascular pressure and relax in response to a decrease of pressure. These responses are thought to be controlled by the oscillations of ionic concentrations, especially Ca^{2+} across the membranes of the vascular smooth muscles. It has been proposed that oscillations in the blood flow around 0.1 Hz may originate from the intrinsic myogenic activity of the vascular smooth muscles caused by pacemaker cells found in the vessel walls [82].

(4) Interval IV around 0.03 Hz: the neurogenic activity

The autonomous nervous system innervates the heart, lungs and blood vessels, except the capillaries. The continuous activity of the autonomous nervous system serves to maintain the basal level of contraction of the vessels. The nervous system controls the peripheral resistance by changing its oscillatory frequency: an increase produces vasoconstriction. The peak around 0.03 Hz is hypothesized to originate from neurogenic activity because there is an indirect evidence that disconnecting nerves from the vessels, thereby suppressing the neurogenic regulation of the vessel radius, causes the oscillation around 0.03 Hz to disappear [70]. It was observed

that there is a significantly lower oscillation amplitude on flaps of transplanted skin, compared to intact skin, in this frequency interval [132]. Brajać *et al.* also observed a significant change before and after denervation on rats [11]

(5) Interval V around 0.01 Hz: the NO-related endothelial activity

The blood supplies the cells with nutrients and removes the waste products of their metabolism while circulating around the circle of vessels. The substances related to metabolism such as O_2 or CO_2 have a direct effect on the state of contraction of the vascular musculature. The control of the blood flow based on the concentrations of metabolites is termed metabolic regulation. There is indirect evidence that the oscillation around 0.01 Hz originate from endothelial activity [83] [139]. The layer of endothelial cells serves as a barrier between the blood and the tissues of vessels and controls the contraction and relaxation of smooth muscle by releasing various substances. It seems that metabolic regulation of the blood flow is mediated by the activity of endothelial cells through adjusting the concentrations of various substances. Nitric oxide (NO) is one of the most important vasoactive substances. It was reported that the interval V was modulated by the inhibition of NO synthetase of endothelium [80] and this interval is related to NO from endothelium.

(6) Interval VI around 0.007 Hz: the endothelial activity

This interval has not been identified until very recently probably because it was filtered out during data pre-processing. However, a strong peak was observed around 0.007 Hz in this study, as well as other studies [14, 81]. This interval may also be related to the endothelial activity.

It has to be noted that the interval I is not shown in Fig. 7.3. The HRV signals are determined according to R peaks as explained in section 5.3.1. The interval of continuous R peaks is usually around 1 Hz. According to Eq. (5.20), the sampling frequency of the HRV signal is also around 1 Hz. It means that the HRV signals do not have enough sampling points so that the frequency of interval I can be resolved.

For calculation, the scaling s varied from 0.5 to 200 by successive multiplication with a factor 1.05 in this chapter.

The effects of aging on the absolute energy within each interval except I, are shown in Fig. 7.4 and Tab. 7.2, and those on relative energy defined by Eq. (7.23)

in Fig. 7.5 and Tab. 7.3. If a few outliers changes results of the significant tests, I got rid of the outliers and showed the results after the removal of them.

It can be seen that total energy decreases significantly with age both for females ($r = -0.33$, $p = 0.02$), which corresponds to the significant decrease with age in the standard deviation in HRV as shown in Fig. 5.3. There is a trend to decrease with age for males, although the p-value does not show significance for males ($r = -0.20$, $p = 0.10$). The decomposition into the six intervals reveals that this decrease of total energy comes from the significant decrease in absolute energy of interval II and interval III both for males and for females. Absolute energy in interval II decreases significantly with age for males ($r = -0.39$, $p = 0.00$) and for females ($r = -0.50$, $p = 0.00$) and absolute energy in interval III decreases significantly with age for males ($r = -0.38$, $p = 0.00$) and females ($r = -0.46$, $p = 0.00$). Absolute energies in intervals IV, V and VI do not show significance age-related changes.

I introduce the results of relative energy because they are closely related to the results of the complexity analysis, which we discussed in the subsection 6.4.1. The relative energy is important rather than the absolute energy for complexity analysis as is discussed in the subsection 7.4. Here I explain the results briefly. It is observed that interval V (endothelial) increases significantly for males ($r = 0.29$, $p = 0.01$) and for females ($r = 0.40$, $p = 0.01$). Relative amplitude in interval III (myogenic) decreases significantly for males ($r = -0.25$, $p = 0.03$) and relative amplitudes decrease for females in intervals II ($r = -0.47$, $p = 0.00$) and IV ($r = 0.56$, $p = 0.00$).

Absolute energy for HRV				
	males		females	
Interval	r	p	r	p
Total	-0.20	0.10	-0.39	0.01
VI	-0.02	0.86	-0.09	0.57
V	-0.09	0.44	-0.08	0.63
IV	-0.16	0.21	-0.27	0.09
III	-0.38	0.00	-0.46	0.00
II	-0.39	0.00	-0.50	0.00

Tab. 7.2: Summary table for age-related changes in absolute energy

The gender differences within each interval for HRV are summarized in Tab. 7.4.

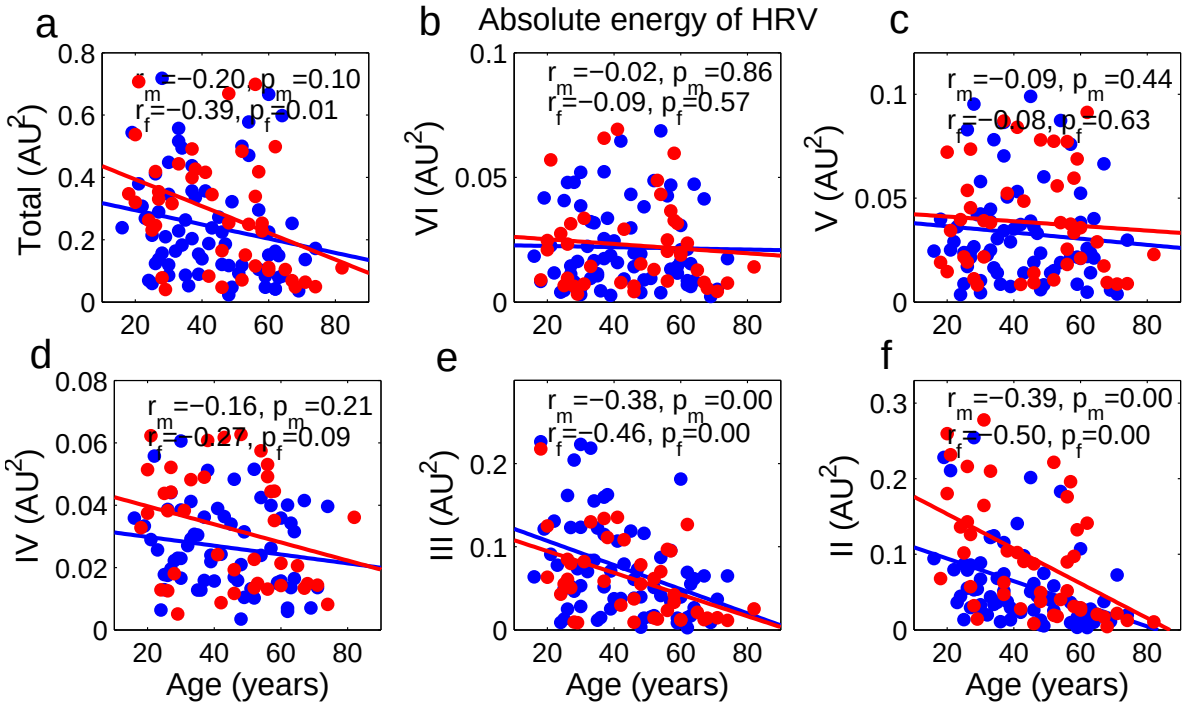

Fig. 7.4: Total energy (a), absolute energy in interval VI (b), V (c), IV (d), III (e), II (f).

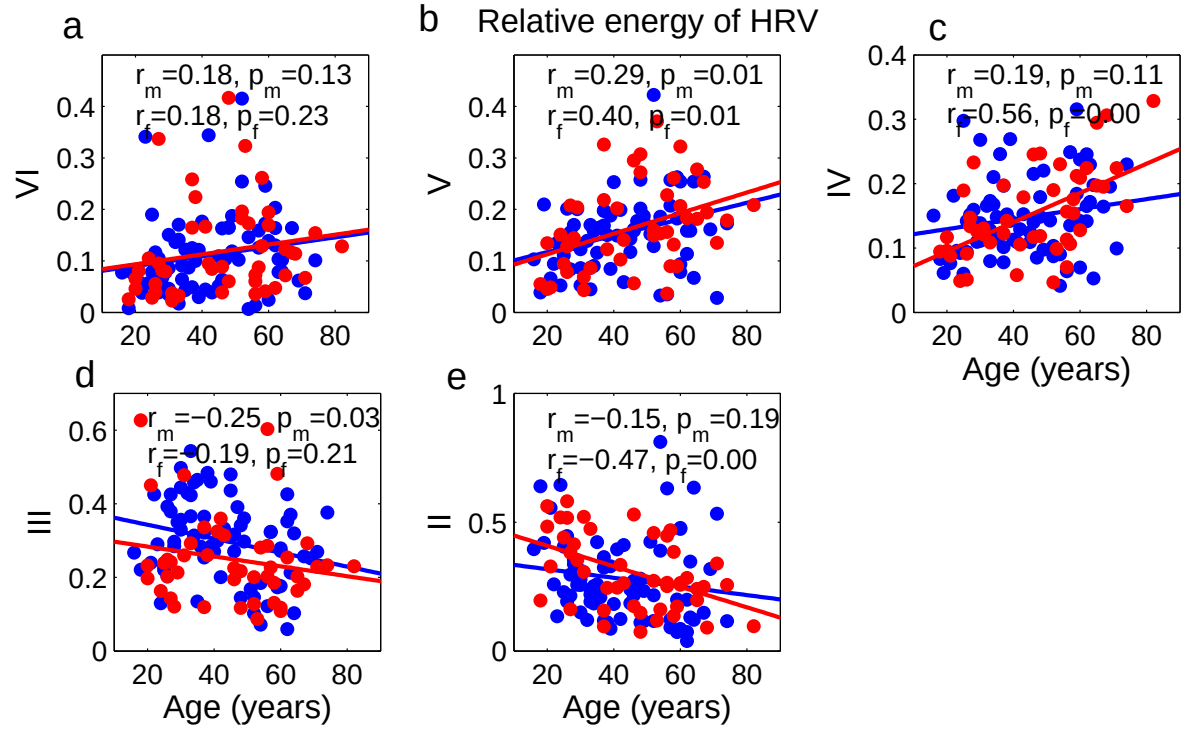

Fig. 7.5: Relative energy in interval VI (a), V (b), IV (c), III (d), II (e).

Relative energy for HRV				
	males		females	
Interval	r	p	r	p
VI	0.18	0.13	0.18	0.23
V	0.29	0.01	0.40	0.01
IV	0.19	0.11	0.56	0.00
III	-0.25	0.03	-0.19	0.21
II	-0.15	0.19	-0.47	0.00

Tab. 7.3: Summary table for age-related changes in relative energy

There is a significant gender difference in absolute energy of interval II in the younger population below 40 years ($p = 0.01$): energy of females are higher than that of males. For relative amplitude, there are significant differences in interval III in the younger population ($p = 0.02$) and in interval II in the younger population ($p = 0.05$). It means that RSA is relatively (and absolutely) stronger for females than for males, whereas the myogenic modulation is relatively stronger for males than females in the younger population.

Gender difference (HRV)				
	Absolute energy		Relative energy	
	below 40 years	above 55 years	below 40 years	above 55 years
Total	$p = 0.09$	$p = 0.44$		
VI	$p = 0.41$	$p = 0.63$	$p = 0.59$	$p = 0.53$
V	$p = 0.56$	$p = 0.40$	$p = 0.53$	$p = 0.64$
IV	$p = 0.12$	$p = 0.75$	$p = 0.22$	$p = 0.61$
III	$p = 0.74$	$p = 0.43$	$p = 0.02$ (m)	$p = 0.36$
II	$p = 0.01$ (f)	$p = 0.06$	$p = 0.05$ (f)	$p = 0.39$

Tab. 7.4: Gender differences between females and males in the results of wavelet analysis of HRV. (m) means that energy for males is significantly higher than that of females and (f) vice versa.

7.2.2 Oscillatory components in the blood flow signal

In this section, we discuss the oscillatory components in blood flow signals. The blood is pumped out from the heart, goes into arteries and arterioles, then branches into capillaries, integrates into veins and comes back to the heart again. Thus the cardiovascular system forms a closed loop of vessels, as first reported by the British physiologist William Harvey in 1628. The cardiac output circulates throughout

the body and is determined by the product of the heart rate and the stroke volume. The amount of the cardiac output is around 5 liters per minute. The oscillation of blood flow propagates from the heart into the microcirculation including the sites on the right wrist, on the inner right ankle and at two sites on the left arm, where we measured the basal flows and the flow with ACh and SNP as we described in chapter 3. One of the blood flow signals is shown in Fig. 3.4.

7.2.2.1 Absolute energy

All the blood flow signals were resampled from 400 Hz to 10 Hz and detrended as discussed in subsection 6.4.2. Then the wavelet analysis was applied to them. The wavelet transform calculated from the signal measured with ACh in Fig. 3.4a is shown in Fig. 7.6, and a time-averaged Wavelet amplitude is shown in Fig. 7.7. The wavelet transform calculated from the signal measured with SNP in Fig. 3.4b is shown in Fig. 7.8, and a time-averaged segment is shown in Fig. 7.9. These signals with ACh and SNP are from the same subject. The six peaks, the physiological origins of which have already been discussed in section 7.2.1, were observed. As we explained in chapter 3, the two vasodilators, ACh and SNP, were applied to assess the change in endothelial function with age. The six peaks still exist but the strength of these oscillatory components is different from endothelial-dependent ACh to endothelial-independent SNP in several intervals as shown in these wavelet results. For example, in this case, the peak at the lowest frequency for ACh is higher than that for SNP. It has to be emphasized again that we measured the signals with ACh and SNP in close proximity (2-5 cm apart) with similar vasculature, on the same person, simultaneously, which indicates the differences come from different actions of the two different substances. The different effect of the substances was documented in a large number of studies with respect to the oscillatory components. The difference with respect to the average flow and energies have to be established.

Age-related changes in average flow and total energy are shown in Fig. 7.10, those in absolute energy for ACh in Fig. 7.11, and in absolute energy for SNP in Fig. 7.12. A summary of these results is shown in Tab. 7.5. If a few outliers changes results of the significant tests, I got rid of the outliers and showed the results after the removal of them.

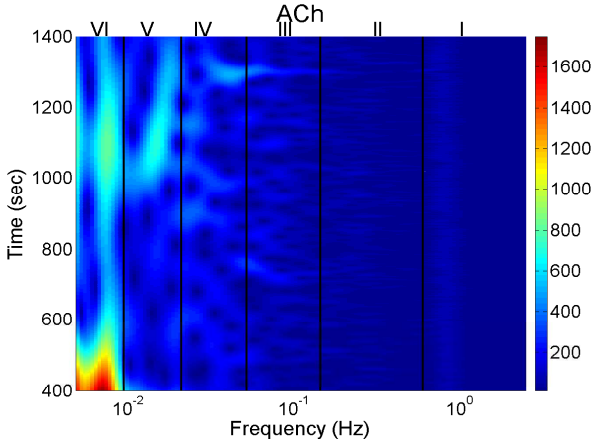

Fig. 7.6: The time frequency domain of wavelet transform of blood flow with ACh.

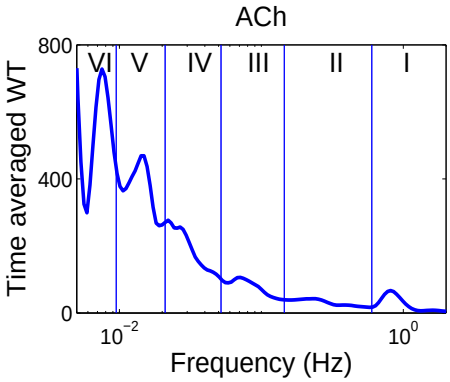

Fig. 7.7: The time-averaged amplitude of blood flow with ACh.

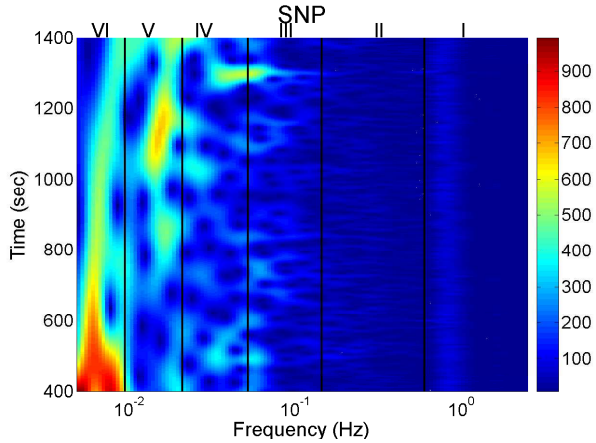

Fig. 7.8: The time frequency domain of wavelet transform of blood flow with SNP.

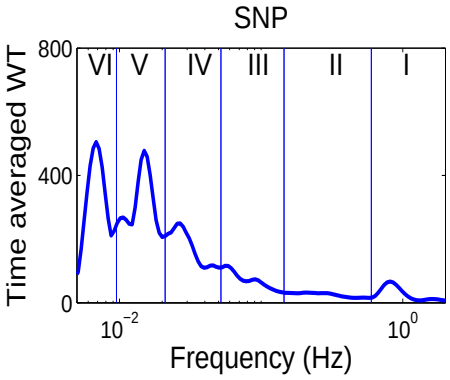

Fig. 7.9: The time-averaged amplitude of blood flow with SNP.

Average flow does not change with age for either ACh or SNP. The total amplitude with ACh increases significantly with age for males but decreases significantly with age for females. It is because the absolute energy in intervals VI and V decreases significantly with age for females, and because the absolute energy in interval I increases significantly with age for males. Actually there are significant gender differences for ACh in interval VI and V as shown in Tab. 7.7. Young females have higher energy in the endothelial related intervals than young males.

The total energy for SNP increases with age for females because of the increase in the absolute energies in the interval I and II.

The differences between ACh and SNP of absolute energy are summarized in Tab. 7.6. For females, the absolute energy with ACh is higher than those with SNP in interval VI, both in the younger population and the aged population in interval V in the younger population whereas for males the absolute energy with ACh is higher in intervals VI and V in the younger population. We can say that with age, humans tend to lose the differences in response to ACh and SNP in intervals V or VI compared to SNP.

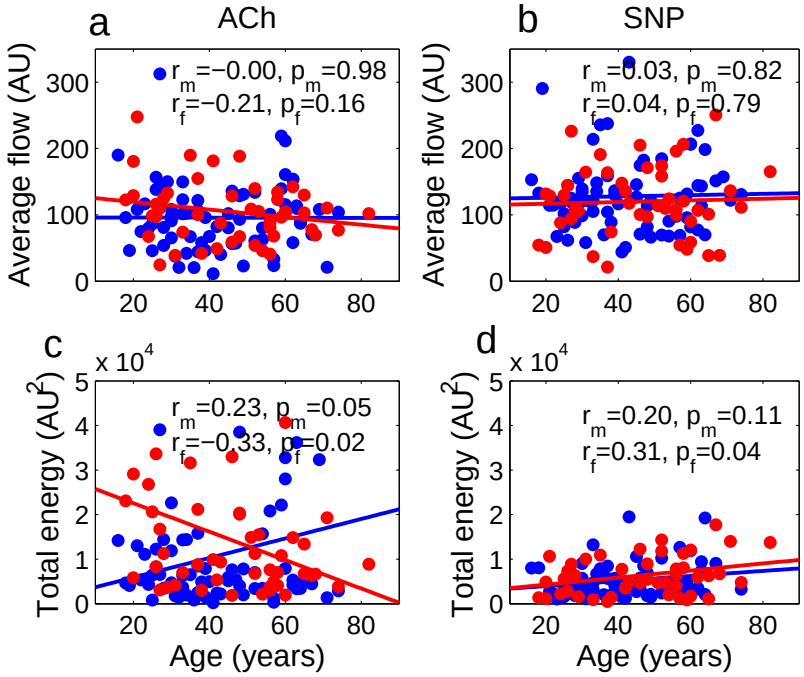

Fig. 7.10: The correlation between age and average flow with ACh (a), average flow with SNP (b), total energy with ACh (c) and total energy with SNP (d).

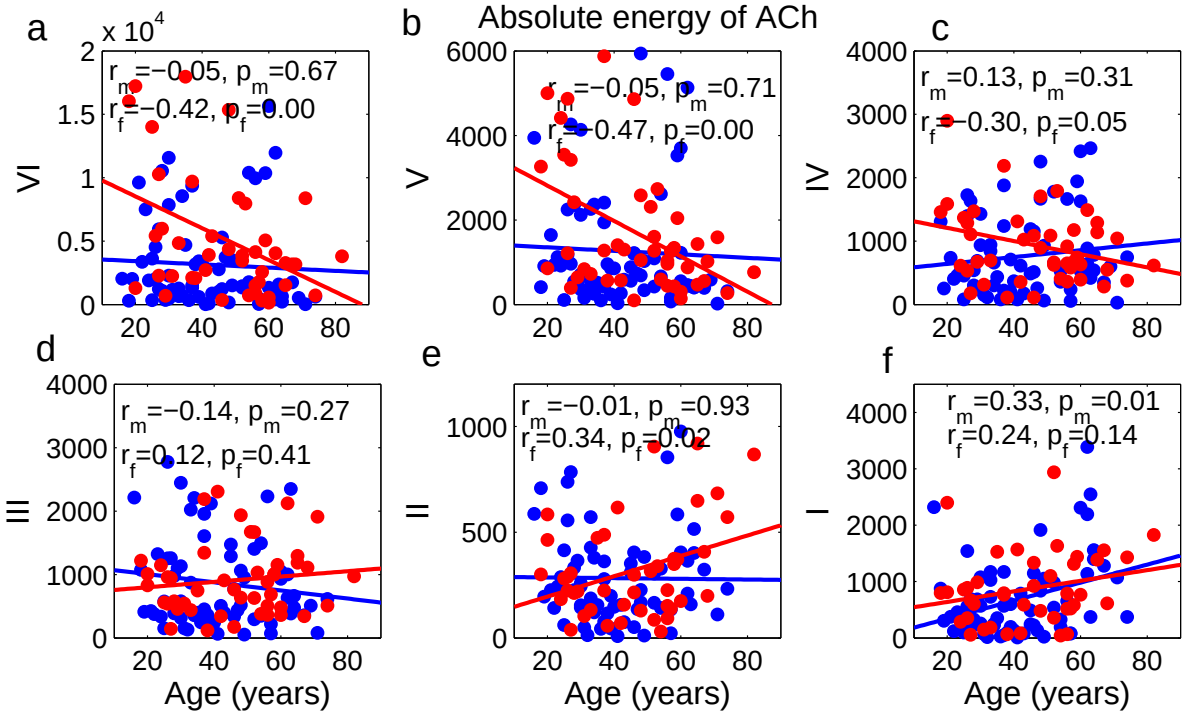

Fig. 7.11: The correlation with age and absolute energy in interval VI (a), V (b), IV (c), III (d), II (e), I (f) for ACh.

Absolute energy								
	males				females			
	ACh		SNP		ACh		SNP	
Interval	r	p	r	p	r	p	r	p
Average flow	-0.00	0.98	0.03	0.82	-0.21	0.16	0.04	0.79
Total energy	0.23	0.05	0.20	0.11	-0.33	0.02	0.31	0.04
VI	-0.05	0.67	0.18	0.15	-0.42	0.00	-0.17	0.26
V	-0.05	0.71	0.16	0.21	-0.47	0.00	-0.16	0.30
IV	0.13	0.31	-0.00	0.99	-0.30	0.05	0.01	0.96
III	-0.14	0.27	0.09	0.51	0.12	0.41	0.24	0.13
II	-0.01	0.93	0.15	0.25	0.12	0.41	0.31	0.05
I	0.33	0.01	0.20	0.11	0.24	0.14	0.37	0.01

Tab. 7.5: Summary table for age-related changes in average flow, total energy and absolute energy.

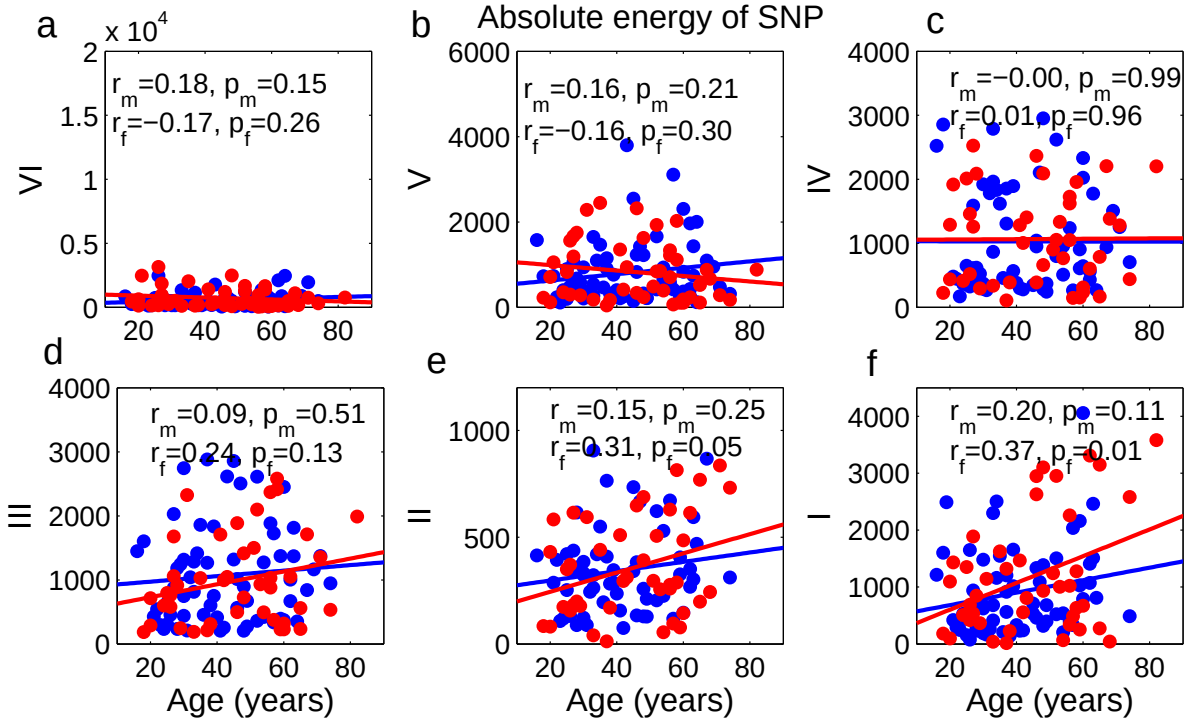

Fig. 7.12: The correlation with age and absolute energy in interval VI (a), V (b), IV (c), III (d), II (e), I (f) for SNP.

The difference between ACh and SNP for absolute energy				
	Males		Females	
	below 40 years	above 55 years	below 40 years	above 55 years
Average flow	$p = 0.00$ (S)	$p = 0.22$	$p = 0.86$	$p = 0.61$
Total energy	$p = 0.28$	$p = 0.95$	$p = 0.01$ (A)	$p = 0.56$
Interval VI	$p = 0.00$ (A)	$p = 0.24$	$p = 0.00$ (A)	$p = 0.00$ (A)
Interval V	$p = 0.03$ (A)	$p = 0.92$	$p = 0.01$ (A)	$p = 0.09$
Interval IV	$p = 0.11$	$p = 0.13$	$p = 0.96$	$p = 0.43$
Interval III	$p = 0.35$	$p = 0.06$	$p = 0.91$	$p = 0.65$
Interval II	$p = 0.10$	$p = 0.97$	$p = 0.69$	$p = 0.65$
Interval I	$p = 0.08$	$p = 0.91$	$p = 0.96$	$p = 0.44$

Tab. 7.6: The difference in average flow, total energy and absolute energy between ACh and SNP. (A) means that ACh is significantly higher than SNP and (S) vice versa.

Gender difference for absolute energy				
	ACh		SNP	
	below 40 years	above 55 years	below 40 years	above 55 years
Average flow	$p = 0.19$	$p = 0.45$	$p = 0.55$	$p = 0.17$
Total energy	$p = 0.01$ (f)	$p = 0.87$	$p = 0.65$	$p = 0.44$
Interval VI	$p = 0.00$ (f)	$p = 0.35$	$p = 0.77$	$p = 0.23$
Interval V	$p = 0.00$ (f)	$p = 0.59$	$p = 0.60$	$p = 0.19$
Interval IV	$p = 0.07$	$p = 1.0$	$p = 0.73$	$p = 0.40$
Interval III	$p = 0.85$	$p = 0.43$	$p = 0.28$	$p = 0.37$
Interval II	$p = 0.83$	$p = 1.0$	$p = 0.31$	$p = 0.61$
Interval I	$p = 0.17$	$p = 0.68$	$p = 0.70$	$p = 0.28$

Tab. 7.7: Gender differences in average flow, total energy and absolute energy of ACh (the left side) and SNP (the right side). (m) means that males' are significantly higher than females' and (f) vice versa.

7.2.2.2 Relative energy

When we measured blood flow signals, we chose measurement sites such that the density of vessels would be same for all the subjects in the measurement area. However, it is still difficult to get exactly the same density because we can not determine the microvasculature under the skin, and because every subject has a different condition of the skin. For this reason, relative energy was calculated so that we could see a normalized value in each interval by dividing the absolute energy by the total energy.

Age-related changes in relative energy with ACh and SNP are shown in Figs. 7.13 and 7.14, respectively and a summary is shown in Tab. 7.8. There is a trend that the relative contribution decreases in intervals VI and V and increases in interval I. The decrease in the relative energy in the intervals VI and V brought partly by the increase in the absolute energy in the intervals I and II. The substance difference is summarized in Tab. 7.9 and the gender difference in Tab. 7.10, for relative energy. For substance differences, the relative contribution of interval VI (endothelial) is higher for ACh than SNP while the other intervals except V are higher in SNP. For gender differences, the energy for females are higher in interval VI whereas the energy for males are higher in intervals III and II in the younger population. However these gender differences disappear in the aged population.

It should be noted that the results of the relative energy has an important

meaning related to DFA as explained in subsection 7.4.

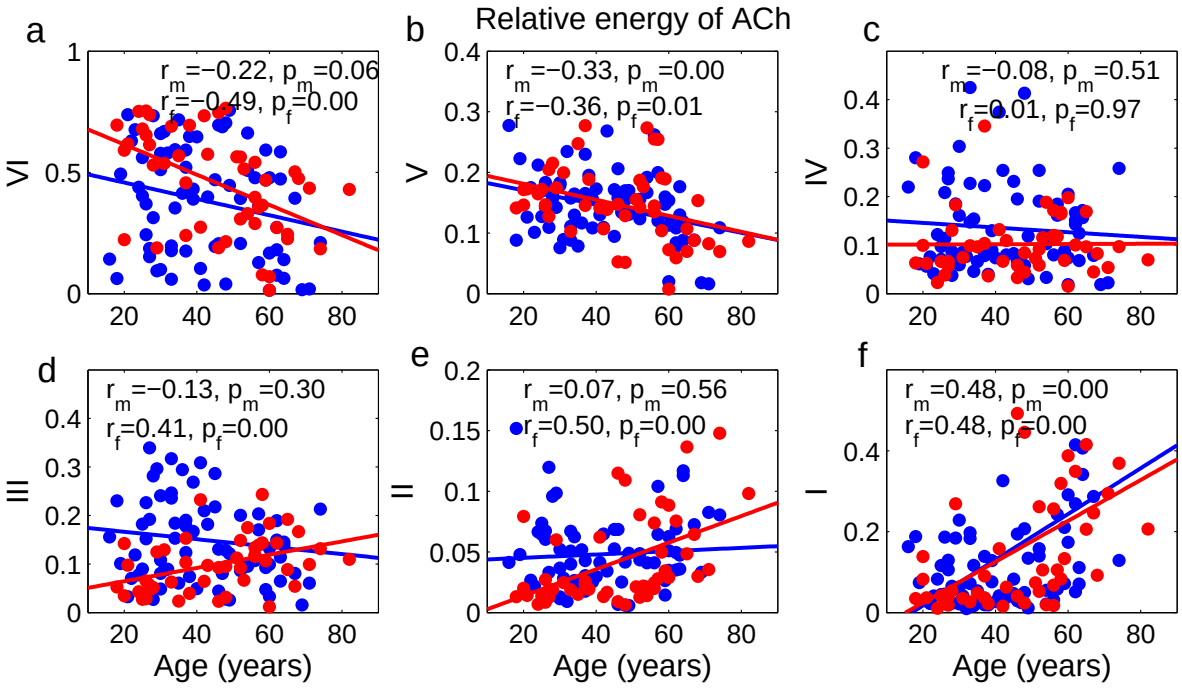

Fig. 7.13: The correlation with age and relative energy in interval VI (a), V (b), IV (c), III(d), II(e), I(f) for ACh.

7.3 Discussion

7.3.1 The HRV signals

Physiological reasons why the gender effect in the interval II exists are a matter for discussion. It is reported in [31]that gender and communal trait such as quarrelsome or agreeable affects the strength of RSA. This may indicate that vagal activity is important for controlling RSA. It also reported in [31] that men had lower RSA values than women in the quarrelsome condition. Combined with the fact which we found that gender effects do not survive after 55 years, we may conclude that the change in the hormonal state of females is one of the reasons for differences in RSA.

The increase with age of relative energy in the interval VI and V comes from the decrease of absolute energy in the interval II and III. The age-related changes in relative energy itself do not indicate the strength of physiological origins. However,

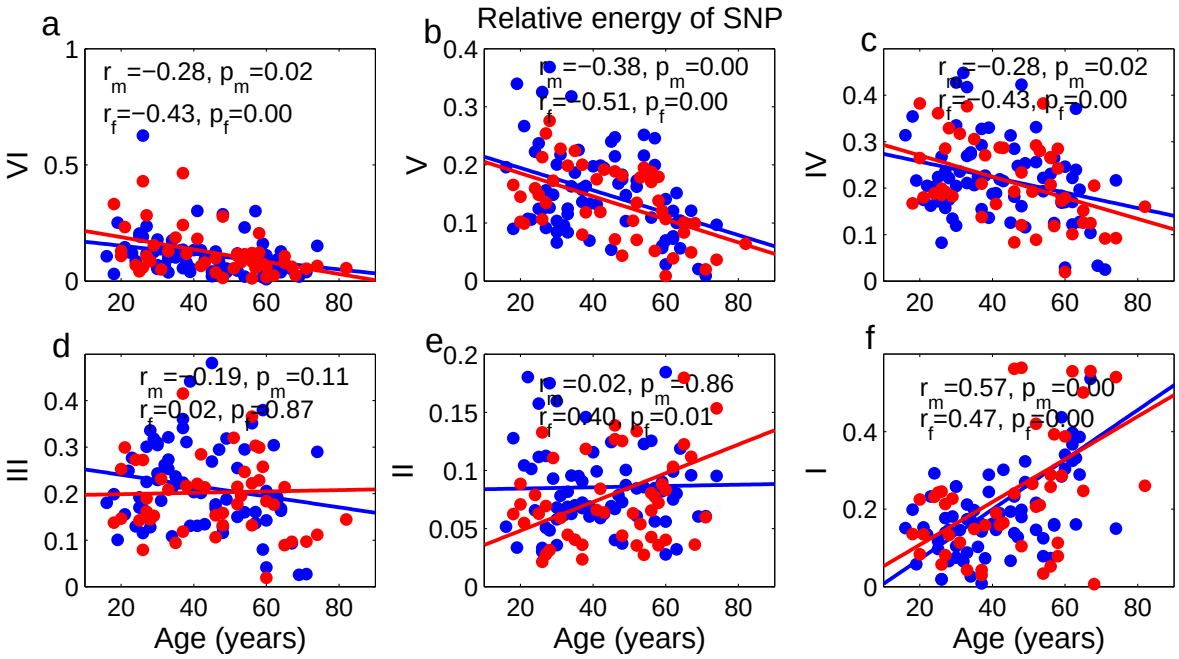

Fig. 7.14: The correlation with age and relative energy in interval VI (a), V (b), IV (c), III(d), II(e), I(f) for SNP.

Relative energy								
	males				females			
	ACh		SNP		ACh		SNP	
Interval	r	p	r	p	r	p	r	p
VI	-0.22	0.06	-0.28	0.02	-0.49	0.00	-0.43	0.00
V	-0.33	0.00	-0.51	0.00	-0.36	0.01	-0.38	0.00
IV	-0.08	0.51	-0.28	0.02	0.01	0.97	-0.43	0.00
III	-0.13	0.30	-0.19	0.11	-0.41	0.00	0.02	0.87
II	0.07	0.56	0.02	0.86	0.50	0.00	0.40	0.01
I	0.48	0.00	0.57	0.00	0.48	0.00	0.47	0.00

Tab. 7.8: Summary table for age-related changes in relative energy.

The difference between ACh and SNP for relative energy				
	Males		Females	
	below 40 years	above 55 years	below 40 years	above 55 years
Interval VI	$p = 0.00$ (A)	$p = 0.00$ (A)	$p = 0.00$ (A)	$p = 0.00$ (A)
Interval V	$p = 0.94$	$p = 0.25$	$p = 0.67$	$p = 0.274$
Interval IV	$p = 0.00$ (S)	$p = 0.04$ (S)	$p = 0.00$ (S)	$p = 0.02$ (S)
Interval III	$p = 0.00$ (S)	$p = 0.14$	$p = 0.00$ (S)	$p = 0.06$
Interval II	$p = 0.00$ (S)	$p = 0.02$	$p = 0.00$ (S)	$p = 0.05$
Interval I	$p = 0.00$ (S)	$p = 0.13$	$p = 0.00$ (S)	$p = 0.20$

Tab. 7.9: The difference in average flow, total energy and relative energy between ACh and SNP. (A) means that ACh is significantly higher than SNP and (S) vice versa.

Gender difference for relative energy				
	ACh		SNP	
	below 40 years	above 55 years	below 40 years	above 55 years
Interval VI	$p = 0.01$ (f)	$p = 0.51$	$p = 0.19$	$p = 0.70$
Interval V	$p = 0.13$	$p = 0.73$	$p = 0.54$	$p = 0.95$
Interval IV	$p = 0.15$	$p = 0.80$	$p = 0.69$	$p = 0.78$
Interval III	$p = 0.00$ (m)	$p = 0.73$	$p = 0.08$	$p = 0.57$
Interval II	$p = 0.00$ (m)	$p = 0.95$	$p = 0.05$	$p = 0.95$
Interval I	$p = 0.15$	$p = 0.95$	$p = 0.90$	$p = 0.80$

Tab. 7.10: Gender difference in average flow, total energy and relative energy with ACh (the left side) and SNP (the right side). (m) means that energy for males is significantly higher than that of females and (f) vice versa.

relative energy affects the complexity of the HRV signals and help to characterize the HRV signals in a different way from absolute energy.

7.3.2 The blood flow signals

A difference in spectral energy between ACh and SNP was observed in intervals VI and V especially for younger subjects. It is thought that higher energies in these intervals were produced by the endothelial activities and young females have higher endothelial function than younger males and aged subjects. It is well known that younger females have less cardiovascular risk than males and aged females. Our results support the idea that the higher endothelial activity which generates the oscillations in interval V and VI leads to a healthier cardiovascular function. On the other hand, the oscillations in the interval I tend to increase with age. It may indicate that external pumping such as heart or respiration dominate, rather than the vessel function, determine the circulation the required amount of blood in the aged population. It might be assumed that the vessels lose elasticity and ability to dilate by themselves through endothelial response decreasing with age and the heart has to work harder. The fact that average flow does not change means that peripheral resistance increases with age, and the hard pumping work of the heart and the increasing stiffness and high resistance of the vessels with increasing age might cause cardiovascular problems such as high blood pressure.

In summary, aging is associated with a decrease of endothelial oscillation and an increase of cardiac oscillation in dilating blood flow.

7.4 The relationship with complexity analysis

7.4.1 Hypothesis

It can be seen that HRV signals have less variability when people get older. The reason is the decrease of RSA and myogenic effects with increasing age. The decrease in RSA is well known, and our result of subsection 7.2.1 is in agreement with it [89]. How the coupling between cardiac and respiratory or cardiac and myogenic systems changes with age needs to be studied.

Now we discuss the relationship between the results of wavelet analysis of HRV and those of the complexity analysis in the previous chapter. As we have already discussed, the HRV signals of younger people are more complex than those of aged

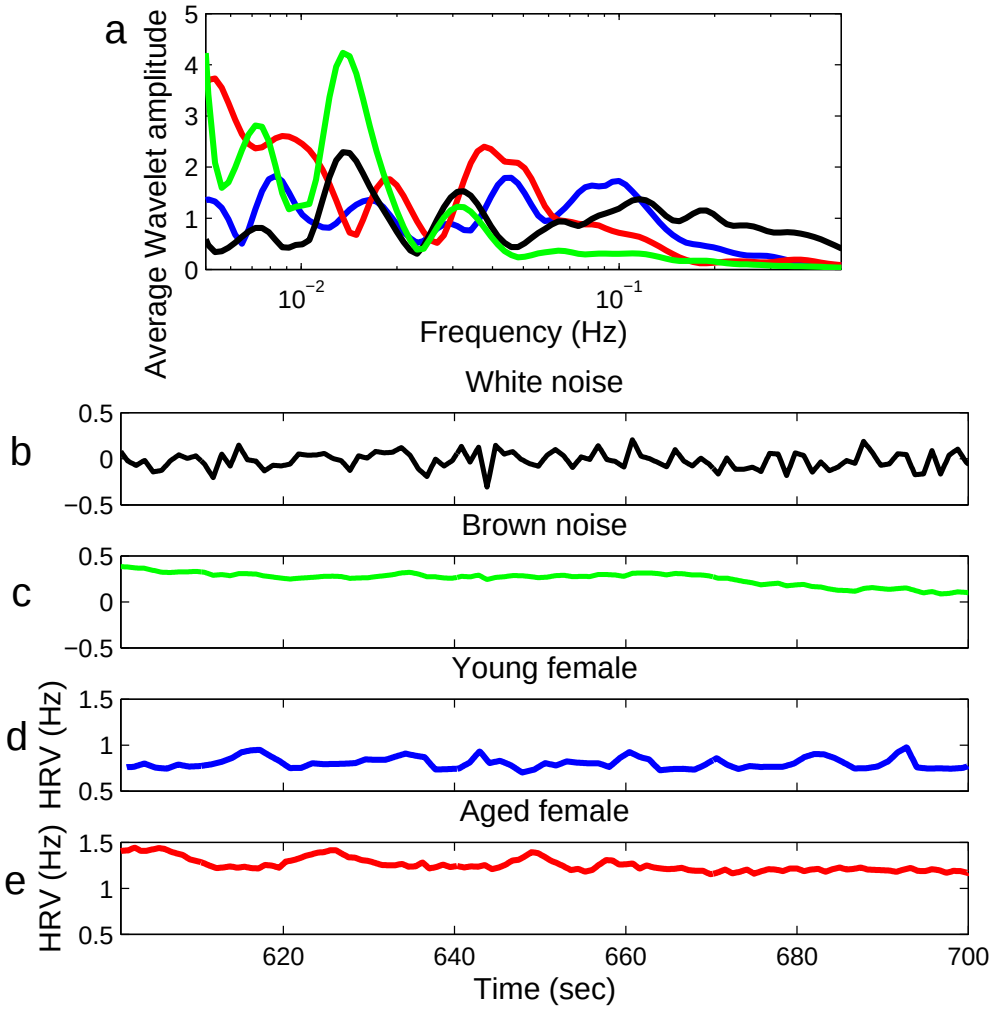

Fig. 7.15: The time average wavelet amplitude of white noise (black), brown noise (green), the heart rate of a young females (blue) and the heart rate of an aged female (red)are shown in (a). The correspondent time series for 100 seconds of white noise (b), brown noise (c), and the heart rate of a young female (d), and the heart rate of an aged female (e). The heart rate of a young female is closer to white noise than that of an aged female because of stronger fluctuations in the higher frequency intervals.

people. It is expected that the shape of the signals of young people are closer to white noise whereas those of aged people are closer to brown noise in the time scale from 10 to 50 seconds. To see the differences of four HRV signals, white noise, brown noise and HRV of a young and an aged person, 100 seconds of these signals are shown in Fig. 7.15. The brown noise looks smoother than the white noise because brown noise has a higher ratio of slow oscillations to fast oscillations than white noise. The HRV of the aged female also looks smoother than that of a young female for the same reason.

The range from 10 to 50 seconds, where the exponents α_i increase significantly with age, corresponds to intervals III and IV. It can be assumed that these aging effects on α_i comes from the significantly increasing ratio of wavelet energy in the slower oscillations in interval IV over wavelet energy in the faster oscillations in interval III with age for males ($r = 0.32,\ p = 0.01$) and for females ($r = 0.42,\ p = 0.00$) as shown in Fig. 7.16a. The aging effect of α_l cannot been seen in the longer time scale from 50 to 300 seconds, which correspond to interval V and VI. This could be because the ratio of wavelet energy of the slower oscillation in interval VI over the faster oscillation in interval V doesn't change significantly with age for males ($r = 0.02,\ p = 0.84$) or for females ($r = -0.12,\ p = 0.45$) as shown in Fig. 7.16b. This assumption will be proved correct by using a simple model in subsection 7.4.2.

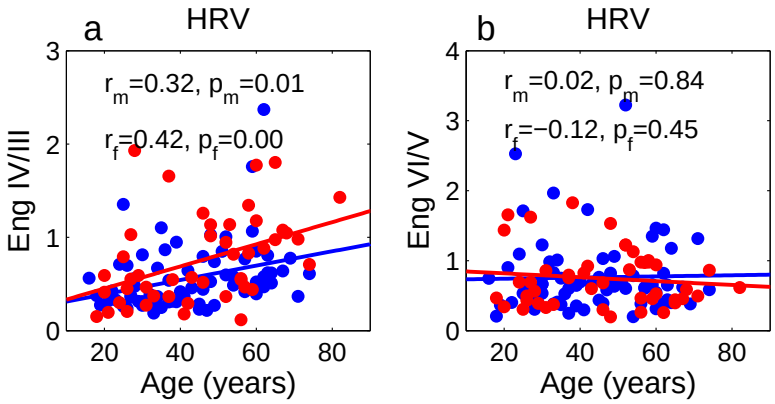

Fig. 7.16: The energy in the interval IV over III (a) and that in the interval VI over V (b).

The exponent α decreases with age both for ACh and SNP. It can be explained by that fact that the relative energy of the slower oscillation (the intervals VI and

V) decrease with age and the relatvie energy of the faster oscillation (the intervals I and II) increase with age as shown in Fig 7.13 and Fig 7.14.

7.4.2 Proof by models

As we explained in section 6.3, there is a relationship between the exponent calculated by DFA and the power spectrum (or auto-correlation function) of the time series. Although the signals which we measured here did not necessarily have power-law correlations, we have assumed that the ratio between the wavelet energy of the faster oscillations and that of the slower oscillations is related to the complexity exponent. In this subsection, we will prove our assumption by using simple models.

The ratio of wavelet energy reflects ${B_s}^2/{B_f}^2$, where B_s and B_f are the amplitude of the slower oscillation and that of the faster oscillation, respectively. To see the case of HRV, we took the time series as $\sin(0.2\pi t)+B\sin(0.02\pi t)$. We changed the amplitude B and calculated the exponent α for each case. It should be noted that the exponent is affected by the ratio between the two amplitudes, but not by the amplitude itself, because $\alpha(\sin(0.2\pi t)+B\sin(0.02\pi t))$ has the same exponent for all values of α. The original signals are shown in Fig. 7.17 and the results of complexity analysis are shown in Fig. 7.18. The exponent α is equal to 0.72 when $B = 0.5$, and 1.27 when $B = 1.5$. Thus if the amplitude B increases, the exponent α increases and the complexity decreases. This confirms in the case of HRV signals that the effect of aging on the self-similar parameter of intermediate time scale α_i is caused by the ratio between the amplitude of the slower oscillation (interval IV) and that of the faster oscillation (interval III) as shown in Fig. 6.3a.

In terms of the blood flow signals measured with ACh and SNP, it is more complicated to confirm the hypothesis because they contained not only two but at least six peaks in the range of n which are analyzed. To see the example, we took the model, $B_1\sin(2\pi t) + \ 0.7\sin(0.2\pi t) + \ 0.7\sin(0.06\pi t) + \ B_4\sin(0.014\pi t)$. We have to keep total energy and change the relative energy since absolute energy does not change the DFA exponent but relative energy does. As the age-related change in relative energy in Fig. 7.13 and 7.14 shows, the fastest oscillation becomes relatively stronger and the slowest oscillation becomes weaker when people get older. In order to imitate the properties, $B_1 = 1.5$ and $B_4 = 0.5$ was chosen for an

aged subject shown in Fig. 7.19a and $B_1 = 0.5$ and $B_4 = 1.5$ for a young subject shown in Fig. 7.19b. For the aged subject, α is equal to 0.78, and for the young subject, α is equal to 1.24. When the relative energy of the slowest frequency becomes bigger, the exponent also becomes bigger. Even though the real blood flow signal is more complicated, it seems valid that the ratio between the slower oscillation (interval VI or V) and the faster oscillation (interval II and I) is related to the self-similar exponent obtained by DFA. The reason the exponent decreases significantly with age is that the slower oscillation is relatively stronger in the younger population than in the aged population.

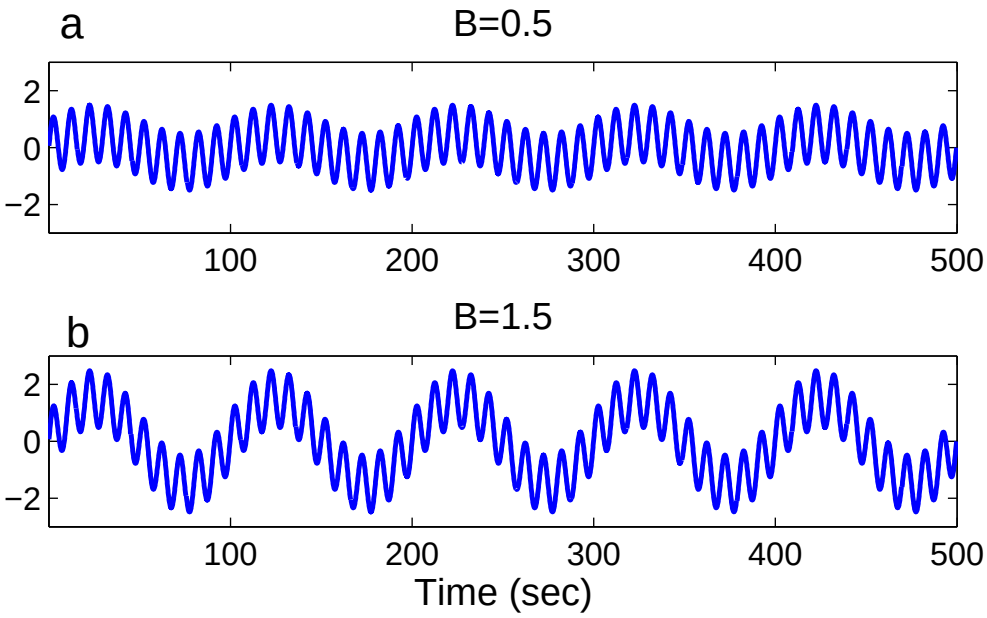

Fig. 7.17: The time series of $\sin(0.2\pi t) + B\sin(0.02\pi t)$. $B = 0.5$ (a), $B = 1.5$ (b).

It has to be noted that we can apply the theory only in the regime where the slope between $\log(F(n))$ and $\log(n)$ can be determined uniquely. If the slope changes dramatically at any point, it means that DFA cannot appropriately be applied and the relation between DFA and spectral analysis does not hold either.

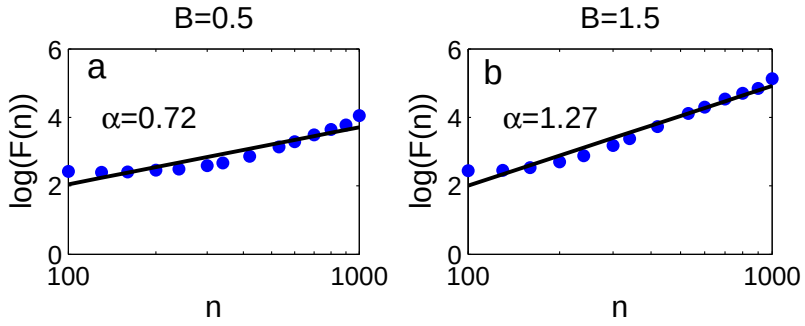

Fig. 7.18: The log-log plot between F and n for $\sin(0.2\pi t) + B\sin(0.02\pi t)$. $B = 0.5$ (a), $B = 1.5$ (b).

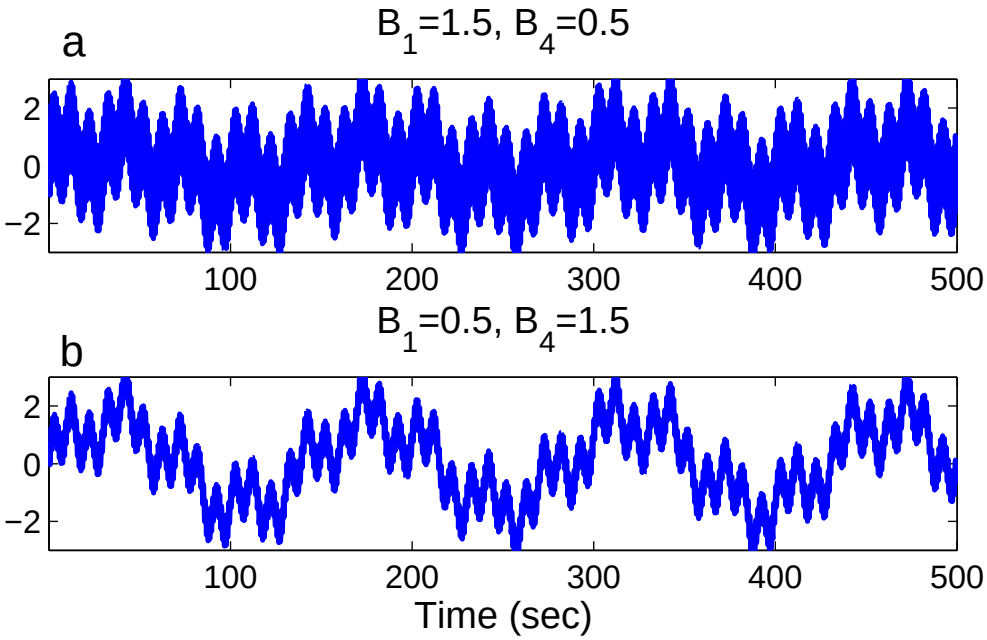

Fig. 7.19: The time series of $B_1\sin(2\pi t) + 0.7\sin(0.2\pi t) + 0.7\sin(0.06\pi t) + B_4\sin(0.014\pi t)$. $B_1 = 1.5$, $B_4 = 0.5$ (a), $B_1 = 0.5$, $B_4 = 1.5$ (b).

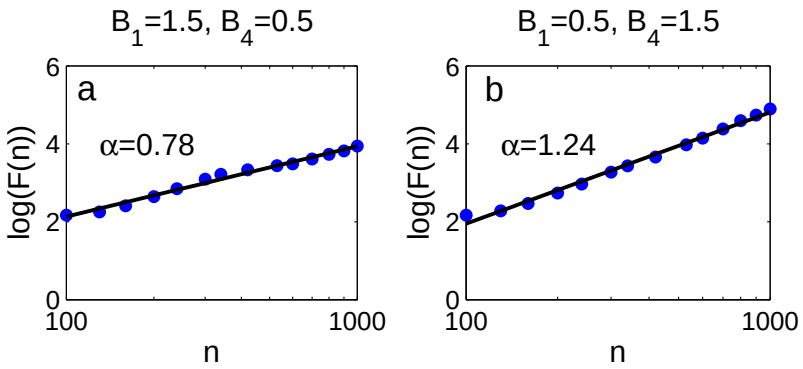

Fig. 7.20: The log-log plot between F and n for $B_1 \sin(2\pi t) + 0.7\sin(0.2\pi t) + 0.7\sin(0.014\pi t) + B_4 \sin(0.06\pi t)$. $B_1 = 1.5$, $B_4 = 0.5$ (a), $B_1 = 0.5$, $B_4 = 1.5$ (b).

8. CARDIORESPIRATORY INTERACTION

The cardiac and respiratory systems are known to be coupled by several mechanism [19], for example, neurologically [49] and mechanically [18]. In the previous section, we discussed one form of cardiorespiratory interaction, the modulation of heart rate by the respiratory system, as well as the modulation by other physiological processes. In this section, we discuss another form of the interaction between the cardiac and respiratory systems, cardiorespiratory synchronization as reported in the study of anesthetized rats [136], young healthy athletes [126, 127], infants [103], healthy adults [148, 88, 149] and heart transplant patients [149]. As discussed in [102], modulation and synchronization can be competing process. In this section, we study the effect of aging on cardiovascular synchronization and compare it with the results of the other sections.

As we saw in section 5.1, in the case that oscillators have weak coupling, or there is a weak external force, the perturbation influences only the phase. This means that the oscillation can be described by only one variable, the phase. Here, we discuss phase synchronization under the assumption that the cardiorespiratory interaction is weak enough to be described by phase dynamics.

8.1 Theory of a pair of coupled oscillators

In this section, we discuss the case where two nonlinear oscillators which are almost identical interact weakly with others. The dynamics of two oscillators is given by

$$\frac{d\mathbf{X_1}}{dt} = \mathbf{F}(\mathbf{X_1}) + \delta\mathbf{F_1}(\mathbf{X_1}) + \mathbf{V_{12}}(\mathbf{X_1}, \mathbf{X_2}), \tag{8.1}$$

$$\frac{d\mathbf{X_2}}{dt} = \mathbf{F}(\mathbf{X_2}) + \delta\mathbf{F_2}(\mathbf{X_2}) + \mathbf{V_{21}}(\mathbf{X_2}, \mathbf{X_1}). \tag{8.2}$$

The dynamics of two oscillators is supposed to be closed. Then $\mathbf{F}(\mathbf{X})$ is the common structure for both oscillators and $\delta\mathbf{F}(\mathbf{X_i})$ is the deviation from $\mathbf{F}(\mathbf{X_i})$. $\mathbf{V_{12}}(\mathbf{X_1}, \mathbf{X_2})$ and $\mathbf{V_{21}}(\mathbf{X_2}, \mathbf{X_1})$ represent the interaction term. By this expression, the phases of oscillator 1 and 2 can be defined commonly based on the dynamics

of $\mathbf{F}(\mathbf{X})$. Then in the same way as in previous subsections, the dynamics of the oscillators is

$$\frac{d\phi_1}{dt} = \omega + (\mathbf{U}^*, \delta\mathbf{F_1}(\phi_1) + \mathbf{V_{12}}(\phi_1, \phi_2)), \tag{8.3}$$

$$\frac{d\phi_2}{dt} = \omega + (\mathbf{U}^*, \delta\mathbf{F_2}(\phi_2) + \mathbf{V_{21}}(\phi_2, \phi_1)), \tag{8.4}$$

which is defined by the Eq. (5.7). New variables are introduced as $\phi_{1,2} = \omega t + \psi_{1,2}$ and, by averaging, the equations of ψ are expressed as

$$\frac{d\psi_1}{dt} = \delta\omega_1 + \Gamma_{12}(\psi_1 - \psi_2), \tag{8.5}$$

$$\frac{d\psi_2}{dt} = \delta\omega_2 + \Gamma_{21}(\psi_2 - \psi_1), \tag{8.6}$$

where

$$\delta\omega_{1,2} = \frac{1}{2\pi}\int_0^{2\pi} d\theta(\mathbf{U}^*(\theta + \psi_{1,2}), \delta\mathbf{F_{1,2}}(\theta + \psi_{1,2})), \tag{8.7}$$

$$\Gamma_{12}(\psi_1 - \psi_2) = \frac{1}{2\pi}\int_0^{2\pi} d\theta(\mathbf{U}^*(\theta + \psi_1), \mathbf{V_{12}}(\theta + \psi_1, \theta + \psi_2)). \tag{8.8}$$

When the interaction is symmetric as $\mathbf{V_{21}}(\mathbf{X_2}, \mathbf{X_1}) = \mathbf{V_{21}}(\mathbf{X_2}, \mathbf{X_1}) \equiv \mathbf{V}(\mathbf{X_1}, \mathbf{X_2})$, it is clear that $\Gamma_{12}(\psi) = \Gamma_{21}(\psi) = \Gamma(\psi)$. In that case, the dynamics of the difference of the two phases $\psi = \psi_1 - \psi_2$ is written as

$$\frac{d\psi}{dt} = \delta\omega + \Gamma_a(\psi). \tag{8.9}$$

where $\delta\omega = \delta\omega_1 - \delta\omega_2$ and $\Gamma_a(\psi) = \Gamma(\psi) - \Gamma(-\psi)$. It has to be noted that $\Gamma_a(0) = \Gamma_a(\pi) = \Gamma_a(-\pi) = 0$. If ψ is constant, it means that the two oscillators are synchronized. This synchronization solution ψ = constant corresponds to $d\psi/dt = 0$ in the Eq. (8.9). Therefore whether synchronization occurs depends on whether the right hand side of Eq. (8.9) has a zero solution and whether the zero solution is stable or not. From this, it is concluded that synchronization occurs if $\delta\omega$ is within a range shown as Fig. 8.1. For example, if the coupling function is a simple sine function like $\Gamma(\psi) = -K\sin(\psi)$, the condition which the frequency difference has to satisfy is $|\delta\omega/K| < 1$.

If phase-locking occurs and $\psi = \psi_0$ (in other words, if ψ_0 is a stable fixed point), the frequency of both oscillators via entrainment becomes $\omega + \delta\omega_1 + \Gamma(\psi_0)$, which is equal to $\omega + \delta\omega_2 + \Gamma(-\psi_0)$.

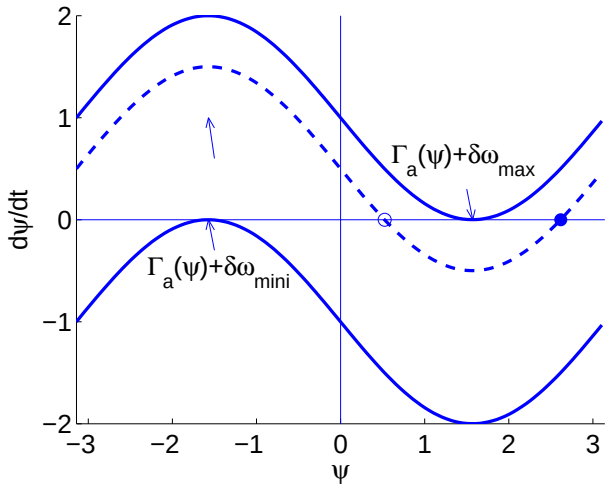

Fig. 8.1: The plot between $d\psi/dt$ and ψ. The two solid curves have a minimum or maximum $\delta\omega$ which allows the curves to cross $d\psi/dt = 0$. The crossing point is the value where the phase-locking occurs. The dashed curve has $\delta\omega$ between the minimum and maximum. The open circle represents a stable fixed point and the solid circle an unstable fixed point.

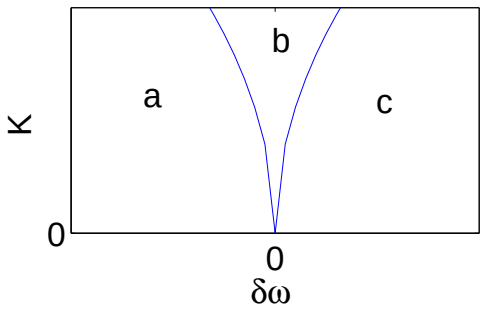

Fig. 8.2: This shows the synchronous region in the $K - \delta\omega$ plane. The region b is one where phase locking occurs and called Arnold tongue whereas the regions a and c are ones where phase locking doesn't occur.

For each coupling strength of K, there is the range of $\delta\omega$ where phase-locking occurs. We can calculate this region in the $K - \delta\omega$ plane, which is called the *Arnold tongue*.

In the case of n:m synchronization, we can carry through a similar discussion by thinking in terms of $n\psi_1$ and $m\psi_2$.

If an oscillator is coupled with many oscillators according to

$$\frac{d\mathbf{X_i}}{dt} = \mathbf{F}(\mathbf{X_i}) + \delta\mathbf{F_i}(\mathbf{X_i}) + \sum_{j=1}^{N} \mathbf{V_{ij}}(\mathbf{X_i}, \mathbf{X_j}), \quad (i = 1, 2, \cdots, N), \tag{8.10}$$

the same method is applied as for a pair of coupled oscillators and the dynamics of $\psi_i \equiv \phi_i - \omega t$ $(i = 1, 2, \cdots, N)$ is

$$\frac{d\psi_i}{dt} = \delta\omega_i + \sum_{j=1}^{N} \Gamma_{ij}(\psi_i - \psi_j). \tag{8.11}$$

In terms of ϕ_i,

$$\frac{d\phi_i}{dt} = \omega_i + \sum_{j=1}^{N} \Gamma_{ij}(\phi_i - \phi_j). \tag{8.12}$$

If the form is

$$\frac{d\phi_i}{dt} = \omega_i - \frac{K}{N} \sum_{j=1}^{N} \sin(\phi_i - \phi_j), \tag{8.13}$$

this is called the Kuramoto model.

8.2 Analytical methods

8.2.1 Synchrogram

One way to detect m:n synchronization between respiration and heartbeat is to make a synchrogram. It is constructed by plotting the normalized relative phase of heartbeats within m respiratory cycles in the following equation,

$$\psi_m(t_k) = \phi_r(t_k) \pmod{2\pi m}, \tag{8.14}$$

where t_k is the time of k-th marked event of heartbeat and $\phi_r(t_k)$ is the instantaneous phase of respiration at the time of t_k. In a perfect m:n phase locking, ψ_m constructs n horizontal strips in the synchorogram. However, in reality these strips are broadened because of noise. One synchrogram can detect synchronization for only one value of m. For example if we choose $m = 2$, the synchrogram detects only 2:n synchronization. In order to cover all possible synchronization state, we

would have to plot synchrogram for all values of m although it is not practical in reality.

While $m : n$ complete synchronization occurs, the phase difference between two oscillators defined by

$$\varphi_{n,m} = n\phi_1 - m\phi_2 \tag{8.15}$$

is constant. The weaker definition is expressed by

$$|n\phi_1 - m\phi_2 - \delta| < \text{const.} \tag{8.16}$$

Under weak noise, the phase difference $\varphi_{n,m}$ flactuates randomly around a constant value. In this case, phase synchronization is detected as an appearance of a peak un the distribution of the relative phase defined by

$$\Psi_{n,m} = \varphi_{n,m} \mod 2\pi. \tag{8.17}$$

8.2.2 Synchronization index

A synchrogram is one of the ways to see synchronization visually but it is not enough to quantify the synchronization in the presence of noise. Especially it is difficult to judge which ratio of synchronization occurs by seeing different synchrograms with different m. To overcome this weakness, synchronization indices were introduced by Tass *et al.* in 1998 [146]. There are two ways to introduce these synchronization indices.

One is based on the conditional probability. We have two phases $\phi_1(t_j)$ and $\phi_2(t_j)$ defined on the intervals [0 $2\pi m$] and [0 $2\pi n$] respectively, where j is an index of time. Each interval is divided into N bins. We take a certain centered time t_{c1} and decide a certain window length around the centered time t_{c1} and call this time interval 'interval-1'. We take all j such that t_j is within the interval-1. Then, for each bin l, $1 \leq l \leq N$, we calculate

$$r_l(t_{c1}) = \frac{1}{M_l} \sum_j e^{\imath\phi_2(t_j)/n} \tag{8.18}$$

for all j, such that $\phi_1(t_j)$ belongs to the bin l and M_l is the number of points in this bin. If there is a complete m:n dependence between two phases, then $|r_l(t_{c1})| = 1$, whereas it is zero if there is no dependence. Finally we calculate the average over all bins in the following equation,

$$\lambda_{nm}(t_{c1}) = \frac{1}{N} \sum_{l=1}^{N} |r_l(t_{c1})|. \tag{8.19}$$

Thus λ_{nm} measures the conditional probability for ϕ_2 to have a certain value provided ϕ_1 is in a certain bin at the time t_{c1}. Then we move the centered time t_{c1} to t_{ci} and calculate the index in the same way. In order to find out m and n, we need to try different sets of values and pick out the set that gives the largest index.

The other approach is based on entropy. It is defined by the following equation,

$$\rho_{nm} = \frac{S_{\max} - S}{S_{\max}}. \tag{8.20}$$

where S is the entropy of the distribution of $\Psi_{m,n}$ and defined as

$$S = -\sum_{k=1}^{N} p_k \ln p_k, \tag{8.21}$$

where N is the number of bins which divide $\Psi_{m,n}$ and p_k is the probability that the phase difference is in the k-th bin.

It has to be noted that $S_{\max} = \ln N$, where N is the number of bins. It is normalized in such a way that $0 \leq \rho_{nm} \leq 1$, where $\rho_{nm} = 0$ corresponds to an uniform distribution (no synchronization) and $\rho_{nm} = 1$ corresponds to a Dirac delta-like distribution (perfect synchronization).

8.3 Results

8.3.1 Synchronization duration of real data

The method to evaluate the degree of synchronization is introduced in order to discuss the age-related changes in synchronization. At first we calculated the synchronization index of 1:n and 2:n cardiac respiratory synchronization for each subject with the window length $5T$ for 1:n synchronization and $10T$ for 2:n synchronization where T is the average respiratory period . The reason for the choice of window length is to see the synchronization during the same periods for all the subjects rather than to use the fixed time by subjects. If the index was above 0.95 and the duration was longer than $5T$ for 1:n synchronization and $10T$ for 2:n synchronization, we judged that synchronization occurred during the interval. When one signal of one subject is exchanged with the signal of another subject or when a signal is randomized, the synchronization index happens to comes up to high values without cardiovascular coupling. To be sure that the synchronization comes from a real cardiovascular interaction, we set minimum thresholds for

the synchronization index and duration. The synchrogram and synchronization index is shown in the Fig. 8.3. It is observed that the state of synchronization changes with time and even the synchronization ratio changes from 1:3 to 2:7. This kind of synchronization transition is quite common among all subjects. It is seen that noise disturbs the synchronization and the synchronization makes frequent transition from one state to another. Finally we calculated the amount of synchronization time for which the index was beyond 0.95 and studied how long the synchronization lasted. In that case, the synchronization duration is proportional to the ratio between synchronization time and the whole measurement time 1800 seconds, which was fixed for all the subjects. Therefore the synchronization duration is equivalent to the percentage of respiratory periods that are in the synchronization state in the whole measurement. Under this interpretation, the difference of average respiratory period does not affect the result.

The results are shown in Fig. 8.4. The synchronization duration increases significantly with age for females ($p = 0.00$) whereas it does not have any correlation with age for males ($p = 0.53$).

8.3.2 The correlation of synchronization duration with HRV and RRV

8.3.2.1 The average and total energy

Here we discuss the correlation between the logarithm of the synchronization duration and the heart and respiratory rate. In this section, we used the logarithm of synchronization duration because the synchronization duration itself does not seem to have the linear relationship with the heart or respiratory rate while the logarithm of synchronization duration does. The results are shown in the Fig. 8.5. The logarithm of the synchronization duration has significant positive correlation with the average respiratory rate both for males ($r = 0.62,\ p = 0.00$) and females ($r = 0.53,\ p = 0.00$) and significant negative correlation with total wavelet energy of HRV for males ($r = -0.26\, p = 0.05$) and total wavelet energy of RRV both for males ($r = -0.37,\ p = 0.00$) and females ($r = -0.33,\ p = 0.03$).

The correlation with average respiratory and synchronization duration could be thought to come from the algorithm because the synchronization threshold is proportional to the average respiratory rate and it is more difficult to keep the

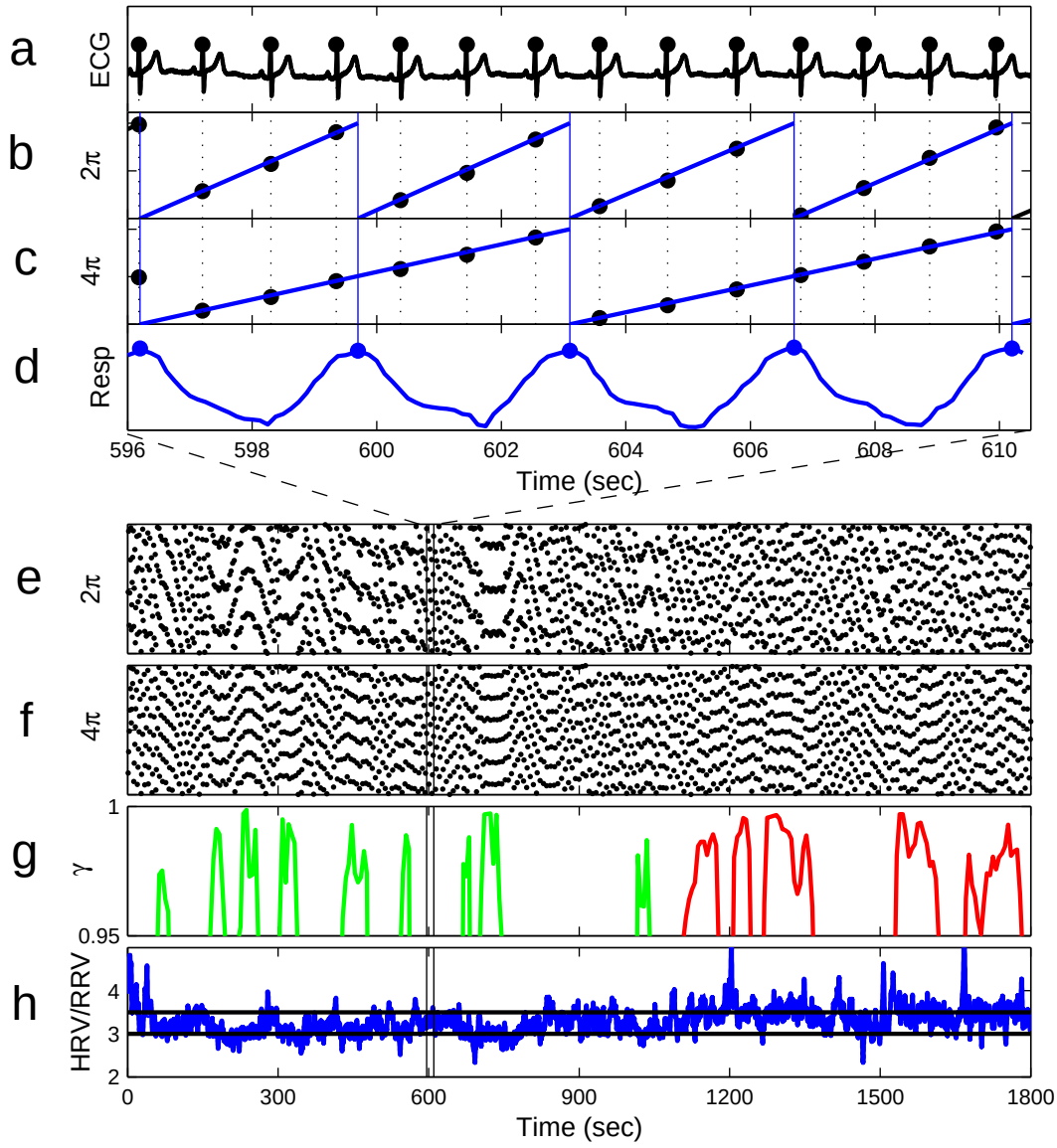

Fig. 8.3: An ECG signal during a time segment where R-peaks are marked (a), the phases (mod 2π) of the respiration signal shown in (d) at the marked R-peaks times in (A) during the time segment (b), the phases (mod 4π) of the respiration signal shown in (d) at the marked R-peaks times in (a) during the time segment (c), a respiratory signal during the time segment where the maxima are marked (d), a synchrogram for 1:n synchronization during the whole measurement (e), a synchrogram for 2:n synchronization during the whole measurement (f), synchronization indices above 0.95 during the whole measurement where 1:3 is drawn in green and 2:7 in red (g) and the ratio between HRV and RRV during the whole measurement where the two lines lie at the ratio 3.0 and 3.5, which corresponds to 1:3 and 2:7 synchronization (h). All data are obtained from the same subject as in Fig. 5.2.

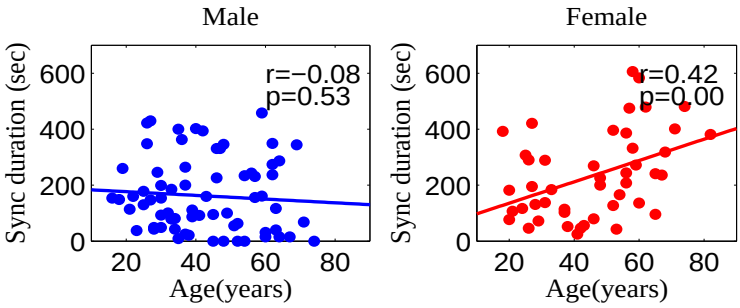

Fig. 8.4: The correlation between the total synchronization duration of the original data and age for males (left, blue) and females (right, red).

synchronization state for the longer threshold. It is difficult to judge the synchronization for people who have different respiratory rate. If we chose a fixed threshold of, for example 30 seconds, the average respiratory rate will not affect the results but it would be doubtful whether we could identify the 2:n synchronization reliably for a person whose average respiratory period is more than 7.5 seconds. It is a problem that we need longer time to judge synchronization state for the people who have longer average respiratory periods to compare the degree of synchronization. Indeed for the body it may be more difficult to maintain the stationary state for a longer time. However, at least these results show that a smaller standard deviation of respiration (for both genders) and a smaller standard deviation of heart rate (only for males) produce a longer synchronization duration in the resting state of healthy subjects. The synchronization study by Lotrič and Stefanovska [88] also revealed that the standard deviation of the heart rate has a negative correlation with the synchronization index

The result that a bigger standard deviation leads to shorter synchronization epochs corresponds well to our picture that if the frequency fluctuates dramatically, the parameters easily move outside the Arnold tongue, thus destroying the synchronization.

Although we could not see any significant correlation between age and duration of synchronization for males, the duration has a significant correlation with the standard deviation of respiration, which is *not* significantly correlated with age. The standard deviation of heart rate, which decreases significantly with age, is also correlated with synchronization, but respiration seems to have bigger influence on synchronization duration. For females, it is certain that respiration has a

significant effect in causing the synchronization. There is a trend of the average respiratory rate to increase with age for females although the correlation is not significant ($p = 0.09$). The fact that the synchronization duration have logarithmic sensitivity with the average respiratory rate supports the hypothesis that the trend of the average respiratory rate for females is one of the reason of the increase in synchronization duration with age. In any case, these results may indicate that the synchronization is related both to the properties which are not related to aging, such as the respiration, and to aging-related properties such as the standard deviation of heart rate.

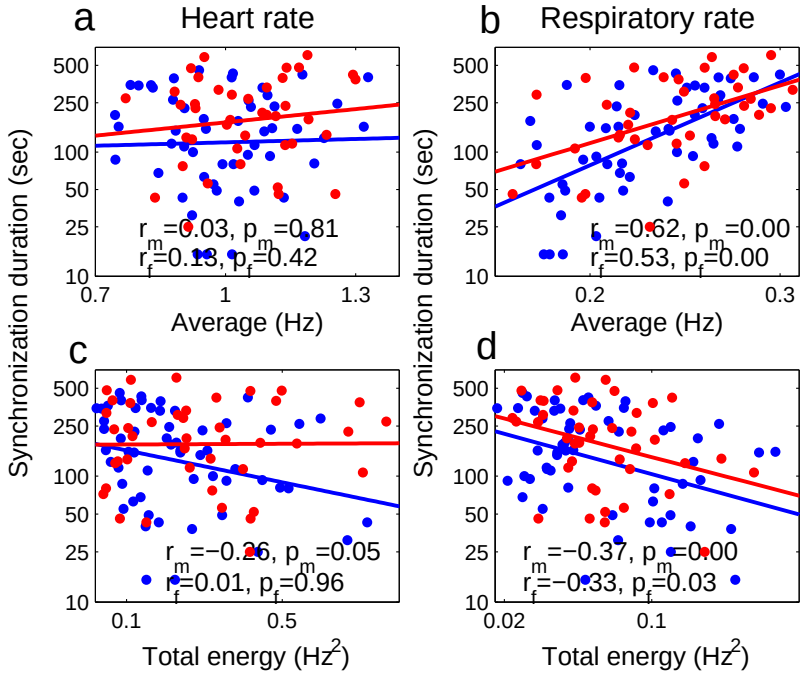

Fig. 8.5: The correlation between the logarithm of the synchronization duration and the average heart rate (a), the logarithm of the synchronization duration and the average respiratory rate rate (b), between the logarithm of the synchronization duration and the standard deviation of heart rate (c) and the logarithm of the synchronization duration and the standard deviation of respiratory rate (d).

8.3.3 Surrogate data

The first point to be settled is whether the synchronization reflects the true cardiovascular interaction or whether it is just noise. This problem was investigated by Toledo *et. al.* [149] by using surrogate date. In the present study, we made

surrogate data from the original signals and used them to calculate the duration of 'synchronization'. Surrogate data are artificially generated data that mimic some of the statistical properties of the data under study, but not the property that is being tested for.

Surrogate data were methodologically introduced into time series analysis as a method to test for nonlinearity [147]. The basic idea is to compute a nonlinear statistic for the data under study and to do the same for an ensemble of realizations of surrogates that mimic the linear properties of the studied data. If the computed statistics for the original data is significantly different from that obtained from surrogates, one can infer that the data were not generated by a linear process. Otherwise, the null hypothesis that a linear model fully explains the data is accepted.

There are several ways to make surrogate data to meet the needs of the study. For bivariate data, four types were proposed by Palus [107]:

- IID1 surrogate are realizations of mutually independent IID (independent identically distributed) stochastic processes (white noise) with the same mean, variance and histogram as the series under study. The IID surrogates are constructed by scrambling the original signal, i.e. the elements of the original series are randomly permutated in temporal order and different random permutation are used for the two components of the bivariate series.

- IID2 surrogates are realizations of IID stochastic processes (white noises), which take into account possible cross dependencies between the two components of the bivariate series. In each realization, the same random permutation is used for both components of the bivariate series. The IID surrogates present the null hypothesis of mutually dependent white noise, i.e. the two series are synchronized in a sense of mutual dependence given, e.g., by cross correlations; but the specific phenomenon as well as other temporal structures are absent.

- FT1 surrogates are independently generated for each of the two components in the bivariate data as a realization of linear stochastic process with the same power spectra under the study. The FT1 surrogates are obtained by computing the Fourier transform (FT) of the series, which is then reverted to

the time domain, with unchanged magnitudes but randomized phases. The FT1 surrogates realize the null hypothesis of two linear stochastic processes which asynchronously oscillate with the same frequencies as the original series under study.

- FT2 surrogates are realizations of a bivariate linear stochastic process that mimic individual spectra of the two components of the original bivariate series as well as their cross-spectrum. When constructing the FT2 surrogates, not only spectra but also the differences between phases of the Fourier coefficients of the two series for particular frequency bins must be kept unchanged. In this case, the same random number must be added to the phases of both coefficients of the same frequency bin. The FT2 surrogates preserve some of the synchronization, if present in the original series, which can be explained by a bivariate linear stochastic process.

In our study, IID1 surrogates were derived from the original cardiac and respiratory signals. Phases of the original signals were decided by the time of marked events according to the Eq. (5.15). The periods between marked events were calculated and permutated randomly. For example, if the time of marked events of an original signal is $[1, 2.5, 3.7, 5]$, the periods of original signals are $[1.5, 1.2, 1.3]$. Then these period are randomly permutated like e.g. $[1.2, 1.3, 1.5]$ and the time of marker events of surrogate is then $[1, 2.2, 3.5, 5]$ and the phases are calculated according to Eq. (5.15). Different randomizations were used for the cardiac and respiratory signals. Then the index and duration of synchronization of surrogates were calculated using the same algorithm as for the original data.

The results are shown in the Fig. 8.6. Surrogate data still have same apparent synchronization durations even after being randomized. However, the duration does not increase significantly with age (males $p = 0.77$; females $p = 0.36$) and the correlation with age is lower than the results of the original time series for both genders. This implies that the results of original data does not come only from noise.

We compared the epochs of synchronization of the original time series and the apparent epochs of synchronization in the surrogate time series for each gender. The original time series have significantly longer synchronization epochs than the

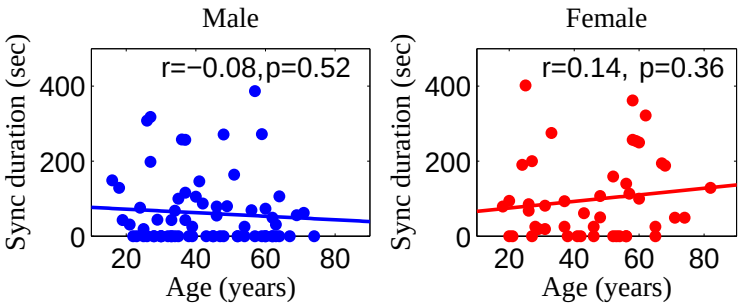

Fig. 8.6: The correlation between the total synchronization duration of the surrogate data and age for males (left, blue) and females (right, red).

surrogate time series (males $p = 0.00$; females $p = 0.00$). This means that the obtained synchronization is real, and not just because of noise.

8.4 Discussion

It was observed that the synchronization ratio was not constant but changed with time. This is because the ratio of heart rate and respiratory rate fluctuate with time as shown in Fig. 8.3h. It seems to be non-stationary as the heart rate and respiratory rate. The synchronization ratio is not only 1:n but also 2:n. There is the possibility that the ratio is m:n where m is more than three. However, it is usually difficult to detect synchronization with higher m because it requires a longer window for calculation and noise becomes larger. The result that females have longer synchronization in older age may be related to the decrease in the standard deviation of HRV with age and the slight increase in the average respiratory rate with age because of the logarithmic relationship. Another factor which affects synchronization is the form of the coupling function $\Gamma(\psi) = \Gamma_{12}(\psi) - \Gamma_{21}(-\psi)$ as we discussed in section 8.1. There are studies about coupling direction [108] [121] [122]. These methods were applied to the cardiorespiratory interaction and it was reported that the coupling is not symmetrical but that the respiration drives the cardiac system. The coupling direction fluctuates with time as the instant frequency, which means that the form of the coupling function $\Gamma(\psi)$ changes with time during measurements as well as $\delta\omega$. It would be an interesting problem to see how the coupling direction changes with age.

Our conclusion is that old females have longer synchronization periods and

that more modulation of the heart rate and the respiratory rate leads to less synchronization. The physiological reasons for longer synchronization of aged females is still not clear.

9. CORRELATION BETWEEN DIFFERENT OSCILLATORY COMPONENTS OBTAINED BY WAVELET ANALYSIS

In chapter 7, different oscillatory components were detected in HRV and blood flow signals. Cardiorespiratory interaction has been studied most intensively in all the combinations in terms of RSA or synchronization as it was mentioned in the previous chapters. In this chapter, the correlation between wavelet absolute energies and amplitudes from different physiological origins, which were calculated in section 7.2.2, are presented to see the interaction between other combinations.

9.1 Results

There seem to be interactions between the oscillations from different physiological origins which were discussed in section 7.2.1. These interactions appeared in correlation between wavelet absolute amplitudes and wavelet absolute energy from the different origins as shown in Fig. 9.1 and Fig. 9.3 for ACh and in Fig. 9.2 and Fig. 9.4 for SNP. The results of the correlation analysis are summarized in Tab. 9.1, Tab. 9.2, Tab. 9.3 and Tab. 9.4.

As we discussed, wavelet energy represents the amplitude of oscillation. The correlation between the absolute energies of oscillations from two different physiological origins indicates that there is the correlation between the amplitudes of the original oscillations. On the other hand, wavelet amplitude contains information about amplitude and frequency variability. Therefore the correlation between wavelet absolute amplitudes indicates that there is an interaction of amplitude and energy. It has to be noted that only the correlation between wavelet absolute amplitudes is not enough to judge whether the correlation comes from, amplitude or frequency variability.

For example, if there is no correlation in wavelet absolute energy, but there is in wavelet absolute amplitude, we could say that there is no amplitude interaction but there is frequency (phase) interaction. If there is no correlation in wavelet

absolute amplitude and there is in wavelet absolute energy, we could say that there is amplitude interaction but there is no frequency (phase) interaction. If there is correlation in both wavelet absolute amplitude and energy, we could say that there is amplitude interaction and maybe something in frequency dynamics. But in any case, it is an indirect evidence about frequency interaction, so further more detailed study will be necessary in details. Here we introduce and summarize only the main results.

All the combinations of different intervals have positive correlation values in terms of both energy and amplitude. All the combinations except VI-I and VI-II for the absolute energy of ACh have significant positive correlations. Most of the combinations of the different intervals have stronger correlation in the absolute amplitude than in the absolute energy, although V-I and IV-I for SNP are not the case. This may indicate that there are both amplitude and phase interaction in the most of different intervals.

The cardiac-respiratory correlation is high in all of the four figures. This means that there is strong cardiorespiratory interaction also in the blood flow signals.

The slopes of the combinations related to the interval V and VI are steeper for ACh than SNP since intervals V and VI are both endothelial-related and react more to ACh than to SNP. The plots were done by using the same size of the axes for ACh and SNP so that we can distinguish these difference between the two substances. For ACh, the figures related to the endothelial activities have broader distribution of points than for SNP.

Absolute energy of ACh					
Interval	VI	V	IV	III	II
I	$p = 0.10$	$p = 0.00$	$p = 0.00$	$p = 0.00$	$p = 0.00$
II	$p = 0.13$	$p = 0.00$	$p = 0.00$	$p = 0.00$	
III	$p = 0.00$	$p = 0.00$	$p = 0.00$		
IV	$p = 0.00$	$p = 0.00$			
V	$p = 0.00$				

Tab. 9.1: Correlation between two intervals for absolute energy of ACh

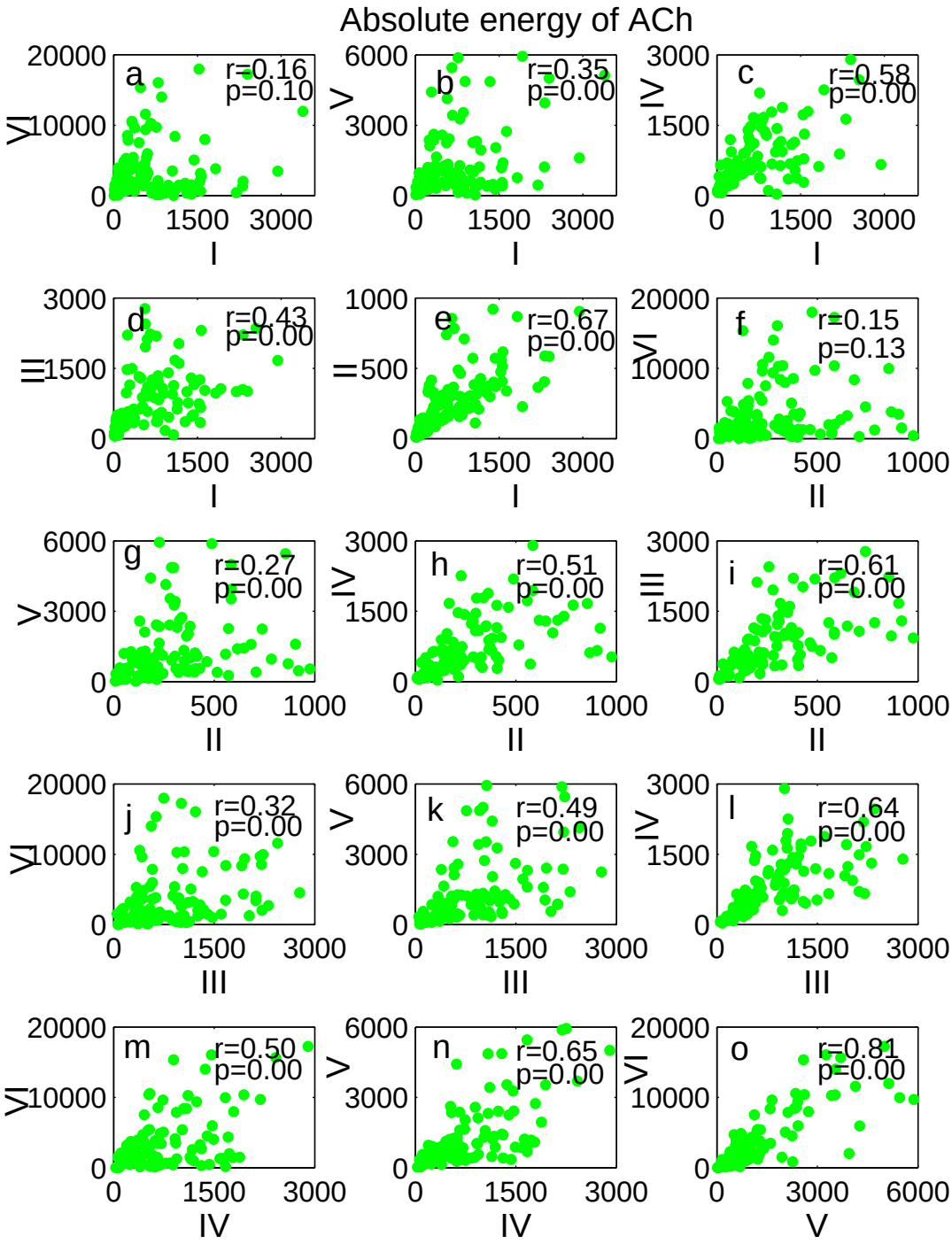

Fig. 9.1: The correlation between absolute energies in the intervals I and VI (a), I and V (b), I and IV (c), I and III (d), I and II (e), II and VI (f) II and V (g), II and IV (h), II and III (i), III and VI (j), III and V (k), III and IV (l), IV and VI (m), IV and V (n) and V and VI (o) and for ACh.

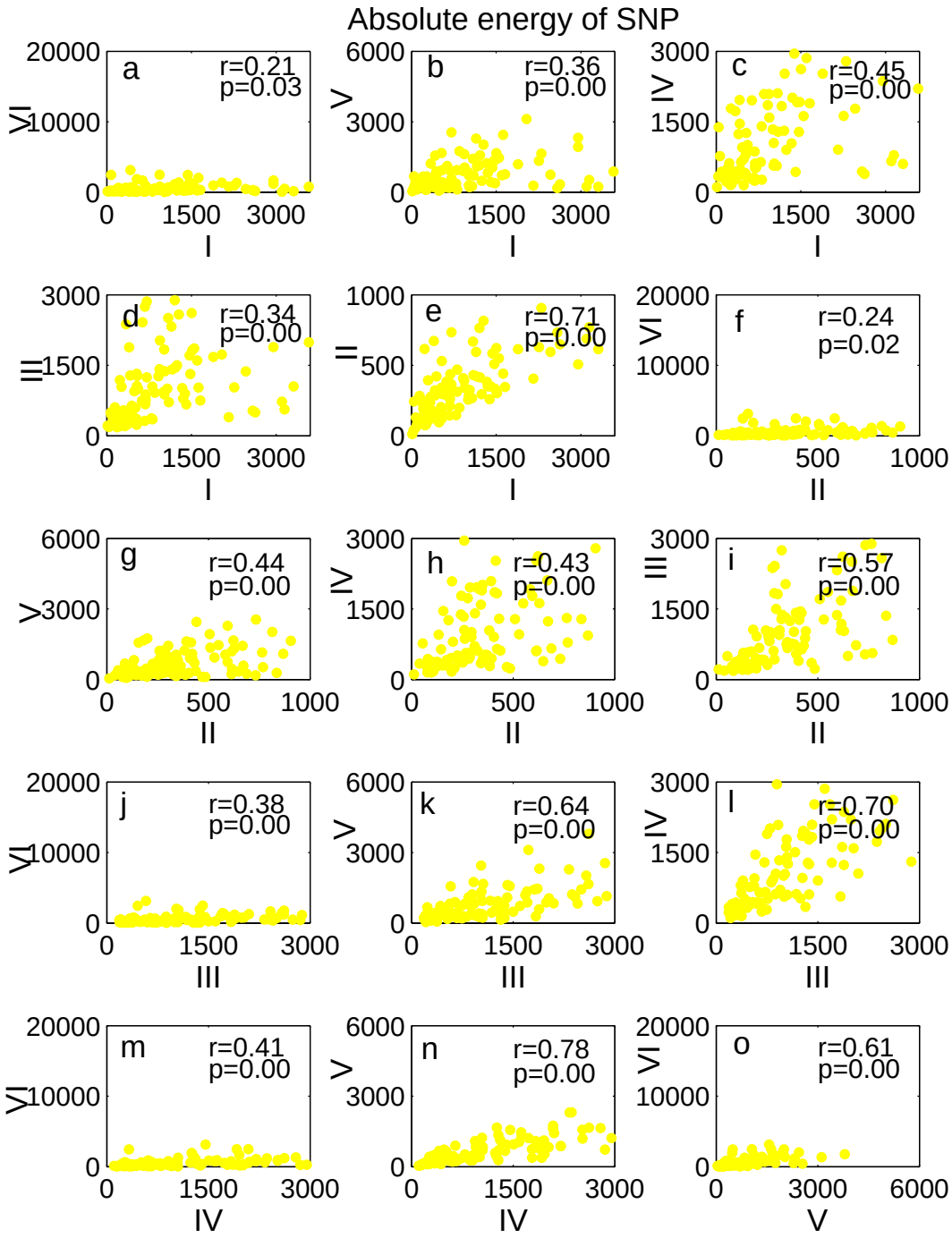

Fig. 9.2: The correlation between absolute energies in the intervals I and VI (a), I and V (b), I and IV (c), I and III (d), I and II (e), II and VI (f) II and V (g), II and IV (h), II and III (i), III and VI (j), III and V (k), III and IV (l), IV and VI (m), IV and V (n) and V and VI (o) and for SNP.

Absolute energy of SNP					
Interval	VI	V	IV	III	II
I	$p = 0.03$	$p = 0.00$	$p = 0.00$	$p = 0.00$	$p = 0.00$
II	$p = 0.02$	$p = 0.00$	$p = 0.00$	$p = 0.00$	
III	$p = 0.00$	$p = 0.00$	$p = 0.00$		
IV	$p = 0.00$	$p = 0.00$			
V	$p = 0.00$				

Tab. 9.2: Correlation between two intervals for absolute energy of SNP

Absolute amplitude of ACh					
Interval	VI	V	IV	III	II
I	$p = 0.02$	$p = 0.00$	$p = 0.00$	$p = 0.00$	$p = 0.00$
II	$p = 0.03$	$p = 0.00$	$p = 0.00$	$p = 0.00$	
III	$p = 0.00$	$p = 0.00$	$p = 0.00$		
IV	$p = 0.00$	$p = 0.00$			
V	$p = 0.00$				

Tab. 9.3: Correlation between two intervals for absolute amplitude of ACh

Absolute amplitude of SNP					
Interval	VI	V	IV	III	II
I	$p = 0.00$	$p = 0.00$	$p = 0.00$	$p = 0.00$	$p = 0.00$
II	$p = 0.00$	$p = 0.00$	$p = 0.00$	$p = 0.00$	
III	$p = 0.00$	$p = 0.00$	$p = 0.00$		
IV	$p = 0.00$	$p = 0.00$			
V	$p = 0.00$				

Tab. 9.4: Correlation between two intervals for absolute amplitude of ACh

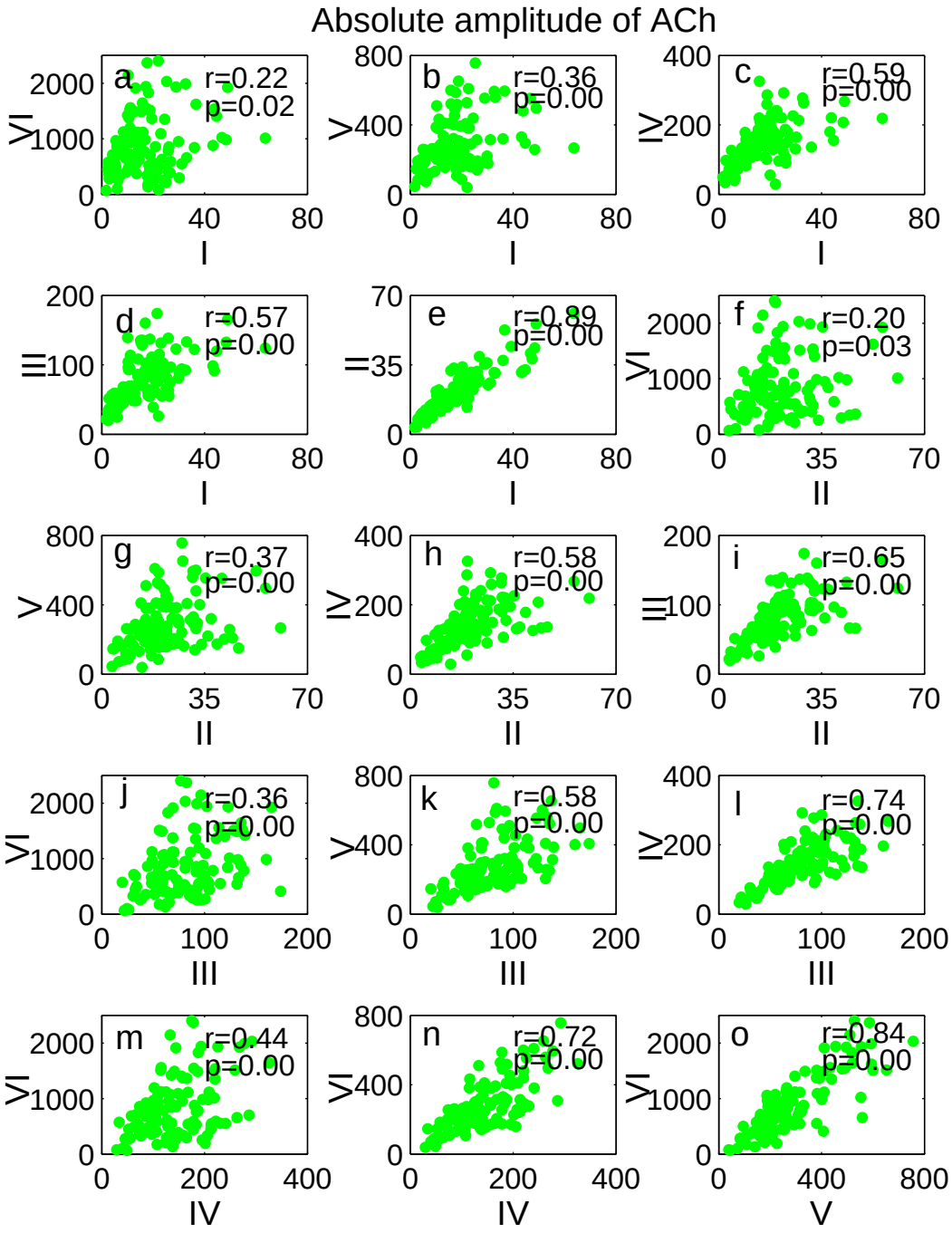

Fig. 9.3: The correlation between absolute amplitudes in the intervals I and VI (a), I and V (b), I and IV (c), I and III (d), I and II (e), II and VI (f) II and V (g), II and IV (h), II and III (i), III and VI (j), III and V (k), III and IV (l), IV and VI (m), IV and V (n) and V and VI (o) and for ACh.

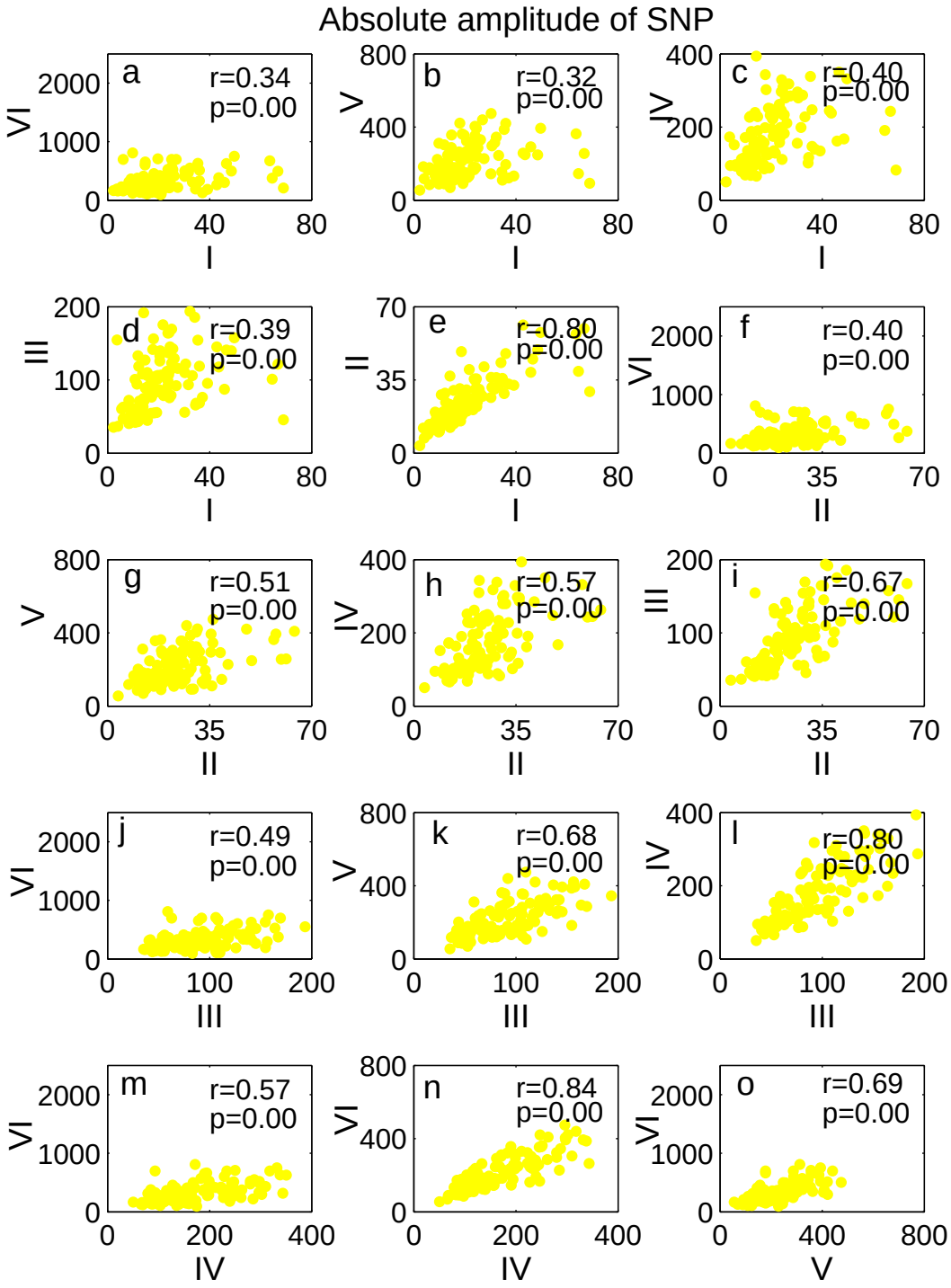

Fig. 9.4: The correlation between absolute amplitudes in the intervals I and VI (a), I and V (b), I and IV (c), I and III (d), I and II (e), II and VI (f) II and V (g), II and IV (h), II and III (i), III and VI (j), III and V (k), III and IV (l), IV and VI (m), IV and V (n) and V and VI (o) and for SNP.

9.2 Discussion

A lot of studies have been done for cardiorespiratory interaction such as cardiorespiratory synchronization and RSA but not much for the interaction between the other combinations. There is a report by Stefanovska *et al.* [134] that the respiration may influence the myogenic activity. A subject were asked to breathe with specific frequencies while the signals of blood flow as well as other cardiovascular function were recorded. Then it was reported the frequency and wavelet amplitude of the myogenic component changed with the respiratory frequency. Our results showed that there are significant correlation in wavelet amplitude and energy between respiratory (interval II) and myogenic (interval III) components for both ACh and SNP. This result also support that there is an interaction between respiratory and myogenic component. In this thesis, we observed strong correlations between the other intervals, which indicates the existence of interaction. At this stage, it is difficult to interpret what these results stand for in terms of the coupling but they are useful to understand the interaction of the cardiovascular system and improve the modelling.

10. CONCLUSIONS

Methods drawn from statistical physics and nonlinear dynamics have been applied to the analysis of cardiovascular time series with particular reference to the identification of physiological processes associated with aging. It is important to emphasize that all measurements on the subjects in order to reveal aging properties were non-invasive. What we have observed is

1. The standard deviation of heart rate decreased significantly with age for both males and females, consistent with previous studies [69, 123, 133, 152].

2. The total energy of HRV decreases with age because the variability which comes from respiratory activities (interval II) and from myogenic activities (interval III) decreases with age. These significant decrease with age of the energy in total, interval II and III were also observed in [89]. We added the low frequency interval VI newly to this thesis and observed that there is no significant change in this interval. In [89], significant decreases in interval III and IV were reported, which we did not observed in the present study. This may be because the number of subjects was smaller. We found in this thesis that females have stronger RSA than males in younger population, which was not reported before.

3. The complexity of HRV decreased significantly with age within the range of 10 to 50 seconds. The decrease arises because the ratio of the energy of the slower oscillation of interval IV (neurogenic activities) over the faster oscillation of interval III (myogenic activities) increases significantly with age. This indicates that the neurogenic control of the heart rate becomes more predominant than the myogenic control with increasing age. The decrease of the complexity with age in HRV was reported in various other studies such as [43, 143]. The difference between this thesis and the previous works is the window size for calculation. We chose a window size according to the

time scales decided by wavelet analysis. Thus we could identify physiological reasons for the decrease of the complexity with age as the increase of the ratio of the neurogenic oscillatory component over the myogenic component.

4. The complexity of blood flow measured with the two vasodilators ACh and SNP increased significantly with age within the range of 1 to 200 seconds. The increase arises because the ratio of the energy of the slower oscillation of intervals VI and V (endothelial activities) over the faster oscillation of interval I (cardiac activities) decreases significantly with age. There is a significant gender difference in the complexity of blood flows with ACh. The blood flows for females are less complex than those for males. We applied the DFA method to blood flows with ACh and SNP, revealed the age- and gender-related changes of the complexity and identified the physiological reasons as the strength of the wavelet relative energy of the low frequency oscillations.

5. The response to the endothelial-related vasodilator ACh of young females is significantly higher than that of young males and aged females, whereas there is no significant gender or aging difference for SNP. It was already known that there is a decrease in endothelial-dependent vasodilation with age and gender difference by using iontophoresis blood flow measurements [36, 42, 27, 1]. We applied the wavelet transform to analyze the iontophoresis blood flow signals and revealed age- and gender-related changes in oscillatory dynamics for the first time. Our results indicate that the endothelial function of females is higher than that of males, which may be connected with the well-known fact that young females has lower cardiovascular risk compared with aged females and males.

6. Oscillations at the cardiac frequency tend to become more dominant with increasing age in the blood flow signals, measured both with ACh and SNP. Combined with the conclusion 5, it might be concluded that the vessels lose the ability to dilate by themselves through endothelial action with age and the heart has to pump more strongly to circulate the necessary amount of the blood in the body. The steady average flow may indicate a high resistance of the vessels as well. This might cause heart problems or a high

blood pressure. Thus we first mentioned age-related changes in the cardiac oscillatory components in blood flows with ACh and SNP.

7. The duration of synchronization epochs increases significantly with age for females. The logarithm of the synchronization duration has a significant correlation with average respiratory rate and total energy of respiration for both males and females, which means that the respiratory rate affects the synchronization duration exponentially. On the other hand, only the total energy for males has significant correlation with the synchronization duration in terms of the heart rate. There are a lot of studies which reported synchronization in wide variety of subjects such as aneasthetized rats [136], young healthy athletes [126, 127], infants [103], healthy adults [148, 88, 149] and heart transplant patients [149]. This thesis first reported the effects of aging on synchronization and the strong correlation between synchronization duration and respiratory rate.

8. Correlations between different oscillatory components were observed in wavelet absolute energy and amplitude in terms of various combinations of the intervals. It was found out that the correlations are positive for all the combinations of the different oscillatory components and that there is an interaction in the amplitude and frequency for most of the combinations.

From all of our results, we conclude that aging is a factor which significantly affects cardiovascular function, and that gender sometimes produces a significant difference as well.

Two approaches to the cardiovascular signals are presented in this thesis. One is based on coupled oscillators and the other is based on the statistical mechanics. The oscillatory components detected by wavelet analysis (Chapter 7) and their significant correlations in wavelet energy and amplitude (Chapter 9) indicate there are interactions of frequency and amplitude between different oscillatory components. The observation of cardio-respiratory synchronization demonstrates a property of nonlinear coupled oscillators (Chapter 8). These results show a possibility that the cardiovascular system may be represented by a set of coupled oscillators with relatively few degrees of freedoms. But at the same time, in reality the system is always exposed to noise from unpredictable sources and may contain a large

number of degrees of freedom. In that case, the statistical approach seems to be more useful. In Chapter 6, we introduced DFA. Although this statistical approach is supposed to be a way to obtain the scaling of a system with a large degree of freedom, this thesis showed that there is a relation between the results of DFA and the six oscillatory components detected by wavelet. Scaling properties of a coupled oscillators model with a relatively small degree of freedom (with noise) should be studied further.

BIBLIOGRAPHY

[1] A. Algotsson, A. Nordberg, and B. Winblad, Inflence of Age and Gender on Skin Vessel Reactivity to Endothelium-Dependent and Endothelium-Independent Vasodilators Tested With Iontophoresis and a Laser Doppler Perfusion Imager, J Gerontol A Biol Sci Med Sci 50 (1995) M121-M127.

[2] S. Akselrod, D. Gordon, F.A. Ubel, D.C. Shannon, R.J. Berger and R.J. Choen, Science 213 (1981) 220-222.

[3] L.A.N. Amaral, A.L. Goldberger, P.C. Ivanov and H.E. Stanley, Scale-independent measures and pathologic cardiac dynamics, Phys. Rev. Lett.81 (1998) 2388-2391.

[4] L.A.N. Amaral, P.C. Ivanov, N. Aoyagi, I. Hidaka, S. Tomono, A.L. Goldberger, H.E. Stanley and Y. Yamamoto, Behavioral-independence features of complex heartbeat dynamics, Phys. Rev. Lett. 86 (2001) 6026-6029.

[5] A. Angelone and N.A. Coulter, Respiratory sinus arrythmia: A frequency dependent phenomenon, J. Appl. Physiol. 19 (1964) 482-497.

[6] G.V. Anrep, W. Pascual and R. Rössler, Respiratory variations of the heart rate, Proc. Rpy. Soc., London, Ser B. 119 (1936) 191-230.

[7] A. Asberg, T. Holm, T. Vasbotn, A.K. Andreassen and A. Hartman, Nonspecific microvascular vasodilation during iontophoresis is attenuated by application pf hypersmolar saline, Microvasc. Res. 58 (1999) 41-48.

[8] Y. Ashkenazy, P.C. Ivanov, S. Havlin, C.K. Peng, A.L. Goldberger, H.E. Stanley, Magnitude and sign correlations in heartbeat fluctuations, Phys. Rev. Lett. 86 (2001) 1900-1903.

[9] B.M. Ayyub and R.H. McCuen, Probability, Statistic & Reliability for Engineers, CRC Press, Boca Raton, New York, 1997.

[10] A. Babloyantz and A. Destexhe, Is the normal heart a periodic oscillator?, Biol. Cybern. 58 (1988) 203-211.

[11] F. Bajrović, M. Cencur, M. Hozic, S. Ribaric and A. Stefanovska, The contribution of lumbar sympathetic neurones activity to rat's skin blood flow oscillations, PFLUGERS ARCHIV-EUROPEAN JOURNAL OF PHYSIOLOGY 439(3) (2000) R158-R160 Suppl. S.

[12] P. Bak, C. Tang and K. Wiesenfeld, Self-organized criticality: an explanation of 1/f noise, Phys. Rev. Lett. 59 (1987) 381-384.

[13] A. Bandrivskyy, A. Bernjak, P.V.E. McClintock and A. Stefanovska, Role of Transdermal Potential Difference During Iontophoretic Drug Delivery, IEEE Trans. Biomed. Eng. 51 (2004) 1683-1685.

[14] A. Bandrivskyy, A. Bernjak, P.V.E. McClintock and A. Stefanovska, Wavelet phase coherence analysis: application to skin temperature and blood flow, Cardiovascular Engineering 4 (2004) 89-93.

[15] J. Beran, Statistics for Long-Memory Processes, New York: Chapman & Hall, 1994.

[16] P. Bernaola-Galván, P.C. Ivanov, L.A.N. Amaral and H.E. Stanley, Scale invariance in the nonstationarity of human heart rate, Phys. Rev. Lett. 87 (2001) 168105.

[17] M.N. Berliner, Skin microcirculation during tapwater iontophoresis in humans, Microvasc. Res. 54 (1997) 74-80.

[18] L. Bernardi, F. Salvucci, R. Suardi, P.L. Solda, A. Calciati, S. Perlini, C. Falcone and L. Ricciardi, Evidence for an instrinsic mechanism regulating heart rate variability in the transplanted and the intact heart during submaximal synamic exercise?, Cardiovasc. Res. 24 (1990) 969-981.

[19] R.M. Berne and M.N. Levy, Physiology, Mosby, St Louis, MO, 1998.

[20] R. Bonner and R. Nossal, Model for laser Doppler measurements of blood flow in tissue, Appl. Opt. 20 (1981) 2097-2107.

[21] M. Bračič and A. Stefanovska, Nonlinear dynamics of blood flow studied by Lyapunov exponents, Bulliten of Mathematical Biology 60 (1998) 417-433.

[22] M. Bračič and A. Stefanovska, Wavelet-based analysis of human blood-flow dynamics, Bulliten of Mathematical Biology 60 (1998) 919-935.

[23] R.P. Brandes, I. Fleming and R. Busse, Endothelial aging, Cardiovasc Res 66 (2005) 286-294.

[24] E.Alessio, A. Carbone, G. Castelli and V. Frappietro, Analysis of clusters formed by the moving average of a long-range correlated time series, Eur. Phys. J. B 27 (2002) 197-200.

[25] A. Carbone, G. Castelli and H.E. Stanley, Time-dependent Hurst exponent in finantial time series, Physica A 344 (2004) 267-271.

[26] A. Carbone, G. Castelli and H.E. Stanley, Analysis of clusters formed by the moving average of a long-range correlated time series, Phys. Rev. E 69 (2004) 026105.

[27] D.S. Celermajer, K.E. Sorensen, D.J. Spiegehalter, D. Georgakopoulos, J. Robinson, and J.E. Deanfield, Aging Is Associated With Endothelial Dysfunction in Healthy Men Years Before the Age-Related Decline in Women, J Am Coll Cardiol 24 (1994) 471-476.

[28] J.D. Croford, Scaling and Singularities in the Entrainment of Globally Coupled Oscillators, Phys. Rev. Lett. 74 (1993) 4341

[29] J.D. Croford and K.R.T. Davies, Synchronization of globally coupled phase oscillators: singularities and scaling for general couplings, Physica D 125 (1999) 1-46.

[30] H.Z. Cummins, N. Knable and Y. Yeh, Observation of diffusion broadning of Rayleigh scatered light, Phys. Rev. Lett. 12 (1964) 150-153.

[31] B. D'Antono, D. Moskowitz,C. Miners and J. Archambault, Gender and communal trait differences in the relations among social behaviour, affect arousal, and cardiac autonomic control, Journal of behaivior medicine. 28 (2005) 267-279.

[32] C.T.M. Davies and J.M.M. Neilson, Sinus arrythmia in men at rest, J. Appl. Physiol. 22 (1967) 947-955.

[33] L. Deng, P. Pei, J. Ma and D.L. Lee, A rank sum test method for informative gene discovery, Proceedings of the tenth ACM SIGKDD international conference on Knowledge discovery and data mining (2004) 410-419.

[34] P.B. DePetrillo, d'A. Speers and U.E. Ruttimann, Determining the Hurst exponent of fractal time series and its application to electrocardiographic analysis, Computers in Biol and Med 29 (1999) 393-406.

[35] S. Durand, B. Fromy, P. Bouyé, J.L. Saumet and P. Abraham, Corrent induced vasodilation during water iontophoresis(5 min, 0.01 mA) is delayed from current onset and involves aspirin-sensitive mechanism, J. Vasc. Res. 39 (2002) 59-71.

[36] K. Egashira, T. Inou, Y. Hirooka, H. Kai, M. Sugimashi, S. Suzuki, T. Kuga, Y. Urabe and A. Takeshita, 1993 Effects of Age on Endothelium-Dependent Vasodilation of Resistance Coronary Artery by Acetylcholine in Humans, Circulation 88 (1993) 77-81.

[37] L.F. Endresen and N. Skarland, Limit cycle oscillations in Pace maker cells, IEEE. Trans. on Biomed. Eng. 47 (2000) 1134-1137.

[38] J. Feder, Fractals. Plenum Press, New York and London, 283 p, 1988.

[39] J.C. Fisher, P.M. Parker and W.W. Shaw, Comparison of two laser Doppler flowmeters for the monitoring of dermal blood flow, Microsurgery 4 (1983) 164-170.

[40] R.F. Furgott, and J.V. Zawadzki, The obligatory role of endothelial cells in the relaxation of arterial smooth muscle by acetycholine, Nature 288 (1980) 373-376.

[41] D. Gabor, Theory of communication, J. of the IEEE 93 (1946) 429-457.

[42] M. Gerhard, M.A. Roddy, S.J. Creager and M.A. Creager, Aging progressively impairs endothelial-dependent vasodilation in forearm resistance vessels of humans, Hypertension 27 (1996) 849-853.

[43] A.L. Goldberger, L.A.N. Amaral, J.M. Hausdorff, P.C. Ivanov, C.K. Peng and H.E. Stanley, Fractal dymanics in physiology: Alternations with disease and aging, Proc. National Acad. of Sciences Suppl. 1. 99 (2002) 2466-2472.

[44] C.H. Goulden, Methods of statistical analysis, New York: John Wiley & Sons, 1956.

[45] P. Grassberger and I. Procaccia, Characterization of Strange Attractors, Phys. Rev. Lett. 50 (1983) 346-349.

[46] P. Grassberger and I. Procaccia, Measuring the strangeness of Strange Attractors, Physica D 9 (1983) 189-208.

[47] P. Grassberger and I. Procaccia, Estimation of the Kolmogorov entropy from a chaotic signal, Phys. Rev. A 28(4) (1983) 2591-2593.

[48] R.A. Gray and N. Chattipakorn, Termination of spiral waves during cardiac fibrillation via shock-induced phase resetting, PNAS 102 (2005) 4672-4677.

[49] A.C. Guyton, Textbook of medical physiology, 8th ed. Philadelphia (PA): Saunders, 1991.

[50] L. Guzman-Vargas. E. Calleja-Quevedo and F. Angulo-Brown, 'Fractal changes in heart rate dynamics with aging and heart failure, Fluctuation and Noise Letters 3 (2003) L83-L89.

[51] S. Hales, Statistical essays II Haemastaticks, London: Innings and Manby,1773

[52] J.M. Hausdorff, C.K. Peng, Z. Ladin, J.Y. Wei and A.L. Goldberger, Is walking a random walk? Evidence for long-range correlations in the stride interval of human gait, J. Appl. Physiol. 78 (1995) 349-358.

[53] J.M. Hausdorff, P. Purdon, C.K. Peng C-K, Z. Ladin, J.Y. Wei and A.L. Goldberger, Fractal dynamics of human gait: stability of long-range correlations in stride interval fluctuations, J. Appl. Physiol. 80 (1996) 1448-1457.

[54] S. Havlin, S.V. Buldyrev, A. Bunde, A.L. Goldberger, P.C. Ivanov, C.K. Peng, H.E. Stanley, Scaling in nature: From DNA through heartbeats to weather, Physica A 273 (1999) 46-69.

[55] T. Higuchi, Approach to an irregular time series on the basis of the fractal theory, Physica D 31 (1988) 277-283.

[56] T. Higuchi, Relationship between the fractal demension and the power law index for a time series, Physica D 46 (1990) 254-264.

[57] G. Hildebrant, The autonomous time structure and its reactive modifications in the human organism, In: L. Resting, U. an der Heiden and M. C. Mackey (Eds), Temporal disorder in human oscillatory system, Berlin: Springer-Verlag (1987) 160-174.

[58] J.A. Hirsch and B. Bishop, Respiratory sinus arrythmia in humans: How breathing patterns modulates heart rate, Am. J. Physiol.: Heart Circ. Physiol. 241 (1981) H620-H629.

[59] H.E. Hurst, Long-term storage capacity of reservoirs, Trans. Am. Soc. Civ. Eng. 116 (1951) 770.

[60] H.E. Hurst, R.P. Black and Y.M. Simaika, Long-Term Storage: An Experimental Study, Constable, London, 1965.

[61] B.W. Hyndman, R.I. Kitney, and B.M. Sayers 1971 Spontaneous rhythms in physiological control systems, Nature 233 (1971) 339-341.

[62] N. Iyengar, C.K. Peng, R. Morin, A.L. Goldberger and L.A. Lipsitz, Age-related alterations in the fractal scaling of cardiac interbeat interval dynamics, Am J Physiol 271 (1996) R1078-R1084.

[63] P.C. Ivanov, M.G. Rosenblum, C.K. Peng, J. E. Mietus, S. Havlin, H. E. Stanley and A. L. Goldberger, Scaling and universality in heart rate variability distributions, Physica A 249 (1998) 587-593.

[64] P.C. Ivanov, L.A.N. Amaral, A.L. Goldberger, S. Havlin, M.G. Rosenblum, Z.R. Struzik and H.E. Stanley, Multifractality in human heartbeat dynamics, Nature 399 (1999) 461-465.

[65] P.C. Ivanov, L.A.N. Amaral, A.L. Goldberger, S. Havlin, M.G. Rosenblum, H.E. Stanley and Z.R. Struzik, From 1/f noise to multifractal cascades in heartbeat dynamics, Chaos 11 issue 3 (2001) 641-652.

[66] J. Jalife and C. Antzelevitch, Phase resetting and annihilation of pacemaker activity in cardiac tissue, Science 206 (1979) 695-697.

[67] N.B. Janson, A.G. Balanov, V.S. Anishchenko and P. V. E. McClintock, Phase synchronization between several interacting processes from univariate data, Phys. Rev. Lett. 86 (2001) 1749-1752.

[68] G. Kaiser, A friendly guide to Wavelet, Boston: Birkhäuser, 1994.

[69] D.T. Kaplan, M. Furman, S.M. Pincus, S.M. Ryan, L.A. Lipsitz and A.L. Goldberger, Aging and the complexity of cardiovacular system, Biophys. J. 59 (1991) 945-949.

[70] J. Kastrup, J. Bühlow and N.A. Lassen, Vasomotion in human skin befire and after local heating recorded with laser Doppler flowmetry. A method for induction of vasomotion, Int. J. Microcirc.: Clin Exp 8 (1989) 205.

[71] R.E. Klabunde, Cardiovascular Physiology Concepts, Lippincott Williams & Wilkins, 2005.

[72] M. Kobayashi, T. Musha, 1/F fluctuation of heartbeat period, IEEE Trans. Biomed. Eng. 29 (1982) 456-457.

[73] Y. Kuramoto, in H. Aoki (ed.) International Symposium on Mathematical Problems in Theoretical Physics 39 (1976) 420.

[74] Y. Kuramoto, Chemical Oscillations, Waves, and Turbulence, Berlin: Springer, 1984.

[75] Y. Kuramoto, Scaling Behavior of Turbulent Oscillators with Non-Local Interaction, Prog. Theor. Phys. 94 (1994) 321-330.

[76] Y. Kuramoto and H. Nakao, Origin of power-law spatial correlations in distributed oscillators and maps with nonlocal coupling. Phys. Rev. Lett. 76 (1996) 4352-4355.

[77] Y. Kuramoto, D. Battogtokh, H. Nakao, Multiaffine Chemical Turbulence, Phys. Rev. Lett 81 (1998) 3543-3546.

[78] Y. Kuramoto, S. Shima, D. Battogtokh and Y. Shiogai, Mean-field theory revives in self-oscillatory fields with non-local coupling, Prog. Teor. Suppl 161 (2006) 127-143.

[79] T.B.J. Kuo, T. Lin, C.C.H. Yang, C.L. Li, C.F. Chen, and P. Chou, Effec of aging on gender differences in neural control of heart rate, Am J Physiol Heart Circ Physiol 277 (1999) H2233-H2239.

[80] P. Kvandal, A. Stefanovska, M. Veber, H.D. Kvermmo and K.A. Kirleboen, Regulation of human cutaneous circulation evaluated by laser Doppler flowmetry, iontophoresis, and spectral analysis: importance of nitric oxide and prostaglandines, Microvasc Res 65 (2003) 160-171.

[81] P. Kvandal, S.A. Landsverk, A. Bernjak, A. Stefanovska, H.D. Kvernmo and K.A. Kirkebøen, Low-frequency oscillations of the laser Doppler perfusion signal in human skin, Microvascular Research 72 (2006) 120-127.

[82] H.D. Kvernmo, A. Stefanovska, M.B. Lotrič, K.A. Kirkebøen and K. Kvernebo, Oscillations in the human cutaneous blood perfusion in human skin before and after exercise, Microvasc. Res. 56 (1998) 173.

[83] H.D. Kvernmo, A. Stefanovska, K.A. Kirkebøen, K. Kvernado, Oscillations in the human cutaneous blood perfusion signal modified by endotheliun-dependent and endothelium-independent vasodilators, Microvasc Res 57 (1999) 298-309.

[84] S.A. Landsverk, P. Kvandal, T. Kjelstrup, U. Benko, A. Bernjak, A. Stefanovska, H. Kvernmo and K.A. Kirkebøen, Human skin microcirculation after brachial plexus block evaluated by wavelet transform of the laser Doppler flowmetry signal, Anesthesiology 105 (2006) 478-484.

[85] B.I. Levy, Artery changes with aging: degeneration or adaptation? Dialog Cardiovas Med 6 (2001) 104-111.

[86] L.A. Lipsitz and A.L. Goldberger, Loss of 'complexity' and aging, JAMA 267 (1992) 1806-1809.

[87] M.B. Lotrič, Couplings among subsystems that regulate blood flow, Ph.D. thesis, University of Ljubljana, 1999.

[88] M.B. Lotrič, and A. Stefanovska, Synchronization and modulation in the human cardio-respiratory system, Physica A 283 (2000) 451-461.

[89] M.B. Lotrič, A. Stefanovska, D. Štajer and V. Urbančič-Rovan, Spectral components of heart rate variability determined by wavelet analysis, Physiol. Meas. 21 (2000) 441-457.

[90] H. Luczak and W. J. Lauring, An analysis of heart rate variability, Ergonomics 16 (1972) 85.

[91] T.H. Maiman, Stimulated optical radiation in ruby, Nature 187 (1960) 493-494.

[92] A. Malliani, M. Pagani, F. Lombardi, and S. Cerutti, Circulation 84 (1991) 482.

[93] B.B. Mandelbrot J.R. Wallis, Noah, Joseph, and Operational Hydrology, Water Resources Research, 4(3) (1968) 909-918.

[94] B.B. Mandelbrot and J.R. Wallis, Computer Experiments with Fractional Gaussian Noises. Part 1, Averages and Variances, Water Resources Research, 5(1) (1969) 228-241.

[95] B.B. Mandelbrot and J.R. Wallis, Computer Experiments with Fractional Gaussian Noises. Part 2, Rescaled Ranges and Spectra, Water Resources Research 5(1) (1969) 242-259.

[96] B.B. Mandelbrot J.R. Wallis, Computer Experiments with Fractional Gaussian Noises. Part 3, Mathematical Appendix, Water Resources Research 5(1) (1969) 260-267.

[97] B.B. Mandelbrot and J.R. Wallis, Some Long-Run Properties of Geophysical Records, Water Resources Research 5(2) (1969) 321-340.

[98] B.B. Mandelbrot and J.R. Wallis, Robustness of the Rescaled Range R/S in the Measurement of Noncyclic Long Run Statistical Dependence, Water Resources Research 5(5) (1969) 967-988.

[99] B.B. Mandelbrot and J.R. Wallis, A Fast Fractional Gaussian Noise Generator, Water Resources Research, 7(3) (1969) 543-533.

[100] B.B. Mandelbrot, Fractals-Form, Chance and Dimension, Freedman, San Francisco, 1977.

[101] R.L. Matz and R. Andriantsitohaina, Age-related endothelial dysfunction, Drugs Aging 20 (2003) 527-550.

[102] P.V.E. McClintock and A. Stefanovska, Interaction and synchronization in the cardiovascular system, Fluctuation and Noise Letters 3 (2003) L167-L176.

[103] R. Mrowka and A. Patzak, Quantative analysis of cardiorespiratory synchronization in infants, Int. J. of Bifurcation and Chaos 10 (2000) 2479-2488.

[104] G.E. Nilsson, T. Tenland and P.L. Öberg, Evaluation of a laser Doppler flowmeter for measurement of tissue blood flow, IEEE trans. Biomed. Eng. 27 (1980) 597-604.

[105] S.M. Ossadnik, S.V. Buldyrev, A.L. Goldberger, S. Havlin, R.N. Mantegna, C.K. Peng, M. Simons, H.E. Stanley, Correlation approach to identify coding regions in DNA sequences, Biophys. J. 67 (1994) 64-70.

[106] H. Oxenham and N. Sharpe, Cardiovascular aging and heart failure, Eur J Heart Failure 5 (2003) 427-434.

[107] M. Paluš, Detecting phase synchronization in noisy system, Phys. Lett. A 235 (1997) 341-351.

[108] M. Paluš and A. Stefanovska, Detection of coupling from phases of interacting oscillators: An information-theoretic approach, Phys. Rev. E 67 (2003) 055201(R).

[109] J. Penaz, J. Roukenz, and H.J. vander Waal, Spectral analysis of some spontaneous rhythms in the circulation, in *Byokibernetik*, edited by H. Drischel and N. Tiedt, (Karl Marx University, Lepizig, 1968), p.233.

[110] C.K. Peng, J. Mietus, J.M. Hausdorff, S. Havlin, H.E. Stanley and A.L. Goldberger, Long-range anticorrelations and non-Gaussian behaviour of the heartbeat, Phys. Rev. Lett. 70 (1993) 1343-1346.

[111] C.K. Peng, S.V. Buldyrev, S. Havlin, M. Simons, H.E. Stanley and A.L. Goldberger, On the mosaic organization of DNA sequences, Phys Rev E 49 (1994) 1685-1689.

[112] C.K. Peng, S. Havlin, H.E. Stanley and A.L. Goldberger, Quantification of scaling exponents and crossover phenomena in nonstationary heartbeat time series, Chaos 5 (1995) 82-87.

[113] H. Peng, V. Matchkov, A. Ivarsen, C. Aalkajær and H. Nilsson, Hypothesis for the initiation of vasomotion,Circ. Res. 88 (2006) 810-815.

[114] S.M. Pikkujämsä, T.H. Mäkikallio, L.B. Sourander, I.J. Räihä, P. Puukka, J. Skyttä, C.K. Peng, A.L. Goldberger and H.V. Huikuri, Cardiac interbeat interval dynamics from childhood to senescence, Circulation 100 (1999) 393-399.

[115] A.S. Pikovsky, M.G. Rosenbulm G.V. Osipov and J. Kurths, Phase synchronization of chaotic oscillators by external driving, Physica D 104 (1997) 219-238.

[116] A.S. Pikovsky, M.G. Rosenbulm and J. Kurths, Snchronization: A universal concept in Nonlinear Sciences, Cambridge University Press, 2001.

[117] C.S. Poon and C.K. Merrill, Decrease of cardiac chaos in congestive heart failure, Nature 398 (1997) 492-495.

[118] W.H. Press, Flicker noise in astronomy and elsewhere, Comments Astrophys 7 (1978) 103-119.

[119] C. Riva, B. Ross and G.B. Benedek, Laser doppler measurements of blood flow in capillary tubes and retinal arteries, Invest. Opthalmol. 11 (1972) 936-944.

[120] M.G. Rosenblum and A.S. Pikovsky and J. Kurth, Phase synchronization of chaotic oscillators, Phys. Rev. Lett. 76 (1996) 1804-1807.

[121] M.G. Rosenblum and A.S. Pikovsky, Detecting direction of coupling in interacting oscillators, Phys. Rev. E 64 (2001) 045202.

[122] M.G. Rosenblum, L. Cimponeriu, A. Bezerianos, A. Patzak, and R. Mrowka, Identification of coupling direction: Application to cardiorespiratory interaction, Phys. Rev. E 65 (2002) 041909.

[123] S.M. Ryan, A.L. Goldberger, S.M. Pincus, J. Mietus and L.A. Lipsitz, Gebder- and age-related differences in heart rate dynamics: are women more complex than men?

[124] H. Sakaguchi and Y. Kurmaoto, A soluble active rotater model showing phase transitions via mutual entertainment, Prog. Theor. Phys. 76 (1986) 576-581.

[125] B. McA. Sayers, Analysis of heart rate variability, Ergonomics 16 (1973) 16.

[126] C. Schäfer, M.G. Rosenblum, J. Kurths and H.H. Abel, Heartbeat synchronised with ventilation, Nature 392 (1998) 239-240.

[127] C. Schäfer, M.G. Rosenblum, H.H. Abel and J. Kruths, Synchronization in the human cardiorespiratory system, Phys. Rev. E 60 (1999) 857-869.

[128] H. Seidel and H. Herzel, Analyzing entrainment of heartbeat and respiration with surrogates, IEEE Eng. Med. Biol. Mag. 17 (1998) 54-57.

[129] T. Schreiber, Measuring information transfer, Phys. Rev. Lett. 85 No.2 (2000) 461-464.

[130] S. Shima and Y. Kuramoto, Rotating waves with phase-randomized core in nonlocally coupled oscillators, Phys. Rev. E 69 (2004) 036213.

[131] Y. Shiogai and Y. Kurmaoto, Wave propagation in nonlocally coupled oscillators with noise, Prog. Theor. Phys. Suppl. 150 (2003) 435-438.

[132] T. Söderström, A. Stefanovska, M. Veber and H. Svensson, Involvement of sympathetic activity in skin blood flow oscillation in humans, Am. J. Physiol. Heart Circ. Physiol. 284 (2003) H1638-H1646.

[133] P.K. Stein, R.E. Kleiger and J.N. Rottman, Differing effects of age on heart rate variability in men and women, Am. J. Cardiol 80 (1997) 302-305.

[134] A. Stefanovska, M.B. Lotrič, S. Strle and H. Haken, The cardiovascular system as coupled oscillators? Physiol. Meas. 22 (2001) 535-550.

[135] A. Stefanovska, D.G. Luchinsky and P.V.E. McClintock, Modelling couplings among the oscillators of the cardiovascular system, Physiol. Meas. 22 (2001) 551-564.

[136] A. Stefanovska, H. Haken, P.V.E. McClintock, M. Hožič, F. Bajrovic and S. Ribarič, Reversible transitions between synchronization states of the cardiorespiratory system, Phys. Rev. Lett. 85 (2000) 4831-4834.

[137] A. Stefanovska and M. Hožič, Spatial synchronization in the human cardiovascular system, Progress of Theoretical Physics Supplement 139 (2000) 270-282.

[138] A. Stefanovska and M. Bračič, Physics of the human cardiovascular system, Contemporary Phys. 40 (1999) 31.

[139] A. Stefanovska, M.B. Lotrič and H.D. Kvernmo, Wavelet Analysis of Oscillations in the Peripheral Blood Circulation Measured by Laser Doppler Technique, IEEE Trans. Biomed. Eng. 46 (1999) 1230-1239.

[140] M.D. Stern, In vivo observation of microcirculation by coherent light scattering, Nature 254 (1975), 56-58.

[141] S.H. Strogatz, R.E. Mirollo and P.C. Matthews, Coupled nonlinear oscillators below the synchronization threshold: Relaxation by generalized Landau damping. Phys. Rev. Lett. 68 (1999) 2730-2733.

[142] S.H. Strogatz, From Kuramoto to Craford: exploring the onset of synchronization in populations od coupeled oscillators, Physica D 143 (2000) 1-20.

[143] Z.R. Struzik, J. Hayano, R. Soma, S. Kwak and Y. Yamamoto, Aging of complex heart rate dynamics, IEEE. Trans. Biomed. Eng. 53 (2006) 89-93.

[144] D. Tanaka and Y. Kuramoto, Complex Ginzburg-Landau equation with nonlocal coupling, Phys. Rev. E 68 (2003) 026219.

[145] Task Force of the ESC and the NASPE, Standards of heart rate variability, Eur. Heart. J 17 (1996) 354.

[146] P. Tass, M.G. Rosenblum, J. Weule, J. Kurths, A. Pikovsky, J. Volkmann, A. Schnitzler and H.J. Freund, Detection of n:m Phase Locking from Noisy Data: Application to Magnetoencephalography, Phys. Rev. Lett. 81 (1998) 3291-3294.

[147] J. Theiler, S. Eubank, A. Longtin, B. Galdrikian, D. Bryan and J.D. Farmer, Testing for nonlinearity in time series: the method of surrogate data, Physica D 58 (1992) 77-94.

[148] E. Toledo, M.G. Rosenblum, J. Kruths and S. Akselrod, Cardiorespiratory synchronization: is it a real phenomenon?, Computers in Cardiology, Los Alamitos (CA), IEEE Computer Society, 26 (1999) 237-240.

[149] E. Toledo, S. Akselrod, I. Pinhas and D. Aravot, Does synchronization reflect a true interaction in the cardiorespiratory system?, Med. Eng. & Phys. 24 (2002) 45-52.

[150] M.P. Tulppo, A.M. Kiviniemi, A.J. Hautala, M. Kallio, T. Seppänen, T.M. Mäkikallio and H.V. Huikuri, Physiologocal background of the loss of fractal heart rate dynamics, Circulation 112 (2005) 314-319.

[151] Y.C. Tzeng, P.D. Larsen and D.C. Galletly, Cardioventilatory coupling in resting human subjects, Exp. Physiol. 88 (2003) 775-782.

[152] K.J. Urstad, N. Storck, F. Bouvier, M. Ericson, L.E. Lindblad and M. J. Urstad, Heart variability in healthy subjects is related to age and gender, Acta. Physiol. Scand 160 (1997) 235-241.

[153] M. Veber, A. Bandrivskyy, P.B.M. Clarkson, P.V.E. McClintock, A. Stefanovska, Wavelet analysis of blood flow dynamics: effect on the individual oscillatory components of iontophoresis with pharmacologically neutral electrlytes, Phys. Med. Biol. 49 (2004) N111-N117.

[154] D. Watkins and G.A. Holloway, An instrument to measure cutaneous blood flow using the Doppler shift of laser light, IEEE Trans. Biomed. Eng. BME-25 (1978) 28-33.

[155] F. Wilcoxon, Individual comparisons by ranking methods, Biometrics 1 (1945) 80-83.

[156] E.P. Windmaire, H. Raff and K.T. Strang, Human physiology 9th edn. Mc Graw Hill, 2004.

[157] A.T. Winfree, Biological rhythms and the behavior of populations of coupled oscillators, J. Theor. Biol. 16 (1967) 15-42.

[158] A.T. Winfree, The Geometry of Biological Time, Springer-Verlag, New York, 1980.

[159] L. Xu, P.C. Ivanov, K. Hu, Z. Chen, A. Carbone and H.E. Stanley, Quantifying signals with power-law correlations: A comparative study of detrended fluctuation analysis and derended moving average techniques, Phys. Rev. E 71 (2005) 051101.